Durham University

Durham E-Theses

Theoretical studies of Van der Waals clusters

Bryan, Robert

How to cite:

Bryan, Robert (1997) *Theoretical studies of Van der Waals clusters*, Durham theses, Durham University. Available at Durham E-Theses Online: http://etheses.dur.ac.uk/4712/

Use policy

The full-text may be used and/or reproduced, and given to third parties in any format or medium, without prior permission or charge, for personal research or study, educational, or not-for-profit purposes provided that:

- a full bibliographic reference is made to the original source
- a link is made to the metadata record in Durham E-Theses
- the full-text is not changed in any way

The full-text must not be sold in any format or medium without the formal permission of the copyright holders.

Please consult the full Durham E-Theses policy for further details.

Academic Support Office, The Palatine Centre, Durham University, Stockton Road, Durham, DH1 3LE
e-mail: e-theses.admin@durham.ac.uk Tel: +44 0191 334 6107
http://etheses.dur.ac.uk

Theoretical Studies of Van der Waals Clusters

Robert Bryan

Ph.D Thesis
Chemistry Department
University of Durham
November 1997

The copyright of this thesis rests with the author. No quotation from it should be published without the written consent of the author and information derived from it should be acknowledged.

19 FEB 1998

Abstract of Ph.D thesis

"Theoretical Studies of Van der Waals Clusters"

Robert Bryan, Durham University, November 1997

The vibrational energy levels of various rare gas trimers, Ar_3, Ne_3, He_3, Ar_2Ne and Ne_2Ar, have been calculated using a coupled channel approach. We have compared results obtained with previous calculations. The existence of Efimov states in He_3 has been investigated, and no evidence of their existence has been found.

The affect of the Eckart conditions on embedding axis into a rotating-vibrating system has been investigated for several rare gas systems. A wide range of rare gas trimers have been studied, Ar_3, He_2Ar, Ar_2He, Ar_2Ne and Ne_2Ar. For each trimer the full range of molecular motion is investigated.

The low energy minima for the Ar_nN_2 and Ne_nN_2 systems have been found using simulated annealing search, and a gradient based minimisation technique, of a pairwise potential energy surface. Clusters with $n \geq 12$ have been studied, and first solvation shells for both systems have been proposed. For each value of n, for $n = 1 - 12$, the first few low energy minima of the potential energy surface have been found. From these studies, we have gained a detailed understanding of the interplay of forces that determine the low energy structures for these systems.

The affect of three-body interactions on the low energy minima both rare gas-N_2 systems has been studied. In both system, rare gas-rare gas and rare gas-N_2 threebody interactions have been taken into account. This study has shown that the three-body forces have a small affect on the low energy structures of each system.

Acknowledgements

To my supervisor Prof Jeremy Hutson, for his guidance over the past three years
To EPSERC for funding
To the Durham theoretical chemistry group, for three very enjoyable years of research. Inparticular I would like to that Keith for his help during my first year of my Ph.D.
To my parents, for their love and support.

Statement

No part of this thesis has been previously submitted by me for a degree to any university. Every effort has been made to ensure that all work which is not ariginal to the author has been properly credited. I placed no restriction upon access to, or copying of, this thesis.

Contents

1 Introduction 4

1.1 The Study of Intermolecular Forces 4

1.2 Rare Gas Trimers 5

1.3 Other Types of Rare Gas Cluster 6

1.4 Rare Gas-Molecule Clusters 7

1.5 Work in This Thesis 8

1.6 Minimisation Techniques 11

1.6.1 Genetic Algorithms 16

2 The Bound States of Rare Gas Trimers 17

2.1 Coupled Channel Calculations 17

2.2 Hyperspherical Co-ordinates 20

2.3 Calculations on A_3 case Rare Gas trimers 23

2.4 Calculations on the He_3 trimer 27

2.4.1 Efimov States 29

2.5 Calculations on AB_2 Case Rare Gas Trimers 33

2.5.1 Results of calculations on Ar_2Ne and Ne_2Ar 38

3 Investigating the Eckart Condition 42

3.1 Rotational Constants 42

3.2 Separation of Rotation and Vibrational Motion 44

3.3 Investigation of Eckart condition 47

3.4 Results and Conclusions 51

3.4.1 Ar_3 . . . 53
3.4.2 AB_2 rare gas trimers . . . 55

4 The Ar_nN_2 system 67
4.1 Studying the Ar_nN_2 system . . . 67
4.2 Discussion and Results for the Ar_nN_2 System . . . 70
4.2.1 Potentials . . . 71
4.2.2 Ar_2N_2 . . . 74
4.2.3 Ar_3N_2 . . . 75
4.2.4 Ar_4N_2 . . . 75
4.2.5 Ar_5N_2 . . . 76
4.2.6 Ar_6N_2 . . . 79
4.2.7 Ar_7N_2 . . . 82
4.2.8 Ar_8N_2 . . . 84
4.2.9 Ar_9N_2 . . . 88
4.2.10 $Ar_{10}N_2$ . . . 92
4.2.11 $Ar_{11}N_2$ . . . 95
4.2.12 $Ar_{12}N_2$ . . . 99
4.2.13 Ar_nN_2 where $n > 12$ . . . 105
4.3 Conclusions . . . 107
4.3.1 $Ar_{2-6}N_2$ . . . 108
4.3.2 $Ar_{7-12}N_2$ . . . 109

5 The Ne_nN_2 system 113
5.1 Ne_nN_2 . . . 113
5.2 Results of Simulated Annealing for Ne_nN_2 . . . 115
5.2.1 Ne_1N_2 and Ne_2N_2 . . . 115
5.2.2 Ne_3N_2 . . . 115
5.2.3 Ne_4N_2 . . . 116
5.2.4 Ar_5N_2 . . . 118
5.2.5 Ar_6N_2 . . . 120

5.2.6 Ne_7N_2 . . . 122
5.2.7 Ne_8N_2 . . . 125
5.2.8 Ne_9N_2 . . . 128
5.2.9 $Ne_{10}N_2$ . . . 131
5.2.10 $Ne_{11}N_2$ . . . 133
5.2.11 $Ne_{12}N_2$ . . . 137
5.2.12 Ne_nN_2 where $n > 12$ . . . 141
5.3 Conclusions . . . 148

6 Three-Body Effects in Rare Gas-Molecule Cluster 151
6.1 Three-Body Effects . . . 151
6.2 Results . . . 159
6.2.1 Ar_nN_2 . . . 159
6.2.2 Ne_nN_2 . . . 161
6.3 Random Move Minimisation(RMM) . . . 163
6.3.1 Energy-Limited RMM Search . . . 167
6.4 Results obtained from RMM for Ar_nN_2 . . . 168
6.5 Results Obtained from RMM for Ne_nN_2 . . . 173
6.6 Conclusions . . . 179
6.7 appendix . . . 180
6.7.1 Argon Three-Body Triad Code . . . 180
6.7.2 main program . . . 180
6.7.3 cheq subroutine . . . 181

7 Conclusions and Future Directions 182

A Conferences, Courses and Seminars Attended 195

Chapter 1

Introduction

1.1 The Study of Intermolecular Forces

The main focus of this thesis is the determination of various properties of rare gas clusters. There has been a range of rare gas clusters studied, with from three to over fifty atoms in the cluster. In my studies I have investigated two main types of cluster. The first type are rare gas trimers, such as Ar_3 or Ar_2Ne. The second type are rare gas-molecule clusters, such as Ar_nN_2 or Ar_nHF. The way in which these two types of cluster were investigated is very different, and therefore I shall introduce them separately. Both rare gas trimers and rare gas-molecule clusters offer excellent prototype systems. This makes insight into these systems all the more valuable.

Both types of system are of interest because they allow the investigation of intermolecular forces. There are many compelling reasons for studying intermolecular forces, as they are of major importance for many processes in chemistry, physics and biology [1]. Intermolecular forces are responsible for the stability of DNA and RNA. A knowledge and understanding of intermolecular forces is also needed for the study of the thermodynamic properties of gases and liquids, and their kinetic properties (e.g. diffusion) [2, 3, 4, 5, 6, 7, 8].

They also play an important role in clustering and solvation processes. Intermolecular forces also play a large part in determining crystal structures (e.g.

equilibrium geometry). One of the results of a better understanding of intermolecular force is the production of "point and click" type modelling packages to aid researchers; this type of package is especially useful for the study of biologically important reactions.

1.2 Rare Gas Trimers

Rare gas trimers exhibit wide-amplitude bending and stretching motion, and they are also the smallest and simplest systems capable of molecular rearrangements. They are easily formed in molecular beam experiments, and high resolution spectra of them can be obtained [9, 10, 11, 12]. This allows detailed information about both two-body and three-body forces to be obtained [13]. They are therefore good trial systems on which to test our understanding of intermolecular forces. In general for rare gas trimers the pattern of vibrational energy levels is of most interest [14, 15, 16, 17, 18, 19], although other properties such as rotational constants can also be calculated [20]. Calculations are commonly performed for systems in which the total angular momentum is zero. This is not to say the rotational-vibrational (ro-vibrational) energy levels are not of interest, but that they are very expensive to calculate. The expense of such ro-vibrational calculations has meant that relatively few have been performed [21, 22, 23].

There are several methods for calculating the vibrational energy levels of rare gas trimers. The first and oldest uses normal co-ordinates, and relies on the existence of a well-defined equilibrium structure about which the molecule undergoes small vibrational motions [24, 25, 26, 27]. This is not a very realistic model for floppy molecules and the method does not work well for excited states of rare gas trimers. An alternative method of calculation involves treating the system as if it were an atom-diatom system [28, 29, 30, 31]. Again this formalism is not physically very realistic as rare gas trimers execute large amplitude motions. Another method, and the one that we use here, is based on the solution of coupled differential equations [32, 14, 15]. In this method all but one of the co-ordinates

is covered with a basis set expansion, and the remaining co-ordinate (usually a distance) is propagated along. This method can be applied to rare gas trimer using a number of different co-ordinate systems. This leads to a set of coupled differential equations that have to be solved. The set of coupled equations can be solved by several methods [32, 33, 34, 35, 36, 37]. The scattering formalism when used within a hyperspherical co-ordinate system [38, 39, 40] works very well, and can accurately predict the spectroscopic properties of the system [14, 15]. The main problem with this method is that it is very expensive as it requires the evaluation of a very large number of matrix elements, which are themselves very expensive. This means that it is very difficult to calculate ro-vibrational energy levels for rare gas trimers.

There is however a way around this problem. It involved the use of an alternative method of solving the Schrödinger equation. The method known as the descrete variable representation (DVR) [41, 42, 43, 44], replaces the basis functions for each co-ordinate with a set of grid points in each co-ordinate, at which the matrix elements of the Hamiltonian are evaluated. This representation has the advantage that the potential energy matrix is diagonal while the kinetic energy matrix in non-diagonal. This is very useful because the potential energy matrix elements are far more expensive to evaluate, as they are normally numerical in nature, than the often analytic kinetic energy matrix elements. The DVR approach has the added advantage that it also reduces the size of the matrices that have to be held in the computer's memory. This has allowed calculations on larger quantum system with up six degrees of freedom [45, 46], as well as ro-vibrational calculations for rare gas trimers [47].

1.3 Other Types of Rare Gas Cluster

Besides the two types of cluster that I have already mentioned there are several other types that have been studied. The first and simplest are pure rare gas clusters [48, 49, 50]. These can be made from a single rare gas species or from

a mixture of rare gas species. They are excellent microcluster systems, and have been widely investigated [1].

Another type of cluster that has not been mentioned so far is clusters made up of two or more molecules. Most of the work so far has involved clusters made from one molecular species, such as $(HF)_2$ [46, 52, 53, 54, 55, 56] and $(HCl)_2$ [56, 57, 58]. There has also been some work on larger $(HF)_n$ and $(HCl)_n$ clusters [59, 60, 61, 62, 63]. In addition to the hydrogen halide systems many other systems have been investigated. The most important systems are probably water clusters [56, 64, 65, 66, 67, 45, 68, 69, 70] and aqueous species such as $C_6H_6 - (H_2O)_n$ [70, 71, 72, 73, 74, 75, 76, 77, 78]. An excellent review covering most types of cluster was published recently by Bačić and Miller [70].

All the clusters so far discussed are neutral, and are held together by van der Waals forces. There are however many studies both experimental and theoretical in the charged species [79, 80, 81]. There are charged analogues of all the rare gas cluster types so far mentioned.

1.4 Rare Gas-Molecule Clusters

Rare gas-molecule clusters are of interest because they allow the study of clustering and solvation process [82, 83, 84, 85, 86, 87, 88, 89, 59] that would be difficult in more every-day solvent-solute system. This is of obvious importance to many physical and chemical processes.

All that has just been said about the experimental usefulness of rare gas trimers is also true for rare gas-molecule clusters. The only complication is that for clusters containing more than three or four rare gas atoms interpreting the spectra becomes very difficult [90, 91, 92, 93, 94]. However for small clusters spectroscopy can be used to determine the structures [92, 93, 94, 90, 91, 95, 96, 97, 98, 99]. Rare gas-molecule clusters are some of the simplest prototype systems that have realistic features in their intermolecular interaction. The solvent-solvent

[1] see references in [51]

and solvent-solute interactions are sufficiently varied to allow many parallels to more every-day chemical systems to be drawn.

1.5 Work in This Thesis

In chapter 2 we discuss our calculations of vibrational energy levels for rare gas trimers. These calculations were performed by a modified version of the BOUND code [100]. In this chapter we study two main types of rare gas trimer. The first type (A_3) has 3 identical rare gas atoms, while the second type (A_2B) is made from a mixture of rare gas atoms.

In chapter 3 we investigate the Eckart conditions [24]. In particular we study how the Eckart conditions embed a rotating axis into a system of three particles executing wide amplitude motions.

In chapters 4, 5 and 6 we will discuss our work on rare gas-molecule clusters. Chapters 4 and 5 contain work on the Ar_nN_2 and Ne_nN_2, while chapter 6 contains work on the effects of three-body forces on these two systems.

All structural data for this project can be obtained by anonymous ftp from krypton.dur.ac.uk.

It is important that we have a clear understanding of what we are going to do, and what information we can obtain. We will construct a potential energy surface that is a function of the co-ordinated of the atoms in a rare gas-molecule cluster. We will then use simulated annealing to search the potential energy surface. We want to find the global minimum and the other low-lying minima. We will then use a gradient technique to refine the local minima found in the simulated annealing search.

It is important to note that we do not calculate the total energy of the system. What we calculate is the potential energy at each configuration. In the following discussion the term energy will refer to the potential energy of the system.

We are interested in the lowest energy structures for each Ar_nN_2 system. The structures that we find represent the likely configurations that might be observed

in a molecular beam cluster experiment. The experimental set up for producing the rare gas molecule clusters is quite simple [95]. A mixture of the two species in a gaseous state is expanded into a chamber at low pressure. After the two gases have been co-expanded into the low-pressure chamber the clusters formed in the expansion chambers may be studied with the usual spectroscopic techniques.

One of the main reasons for studying rare gas-molecule clusters is that they provide excellent prototype systems on which to test our understanding of the role played by intermolecular interactions in solvation structures. It is important to state precisely what we mean by a solvation structure. If a substance is dissolved in a solvent each molecule of the solute is surrounded by a large number of solvent molecules. In trying to understand the physical factors that determine solvation structures, we concentrate on one of the solute molecules. In the present work, we try to find the lowest energy structures formed by the solvent$_n$-solute system. If we find a structure in which the solvent completely encases the solute molecule, with no room for any additional solvent molecules in contact with the solute, and this structure is the lowest energy configuration, then we have probably found the solvation structure for the system that would exist in a bulk sample.

The systems that we will study are rare gas-N_2 clusters. These are obviously far simpler than most solvent-solute systems of real chemical interest. Nevertheless studying a number of different prototype systems [101, 95, 91] we will be able to build up a deeper understanding of the effects on solvation of the potential energy surface topology, and the interplay between solvent-solvent and solvent-solute interactions.

It is however possible to calculate the infrared red shift of a cluster, which is an experimentally measurable quantity [102, 103]. The red shift is the change in the frequency of a particular transition between the 'bare' molecule and the molecule when it is part of a cluster. In general terms the frequency is shifted to the red because the molecular interactions with the rest of the cluster reduces the force constant for the molecular vibration. As the number of rare gas atoms in a cluster increases the magnitude of the red shift generally increases, though not

in a uniform manner. Because the red shift depends sensitively on the interaction between the cage and the molecule, it is a sensitive probe of the structure of a system.

Experimentally it is difficult to size-select each solvent$_n$-solute system of interest. For instance the experimental results on Ar_nHF [90] only go up to $n = 4$. There can also be a number of different species formed (i.e. structures) in the experiment, which makes it more difficult to distinguish one possible structure from another. Therefore the observed red shift may have a value between the predicted values for two structures. This can however still be useful as it may provide an estimate of the relative populations of the different cluster species. It is also often possible to measure a bulk red shift for a system, where the molecule is completely solvated. The red shift therefore gives detailed information on the structures formed by each rare gas-molecule system in the experiment. This means that in theory an experiment could test the predictions made by a study of the potential energy surface. If a global minimum can be found in which the solvent forms a complete cage around the molecule, the structure could be used to compare the calculated red shift against the experimental bulk red shift.

The problem with the above discussion is that it requires the potential energy function of the rare gas-molecule interaction to have a vibrational dependence built into it. This would allow the structures for the two potential energy surfaces to be found. The two potential energy surfaces would represent the cluster structures when the N_2 is in its v and v' vibrational states. If we were to calculate the total energy, rather than the potential energy, the difference between global minimum on the two surfaces would give a transition frequency, for which we could calculate the red shift. If there was an experimentally determined proportionality constant for the red shift, such as Nesbitt measured for the Ar_nCO_2 system, then it would be possible to use the red shift constant to estimate the red shift for each of the structures we find. Without the vibrational dependence though we cannot calculate the red shift, and we must wait for the development of more potential energy surface with vibrational dependence.

1.6 Minimisation Techniques

Finding the minimum value of a function is a long standing problem in both mathematics and the physical sciences. As the number of variables in the function increases, it becomes increasingly hard to find the global minimum. This problem has historically been solved by numerical searches [104, 48, 105, 106, 107]. The question then becomes how to be confident that the global mimimum has been found.

For a fairly simple function, one can imagine searching over a grid covering all the dimensions. This grid would obviously be of a finite size in each dimension. The finite range of the search is in general not a major problem, as the range in each dimension can be set to cover the active range. That is to say the range of each dimension in the search is large enough to cover all values of the variable which could contribute to a low value of the function. For example if you were looking for the minimum in the potential energy between two rare gas atoms, where the potential energy function depends only on the interparticle distance R, you would probably search from zero, or close to zero, to some large distance (perhaps 20 Å). There is no point in continuing to $R = \infty$ because the asymptotic limits of the function are known.

As the number of variables increases, it becomes increasingly difficult to continue with a grid strategy. This is due to increase in the size of the space that need to searched, and the commensurate number of grid points needed to cover that space. To illustrate this point consider that if we need q points in each dimension then as the number of atoms in a cluster (n) increases the number of grid point increases as q^{3n}. This would lead to a huge number of grid points being needed even for a fairly small rare gas-molecular cluster.

We need a more 'intelligent' way of searching the active space of the function [104]. The most obvious way of doing this is to use the properties of the function at a given point to determine the future direction in which to search. This is the principle behind gradient-based search techniques. In gradient-based techniques the search is started at a given point, and the direction of the first step in the

search is determined by the gradient at that point. When the search routine has completed the first step, the gradient of the function at the new position in parameter space is calculated. This information is then used to determine the direction of the next step in the search. This process is repeated until the change in the value of the function is smaller than a convergence parameter. Methods based on this principle have been very widely applied to many different problems. The way in which the gradient information is used is however very important. The simplest way of using the gradient information involves taking the path of steepest descent. This however is not the most efficient use of the gradient information. It has been found [104] that using the gradient information to generate a new search direction that is conjugate to the previous search direction is much more efficient.

The main disadvantage of gradient-based techniques is that they can be trapped in a minimum that is not the global minimum. This problem occurs commonly for clusters. If an atom interacting at its pair potential equilibrium distance with n neighbouring atoms in a cluster is then moved so it can interact with $n+1$ atoms at its equilibrium distance, clearly the second structure is lower in energy that the first. But because the atom in the first structure is in its optimal configuration in that particular volume of parameter space, whichever way the cluster is distorted to try and get to the second structure will initially lead to an increase in the energy. It will appear to the gradient minimisation technique that it has found the minimum value of the function, as all moves lead to an increase in the energy of the cluster.

As the number of atoms in the cluster increases the number of dimensions in the parameter space will also increase. This makes it more likely that a gradient-based technique will become trapped in a local minimum. One way around this problem is to start from many different points in parameter space. If the surface is not too complicated, then eventually the global minimum is located. If you are looking for the minimum energy of a cluster, you can use your intuition about what the low-energy structures will look like to help determine the starting positions used to search the surface. So for example we know that all the atoms

in a low-energy structure will interact with the other atoms in the system at approximately their equilibrium configuration, as defined by their pair potentials. It would therefore make no sense to start the search from a point in parameter space where two or more atoms are very close together. Equally the search should not be started from a point in parameter space where the atoms in the cluster are too widely separated. Otherwise the search will tend to find an $n-1$ or $n-2$ structure with the remaining atoms attaching to the side of the $n-1$ or $n-2$ structure, whereas the global minimum structure may be completely different. The problem with gradient methods is that, as the number of dimensions increases, the number of starting points needed to search the space increases. In addition the space becomes more complicated, and the likelihood of being trapped in a local minimum increases.

If we now turn our attention to the problem of rare gas-molecule clusters, the above discussion will become more physically obvious. Our function is the potential energy surface of a rare gas-molecule cluster, where argon or neon atoms cluster around an N_2 molecule. The potential energy surface is itself a summation over the pairwise interactions of the rare gas cluster, and the pairwise interactions of the rare gas atoms with the N_2. It is therefore a function of $3n-6$ parameters (the bond length of N_2 is fixed) , where n is the number of atoms in the cage. If we consider a simple system such as Ar_2N_2 then with our knowledge of the potential energy function of Ar-Ar, dependent only on R, and Ar-N_2, which has a 'T shaped' minimum, we can guess that the global minimum will have the two Ar atoms interacting in a 'T shaped' configuration with the N_2, and separated from each other by about their equilibrium distance. It is therefore easy to investigate this system using a gradient-based technique, by choosing several starting positions where the Ar atoms are around the middle of the N_2. Using similar logic you could investigate simple Ar_nN_2 systems where $n = 3$ to 5. Even for $n = 5$ however it would be difficult to know for certain that you have found the global minimum as the potential energy surface is a function of fourteen variables. The large number of variables means that it would be easy to miss a low energy minimum that is not

accessible from one of the starting position used in the search.

We are also interested in the first few minima above the global minimum. We are interested in these low-lying minima because they show the evolution of structures that for larger clusters may become the global minimum. They also help to illuminate the interplay of forces in the system, such as the balance between the rare gas-rare gas and rare gas-molecule interactions. Understanding such considerations become increasingly important in larger clusters if we are not to miss low energy structures. In addition the gap between the global minimum and the first few low-lying minima gives an indication of the likely population distributions between the structures that would be found in an experiment.

To be able to search the more complex and subtle potential energy surfaces of the larger clusters, we need to be able to escape local minima and continue the search. We need a search algorithm that is less 'greedy' in its attempt at reaching the global minimum. To achieve this we use a Simulated Annealing algorithm [104, 108, 109]. In a simulated annealing search, the search starts from some arbitrary point on the potential energy surface. From this point each of the variables is altered in turn by a small random amount. After each alteration of a variable the value of the function at the new point in parameter space is calculated. If the value of the function has decreased then the alteration is accepted, and the search moves to a new point in parameter space. This is similar to the gradient techniques in that it is assumed that any alteration that reduces the value of the function is a good step on the road to the global minimum. What saves simulated annealing from being so easily trapped in a local minimum is that, if a random alteration increases the value of the function, the alteration has a chance at been accepted. Simulated annealing achieves this by accepting a proportion of the alterations with a positive ΔE. The probability of an 'up hill move been accepted is thus given by

$$P[\Delta \mathrm{E}] = 1 - e^{\Delta \mathrm{E}}/kT, \tag{1.1}$$

where k is the Boltzmann constant.

In a simulated annealing run the temperature is started at a high level and

then is slowly reduced, after a given number of random alterations to the variables (known as steps). A typical simulated annealing run starts with a simulated temperature of several thousand Kelvins. The temperature is reduced during the run to tens of Kelvins. As can be seen from the equation above, the probability of a given ΔE being accepted depends on the temperature. At the beginning of a simulated annealing search when the temperature is high, the probability of a given positive ΔE being accepted is greater than when the temperature is lower. This allows the simulated annealing algorithm to escape from a local minimum, and efficiently search a greater volume of configuration space.

A simulated annealing search therefore has a greater chance of finding the global minimum than a gradient search. Although the result of a simulated annealing search is not completely independent of the starting position, it does have a greatly reduced dependence. The final temperature of a simulated annealing run is finite so the system is not precisely at the minimum. We therefore refine each structure that the simulated annealing run finds using a gradient-based technique. Using simulated annealing we can quite easily find the low-lying minima of the potential energy surface as well as the global minimum.

If a simulated annealing run is started twice from the same starting position, it is quite likely to give different results because of the random nature of the perturbations. This may seem to be a disadvantage to the technique but in reality is one of it's strengths: we actually run the program many times (usually 32 times) from the same starting position. In this way we can to cover the largest possible volume of the parameter space, for a given starting position, and therefore increase the likelihood of finding the global minimum and low-lying minima.

It can be seen that as the clusters become bigger the problem of finding minima become increasingly hard. The problems of finding the global minimum of a protein [110, 111] or a cluster [112] are 'hard' computer problems [113]. Thus we are limited in the size of system that we can study, but within this limitation we can learn a lot about these complex and fascinating systems.

1.6.1 Genetic Algorithms

Until very recently simulated annealing was the only way in which to search very complicated functions. However very recently there has emerged a new algorithm. Interestingly this new search algorithm, called a genetic algorithm [48, 114, 51, 115, 109], also takes its inspiration from nature, just as simulated annealing did. In a genetic algorithm the solution to the problem, i.e. the lowest few minima of a function, are bred by a pseudo-natural selection process. The algorithm works by starting with a set of parents, of fixed size m. These parents are bred together to produce a set of 'child' structures. At the end of each breeding cycle the m fittest structures are kept as the next generation of parents, where the fitness of a structure is measured by how low the energy is. This process is repeated until the set of parents has converged to a stable population. There are several different methods for breeding new solutions, and for picking the new set of parents for the next breeding cycle.

Although this method is new and has only been tested on a few problems, it has proved to be as effective at finding the global minimum of a complicated function as simulated annealing. Indeed in one study of pure rare gas clusters it found a new global minimum for one of the Ar_n systems which had not been found by any previous search method [114]. Not only are genetic algorithms at least as good as any other search technique for complicated surfaces, they are also significantly quicker that simulated annealing.

Chapter 2

The Bound States of Rare Gas Trimers

2.1 Coupled Channel Calculations

To calculate the properties of the van der Waals molecules it is necessary to solve the Schrödinger equation for the system,

$$H\Psi_n = E_n\Psi. \tag{2.1}$$

The hamiltonian H is of the form

$$H = \frac{\hbar^2}{2\mu}R^{-1}\frac{d^2}{dR^2}R + H_{\text{int}} + V(R,\vartheta) \tag{2.2}$$

where R is the separation of 2 particles, ϑ represents all other coordinates, and H_{int} is the Hamiltonian of the isolated particles and does not depend on R. To solve this equation and find its eigenvalues, I used a program called BOUND [100] which solves the problem using the log derivative propagator method of Johnson [116, 33, 32, 117]. This is best understood if the problem is considered in a more general way first. It is possible to find eigenvalues and eigenvectors by a matrix method, in which all degrees of freedom are handled by basis sets [118, 119, 41]; alternatively all the co-ordinate could be described on a grid [120]. The method that BOUND uses is in-between these two extremes and is called the coupled channel method. In this method [34, 35, 36, 37, 121] the R co-ordinate is handled by a grid, where the grid ranges from R_{min} to R_{max} with a grid spacing h, and all

other co-ordinates are handled by basis sets. This method has the advantage that it is not necessary to use a basis set for R, which generally show poor convergence. The wavefunction in the coupled channel case is

$$\Psi_n = R^{-1} \sum_j \phi_j(\vartheta)\psi_{jn}(R) \tag{2.3}$$

where the functions $\phi_j(\vartheta)$ form a complete orthonormal basis set for motion in the ϑ co-ordinates, and the factor R^{-1} simplifies the action of the radial kinetic energy operator. Substituting Ψ_n into the Schrödinger equation gives

$$\frac{d^2\psi_{in}}{dR^2} = \sum_j [W_{ij}(R) - E_n\delta_{ij}]\psi_{jn}(R), \tag{2.4}$$

where δ_{ij} is the Kronecker delta and E is the energy scaled by $2\mu/\hbar^2$ and

$$W_{ij}(R) = \frac{2\mu}{\hbar^2} \int \phi_i^*(\vartheta)[H_{int} + V(R,\vartheta)]\phi_j(\vartheta)d\vartheta. \tag{2.5}$$

Similar equations arise for each channel and the channels are coupled by the of diagonal terms, ie the $W_{ij}(R)$ with $i \neq j$. Equation 2.5 can be expressed in matrix form

$$\frac{d^2\Psi_n}{dR^2} = [W(R) - E_n I]\Psi_n \tag{2.6}$$

where $\Psi(R)$ is a column vector of order N with elements $\psi_{ij}(R)$, $W(R)$ is an $N \times N$ matrix with elements $W_{ij}(R)$ and I is an $N \times N$ unit matrix. Equations 2.6 can be solved by approximate techniques, in which off-diagonal terms are ignored or their effect is added by perturbation theory [122, 123, 124, 125, 126]. However BOUND does not do this, and finds exact solution within the errors of truncating the basis set. These types of calculations are called close coupled calculations.

To solve the Schrödinger equation we must solve the set of coupled differential equations. There are several methods for solving such problems, which have been reviewed by Hutson [32] and [34]. The method used by BOUND is that of the log derivative propagator. The log derivative [117, 32, 116] is defined as

$$Y(R) = \frac{d\ln\Psi}{dR} = \Psi'(R)[\Psi(R)^{-1}], \tag{2.7}$$

where ' $\prime$ ' denotes the derivative of the wavefunction. If E is an eigenvalue of the coupled equations there must exist a wavefunction

$$\psi(R_{\text{mid}}) = \psi^{+}(R_{\text{mid}}) = \psi^{-}(R_{\text{mid}}) \tag{2.8}$$

for which

$$\left[\psi^{+}\right]'(R_{\text{mid}}) = \left[\psi^{-}\right]'(R_{\text{mid}}), \tag{2.9}$$

where $+$ and $-$ refer to the direction of propagation. The point R_{mid} is a point on the grid in the classically allowed region (e.g. $W(R) < E$) where the two propagated wavefunctions meet. Two propagation directions are use because it is more stable to propagate on of the two classically forbidden regions, at small and large R where $W(R) > E$, than to propagate from R_{min} to R_{max} [32]. From equations 2.8 and 2.9 we can define

$$Y^{+}(R_{\text{mid}})\psi(R_{\text{mid}}) = Y^{-}(R_{\text{mid}})\psi(R_{\text{mid}}) \tag{2.10}$$

or equivantly

$$[Y^{+}(R_{\text{mid}}) - Y^{-}(R_{\text{mid}})]\Psi(R_{\text{mid}}) = 0. \tag{2.11}$$

A non trivial solution to 2.11 exists only if the determinant at R_{mid} is zero. Therefore it is sufficient to propagate the log derivative matrix and look for zeros as a function of energy [37], instead of having to propagate ψ and ψ'. A better algorithm, and the one used by the current version of BOUND, is to consider equation 2.11 as a eigenvalue equation where $\psi_{R_{\text{mid}}}$ is the eigenvector of the matching matrix $\mid Y^{+} - Y^{-} \mid$, with the eigenvalue zero. Thus BOUND simply find the smallest eigenvalue at each energy, and then use the secant method to converge upon an energy at which it is zero.

BOUND has a node count facility, to work out the quantum number of the vibrational wavefunction for each of the eigenstates it finds. This is a very useful feature when you are trying to find the groundstate. The node count is done by counting the number of poles in $\mid Y \mid$, which can be monitored by seeing how many times the Z matrix has negative eigenvalues, for a detailed discussion see [32], in the range R_{min} to R_{max}.

2.2 Hyperspherical Co-ordinates

In all my calculations a hyperspherical basis set [14] was used. The reason for using a hyperspherical basis is that although computationally expensive, they handle wide-amplitude motions more naturally than normal basis set expansion methods. This is because for wide amplitude motions the idea of motion about an equilibrium geometry in not valid. A hyperspherical co-ordinate system does not have this problem because it does not distinguishing between particles, they are just labelled by the indices i j k, as the particles have been mass normalised. This means that wide amplitude motions and even inversions of the molecular geometry can be easily handled.

In hyperspherical co-ordinate there are both, the internal and external co-ordinates. The internal co-ordinates consist of two angles θ and χ and a distance ρ called the hyperadius. They are derived from the Jacobi co-ordinates [14, 38, 39, 40, 127, 128, 129]

$$\begin{aligned} \vec{r}_i &= \vec{X}_k - \vec{X}_j \\ \vec{R}_i &= \vec{X}_i - \frac{M_j\vec{X}_j + M_k\vec{X}_k}{M_j + M_k}, \end{aligned} \tag{2.12}$$

where the jacobi co-ordinates $\vec{R}_i$ and $\vec{r}_i$ are as shown below in figure 2.1. The external co-ordinates are the usual Euler angles. A set of corresponding mass-scaled Jacobi co-ordinates is defined by

$$\vec{s}_i = \vec{r}_i/d_i \tag{2.13}$$

and

$$\vec{S}_i = d_i\vec{R}_i. \tag{2.14}$$

Where d_i^2 is the dimensionless scaling factor

$$d_i^2 = \frac{M_i(M_j + M_k)}{\mu(M_i + M_j + M_k)} \tag{2.15}$$

and μ is given by

$$\mu^2 = \frac{M_iM_jM_k}{M_i + M_j + M_k} \tag{2.16}$$

The interparticle distances are then given by

$$\begin{aligned}
\vec{X}_3 - \vec{X}_2 &= d_1 \vec{s}_1 \\
\vec{X}_1 - \vec{X}_3 &= \frac{1}{d_1}\left[\vec{S}_1 - \frac{M_2 d_1^2}{M_2 + M_3 \vec{s}_1}\right] \\
\vec{X}_1 - \vec{X}_2 &= \frac{1}{d_1}\left[\vec{S}_1 - \frac{M_3 d_1^2}{M_2 + M_3 \vec{s}_1}\right].
\end{aligned} \tag{2.17}$$

The Schrödinger equation for the system is then

$$\left(\frac{\hbar}{2\mu}[\nabla^2_{\vec{S}_i} + \nabla^2_{\vec{s}_i}] - V(\vec{S}_i, \vec{s}_i) - E\right)\psi(\vec{S}_i, \vec{s}_i) = 0 \tag{2.18}$$

where $\nabla^2_{\vec{S}_i} + \nabla^2_{\vec{s}_i}$ is the six dimensional Laplacian. The hyperspherical co-ordinates $\alpha, \beta, \gamma, \rho, \theta$ and χ, where α, β, γ are the Euler angles and ρ, θ, χ are the internal co-ordinates, are defined implicitly in terms of the mass scaled co-ordinates. The Cartesian components of $\vec{S}_i$ and $\vec{s}_i$ are

$$\begin{aligned}
S_{1x} &= \rho \cos\theta \sin\chi \\
S_{1y} &= \rho \sin\theta \cos\chi \\
s_{1x} &= \rho \cos\theta \cos\chi \\
s_{1y} &= -\rho \sin\theta \sin\chi
\end{aligned} \tag{2.19}$$

where the range of θ and χ is

$$\begin{aligned}
&0 \leq \theta \leq \pi/4 \\
&0 \leq \chi \leq 2\pi.
\end{aligned} \tag{2.20}$$

This gives

$$\rho^2 = [S_1]^2 + [s_1]^2. \tag{2.21}$$

Using equations 2.17 to 2.21 expressions for the interparticle distances in terms of the hyperspherical co-ordinates can be calculated; these are used in BOUND in the evaluation of the potential energy matrix elements.

$$| r_1 |^2 = \frac{\rho^2 d^2}{2}[1 + \cos 2\theta \cos 2\chi], \tag{2.22}$$

$$|r_2|^2 = \frac{\rho^2 d_1^2}{2}\left[\frac{1}{d_1^4} + \left(\frac{M_2}{M_2+M_3}\right)^2\right] \times [1+\cos 2\theta \cos 2(\chi+\delta_2)] \quad (2.23)$$

and

$$|r_3|^2 = \frac{\rho^2 d_1^2}{2}\left[\frac{1}{d_1^4} + \left(\frac{M_3}{M_2+M_3}\right)^2\right] \times [1+\cos 2\theta \cos 2(\chi-\delta_3)], \quad (2.24)$$

where

$$sin2\delta_i = \frac{2M_1}{d_i^2(M_2+M_3)}. \quad (2.25)$$

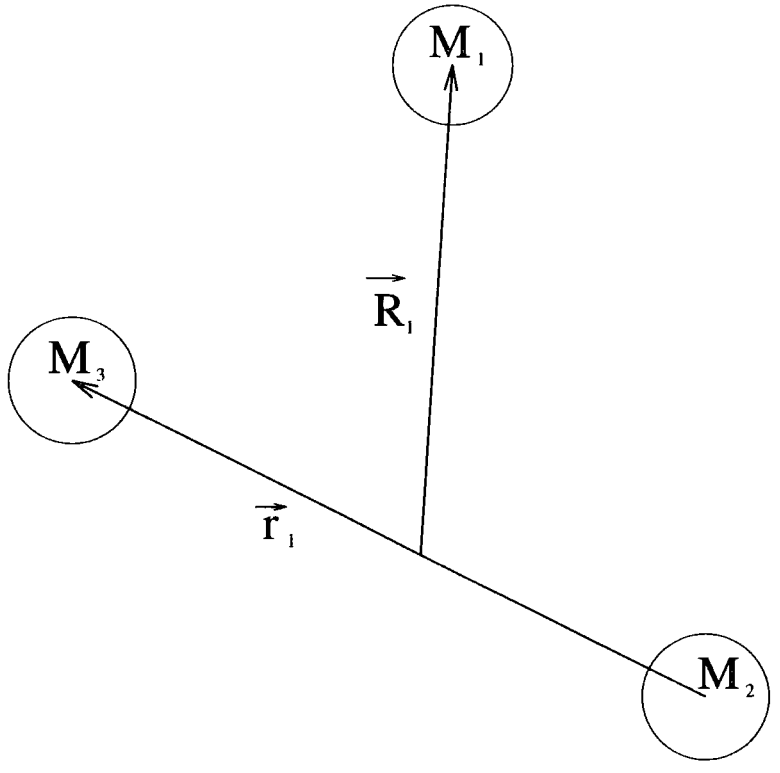

Figure 2.1: Rare gas trimer in Jacobi co-ordinates.

2.3 Calculations on A_3 case Rare Gas trimers

In the version of BOUND we are going to use to calculate vibrational energy levels of rare gas trimers hyperspherical harmonics are used to form a complete basis in θ and χ [14], and are given by

$$\begin{aligned} f^S_{\lambda,\nu}(\theta,\chi) &= (2-\delta_{\nu 0})^{1/2}\left(\frac{\lambda+2}{2\pi^3}\right)^{1/2} d^{\lambda/4}_{\nu/4,\nu/4}(4\theta) \\ &\times \begin{cases} \cos\nu\chi & for \quad S=0 \\ \sin\nu\chi & for \quad S=1 \end{cases} \end{aligned} \tag{2.26}$$

The quantum numbers λ and ν describe the grand angular momentum and its projection onto the molecule fixed z axis of a reduced rotation matrix $d^{\lambda/4}_{\nu/4,\nu/4}(4\theta)$ [130]. The coupled channel equations in hyperspherical harmonics are then solved by propagating the log derivative matrix. The number of open channels in a calculation, and therefore the level of convergence, is governed by λ. In the BOUND program the maximum value of is set by an input parameter $\lambda_{\max}$.

The vibrational energy levels for several rare gas trimers have been calculated by Ernesti and Hutson (EH) [131] using a hybrid basis set method in Jacobi coordinates, and diagonalising the subsequent matrix. His method is believed not to treat the wide-amplitude motions as well as the hyperspherical based code of BOUND. Hutson and Jain [14] and Cooper et al. [15] have calculated equivalent energy levels for Ar_3 system but using a different potential than EH, which makes a comparison of the two sets of results difficult. The Ar-Ar potential [132] 2.27 used both here and by EH is of the form

$$V(r) = \varepsilon V^*(R) \tag{2.27}$$

where

$$V^* = V_{\rm SCF} + V_{\rm Cor}, \tag{2.28}$$

and

$$\begin{aligned} V_{\rm SCF} &= A\exp(-\alpha^* R + \beta R^2) \\ V_{\rm Cor} &= -\left[\sum_{j=0}^{4} C_{2j+6} R^{-(2j+6)} g_n(\rho R)\right] F(\rho R). \end{aligned} \tag{2.29}$$

The expressions for $F(R)$ and $g_n(R)$ are

$$F(R) = 1 - R^{1.68} \exp -(0.78R) \tag{2.30}$$

and

$$g_n(R) = [1 - \exp(-2.1R/n - 0.109R^2/n^{1/2}]^n. \tag{2.31}$$

In the case of a fairly rigid molecule such as Ar_3 our results are in quite close agreement with those of EH (compare tables 2.1[1] and 2.2).

energy level	A state/cm^{-1}	E state/cm^{-1}
1	−254.891	−232.373
2	−224.290	−211.826
3	−211.950	−205.036
4	−198.242	−195.389
5	−185.992	−184.268

Table 2.1: Results for Ar_3 in hyperspherical basis set

The next system that we studied was the neon trimer, which was also studied by Ernesti. By the standards of rare gas molecules Ar_3 is a quite rigidly bound system. The Ne_3 system on the other hand is very floppy. This should make an interesting test of how well the method used by EH copes with very wide amplitude motion. The Ne-Ne potential used both here and by EH is the HFD-B potential by Aziz [133], and is of the form

$$V(r) = \varepsilon V^*(x). \tag{2.32}$$

Where x is the interparticle distance divided by the equilibrium distance. The expression for V^* is

$$\begin{aligned} V^*(x) &= A^* \exp(-\alpha^* x + \beta^* x^2) \\ &- F(x) \sum_{j=0}^{2} \frac{C_{2j+6}}{x^{2j+6}}, \end{aligned} \tag{2.33}$$

[1]With the following input parameters $R_{\text{min}} = 4.0$ Å, $R_{\text{mid}} = 5.0$Å, $R_{\text{max}} = 6.5$Å, $h = 0.05$Å, reduced mass = 23.0722926345, Jmax = 84

Energy Level	Energy/cm^{-1}
1	−254.893
2	−232.366
3	−224.280
4	−211.900
5	−211.741
6	−204.957
7	−197.787
8	−194.536
9	−192.934
10	−186.917

Table 2.2: EH results for Ar_3

and where the value of the function $F(x)$ is defined as

$$F(x) = \begin{cases} \exp\left[-(\frac{D}{x} - 1)^2\right] & \text{for } x < D \\ 1 & \text{for } x \geq D \end{cases}$$

In the case of Ne_3 system we did not obtain as good an agreement with EH for the ground state as for Ar_3, and we did not agree at all about the excited state energy levels. The BOUND code predicts much deeper excited states, showing that it does indeed handle floppy molecules wide-amplitude motions better that normal basis set method (see tables 2.4[2] which shows our results for Ne_3 and 2.5 which shows EH's results for Ne_3).

Table 2.3[3] shows the convergence for the Ne_3 system. It is interesting to note that the Ne_3 system converges more quickly than the Ar_3 system [15]. This is exactly the opposite behaviour to that of the basis set method of Ernesti, which

[2]With the following input parameters $R_{\text{min}} = 3.0$Å, $R_{\text{mid}} = 6.0$Å, $R_{\text{max}} = 10.0$Å, $h = 0.035$Å, reduced mass = 11.54263773, Jmax = 66

[3]With the following input parameters $R_{\text{min}} = 3.0$Å, $R_{\text{mid}} = 6.0$Å, $R_{\text{max}} = 10.0$Å, $h = 0.035$Å, reduced mass = 11.65035108

requires many more basis functions to calculate the energy levels of Ne_3 that those of AR_3. Even with many more basis functions, however, the excited states as calculated by EH are not very accurate. The reason for the poor performance of the basis set method can be understood if we consider how many states are near to the energy require to flip from a triangular geometry through a linear geometry to the mirror image of the starting triangle. The barrier for this motion is approximately the pair potential well depth, which for the neon trimer is about 29 cm^{-1}. Even some of the low-lying states in table 2.4 have enough energy to flip. More importantly there are eight states within 10 cm^{-1} of being able to flip. With such wide amplitude motions the basis set method can not cover the full space of the problem. This means that even with a 'complete' basis we could not cover the full range of motion of the problem. In hyperspherical co-ordinates, however, this is not the case. Wide amplitude motions, and even inversions of a structure, are 'naturally' treated. The difference in the values of the energy levels for the convergence and energy level tables is due to the fact that the two calculations use different values for the mass of Neon. This will not effect the convergence properties of the system. It will only effect the magnitude of the energy levels.

λ_{max}	E_1/cm^{-1}	E_2/cm^{-1}	E_3/cm^{-1}	E_4/cm^{-1}	E_5/cm^{-1}
32	−51.276	−35.685	−31.752	−29.020	−26.060
40	−51.482	−36.292	−33.427	−30.870	−27.413
48	−51.503	−36.413	−34.076	−31.539	−27.948
56	−51.505	−36.433	−34.188	−31.611	−28.023
66	−51.505	−36.437	−34.220	−31.633	−28.041
72	−51.505	−36.437	−34.222	−31.634	−28.042

Table 2.3: Convergence for Ne_3 in hyperspherical basis with a reduced mass of 11.650 amu

energy level	A states/cm^{-1}	E states/cm^{-1}
1	−51.360	−38.604
2	−36.300	−34.516
3	−34.101	−32.275
4	−31.480	−28.464
5	−27.857	−24.367
6	−23.888	−23.253
7	−22.318	−22.227
8	−21.752	−20.090

Table 2.4: Results for Ne_3 in hyperspherical basis set

Energy Level	Energy/cm^{-1}
1	−51.354
2	−38.484
3	−35.589
4	−31.589
5	−27.881
6	−24.761
7	−23.755
8	−21.934
9	−18.582
10	−17.568

Table 2.5: EH results for Ne_3

2.4 Calculations on the He_3 trimer

The work on He_3 was started off by a comparison of the results for Ne_3, where the hyperspherical BOUND code had been shown to be much better at handling floppy molecules than a basis set method in Jacobi co-ordinates. He_3 is the most

weakly bound rare gas trimer, and there has been much debate as to whether or not the helium dimer exists [134, 135, 136]. The problem for experimentalists trying to find evidence of the dimer in a molecular beam experiment, is that the usual means of detecting clusters is by mass spectrometry. The He_2 and He_3 bound states are very weakly bound. He_2 for example has a calculated binding energy of 1×10^{-3} K on a recent potential energy curve. There was therefore some discussion about whether the He_2^+ signal detected experimentally was formed from ionising the helium dimer, or by some other path. The creation of ions in the mass spectrometer leads to several alternative pathways such as creation of He_2^+ via collisions of He_n^+ with neutral atoms to form He_2^+. An alternative path could be the ionisation of a helium trimer, which then disintegrates into He_2^+ and He. These different possibilities make assignment of the spectra difficult and open to differing interpretation.

Although there has been much work on He_2, both in determining pair potentials [137, 138, 139, 140, 141] and in experimental investigation of the He_2 bound state [139, 142, 143]. There has however been little interest over the last ten years in calculation of the bound states of He_3 [144, 145, 146], as a result the vibrational energy levels of the helium timer have not been calculated with modern pair potentials. As our method of calculation suits very floppy molecules we decided to investigate the bound states of the helium trimer using modern pair potential. We wanted to know how accurate the previous calculations were, as an increase in the strength of the bound states of helium might be pertinent to the discussion of pathways to He_2^+ in mass spectrometry experiments [134, 135, 136]. The previous calculations of the bound states of He_3 used different methodologies to BOUND. As well as the mass spectrometry evidence, which was disputed due to the weakness of the helium interaction, a novel diffraction technique was used to prove the existence of the helium dimer [147, 148]. In our calculations we used the best He-He pair potential available [137], which is a modified HFD-B potential of the form

$$V(r) = \epsilon[V_a^\star(x) + V_b^\star(x)], \tag{2.34}$$

where $V_a^*(X)$ is an add-on-part of the potential, for a small region about the equilibrium distance, and $V_b^*(X)$ is the standard HFD-B potential.

$$V_a^\star(x) = \begin{cases} A_a\{\sin[B(x-x_1)-\pi/2]+1\} & x_1 \le x \le x_2 \\ 0 & x < x_1 \ \ or \ \ x > x_2. \end{cases} \tag{2.35}$$

Where $x = r/r_m$, $B = 2\pi/(x_2 - x_1)$, and x_1 , x_2 and A_a are adjustable parameters. The second part of the potential $V(r)$ is a HFD-B type potential of the form

$$\begin{aligned} V_b^\star &= A^\star \exp(-\alpha^\star x + \beta^\star x) - F_6 C_6/x^6 \\ &- F_8 C_8/x^8 - F_{10} C_{10}/x^{10} - F_{12} C_{12}/x^{12}, \end{aligned} \tag{2.36}$$

where

$$F_n(x) = \begin{cases} \exp\left[-\left(\frac{D_n}{x}-1\right)^2\right] & x \le 1 \\ 1 & x > 1 \end{cases} \tag{2.37}$$

With the helium trimer being so floppy the propagation range had to be very large ($R_{\max} = 75$Å) compared to other rare gas trimers. The result of our calculations was that a bound state with an energy of -0.12 K was found, see table 2.6[4] below, this result was in close agreement with the most recent calculation of Cornelius and Glöckle [144]. Their value for the ground state was -0.11 K, where the small difference in the ground state energy was due to their use of an older version of the HFD-B type He-He pair potential [138]. When we re-calculated the bound states of the system using the older helium pair potential, as used in the most recent previous calculation [144], I got the same answer for the energy of the ground state as previously published.

2.4.1 Efimov States

The main difference between our results and those previously published was that the previous studies [144, 145, 146] of the helium trimer found two Efimov states [149], and we did not find any Efimov states. Efimov states are formed by

[4]With the following input parameters $R_{\min} = 1.0$ Å, $R_{\mathrm{mid}} = 20.0$ Å $R_{\max} = 75.0$ Å $h = 0.75$ Å reduced mass = 2.3109 amu, N° quadrature points = 128

λ_{max}	Energy/cm^{-1}	Energy/K
66	−0.07977	−0.11478
72	−0.08211	−0.11814
84	−0.08486	−0.12210
90	−0.08567	−0.12327
96	−0.08627	−0.12413

Table 2.6: Convergence for He_3 in hyperspherical basis set

three-body systems, interacting with a pairwise potential, and lie very close to the dissociation limit. They show a very sensitive dependence on the pair potential. If the pair potential well depth is increased or if the equilibrium distance is increased, then the Efimov states will disappear.

An Efimov state can be thought of via the following discussion. If two particles are brought together slowly they can be strongly correlated at their scattering length (a), which is a constant that controls the scattering cross section [150], which can be much larger than the range of interaction between the two particles (r_0) [151]. If a third atom is now added. It can feel the presence of the two particles when it gets within a of either of them, and can become highly correlated. This interplay of the three particles results in an effective three-body interaction, which is very long range in nature [5].

We were unsure why we did not find any Efimov states, as we would expect to find all bound states that exist with the BOUND code. I therefore tried increasing the propagation range, as it was possible that R was not large enough to cover the excited states. I increased R up to 200 Å and found no bound states, and for R_{max} greater than 200 Å the propagation of solutions became unstable and failed to converge on any state, including the ground state. It was therefore decided to just do a node count, as this would pick up any excited states and it is much quicker that trying to find eigenvalues especially with large propagation ranges. This did

[5] see [152]

not work out as expected, because the result of a node count at different values of R_{max} was always different. The reason for this is that the BOUND program is only variational as long as there are enough points used in the Guassian quadrature to evaluate the matrix in equation 2.6, and with the very long propagation ranges needed for the Efimov states this is not true. This result cast doubt on our work on the Helium trimer, even though we were in such good agreement with previous work. There was a question to whether enough quadrature points had been used in calculations on the ground state. The solution of this problem was to alter the BOUND program, to allow the number of quadrature points used in the calculation to be varied. I therefore ran a series of calculations with differing numbers of quadrature points, the results of which are shown below in table 2.7[6]. When

Number of quadrature points	Energy/10^{-1}cm^{-1}
48	−0.797145571
66	−0.797777973
128	−0.797684658
256	−0.797674017
300	−0.797673474
356	−0.797673105
400	−0.797672942

Table 2.7: convergence of He_3 in hyperspherical basis set

BOUND had been altered it was found that with 256 Guassian quadrature points that only one node was found. With the increased number of quadrature point I was able to check of the number of nodes up to an R_{max} of 1000Å. Even with this enormous propagation range we only found one node. A rough calculation based on equation 2.38 shows that there should be an Efimov state when a is

[6]The input parameters were R_{min} = 1.0 Å, R_{mid} = 20.0 Å, Rax = 75.0 Å, h = 0.75 Å, reduced mass = 2.3109 amu, Jmax = 66

approximately twenty times r_0. It is therefore necessary to search out to at least this range, if we are to find an Efimov state. For Helium this condition on the propagation range would mean searching out to roughly 140Å. We have clearly exceeded this requirement for the discovery of an Efimov state.

Further evidence that the results obtained from the BOUND code are correct, and that there are indeed no Efimov state in the helium trimer, was given in a paper published after our work was completed, by Aziz et al. [139]. In his paper Aziz took a large selection of helium dimer potentials from the literature, and calculated the dimer binding energy, the effective range (r_0) and the scattering length (a), for each of the potentials. With the calculated scattering lengths and effective ranges Aziz was able to calculate N_E, which is the estimated number of Efimov states that each potential can support. The formula for the number of Efimov states that each potential can support is

$$N_E = \frac{1}{\pi} \ln \left| \frac{a}{r_0} \right|, \tag{2.38}$$

and comes from the original Efimov paper [149]. For an Efimov state to exist the value of N_E has to be greater than one. Aziz shows that for all recent realistic potentials the value of N_E is less than one. This is strong evidence that the helium trimer does not have an Efimov state; and that the BOUND calculations are correct in not finding any Efimov states.

An interesting point to note is though is that two of the papers which found Efimov states [144, 145] used an earlier Aziz HFD type potential [138]. This is strange because according to the Aziz calculations of the value of N_E an Efimov state should not be found. Given the accuracy of BOUND and the work by Aziz and the age of the two calculations it is tempting to conclude that both calculations have found a state that does not exist. This could be due to an approximation in the calculations or some other factor. We cannot be that categorical in our conclusions. All that it is possible to say is that the BOUND code was pushed as hard as possible with present computational capabilities and found no evidence of an Efimov state, and that this conclusion is supported by the new work of Aziz.

The oldest of the papers [146] which claimed to find an Efimov state uses

three different potentials, all of which give a N_E value greater than one. The potentials however are quite old and do not reproduce all the experimental data; and are by the standards of modern day helium dimer potentials consider to be poor representations of the helium-helium interactions.

A final piece of evidence that BOUND has found all the bound states of the helium trimer is found in a consideration of exactly what an Efimov state is. We can define a modified pair potential $gV(r)$, where at the value $g = g_0$ the two particle just form a bound state. As g is varied, Efimov [149] showed that if g was slightly less than g_0 there would emerge a series of bound states of the system. The number of bound states of the system tends towards infinity in the limit of $g \rightarrow g_0$. As the value of g continues to increase past g_0, levels leave into the continuum one after another. The result can be restated as follows [152]. If there is a two-body system that is just unbound, then the three-body system can have many Efimov states. In the case of the helium dimer however, for all modern potentials, the system has one bound state.

2.5 Calculations on AB_2 Case Rare Gas Trimers

All the rare gas trimers so far have been of the same A_3 type. It is also possible to form mixed trimers, denoted AB_2, such as Ar_2Ne or Ne_2Ar. Some work had already been done on these systems by EH [131] using a more conventional basis set method (see tables 2.11 and 2.9). Some AB_2 systems have also been observed experimentally by microwave spectroscopy [11]. The BOUND code could not initially do hyperspherical calculations on this type of rare gas system. We therefore had to alter it to allow calculations of AB_2 rare gas clusters. We were then able to compare the results of EH with those of BOUND.

The equations given above to calculate the interparticle distances, which are then used to calculate the potential energy, are only valid for the A_3 case rare gas trimers. To evaluate the potential energy matrix of equation 2.6 for the AB_2 case, we required modified equations for the interparticle distances, in terms of the

hyperspherical co-ordinates.

From the equations 2.17 we know that

$$\vec{X}_3 - \vec{X}_2 = d_1\vec{s}_1. \tag{2.39}$$

We therefore have only to evaluate $\vec{s}_1$ to obtain the expression we want. The value of $\vec{s}_1$ is

$$\vec{s}_1 = \sqrt{\vec{s}_{1x}^2 + \vec{s}_{1y}^2}, \tag{2.40}$$

which becomes

$$\vec{s}_1 = \rho(\cos^2\theta\cos^2\chi + \sin^2\theta\sin^2\chi)^{\frac{1}{2}} \tag{2.41}$$

when the relevant expressions from equations 2.19 are substituted in. This expression can be rearranged to give the following expression

$$\vec{s}_1 = \frac{\rho}{\sqrt{2}}[1 + \cos 2\theta\cos 2\chi)]^{\frac{1}{2}}. \tag{2.42}$$

Thus the final expression for $\mid r_1 \mid^2$ is

$$\mid r_1 \mid^2 = \frac{\rho^2 d^2}{2}[1 + \cos 2\theta\cos 2\chi]. \tag{2.43}$$

From the equations 2.17 we know that

$$\vec{X}_1 - \vec{X}_3 = \frac{1}{d_1}\left[\vec{S}_1 - \frac{M_2 d_1^2}{M_2 + m_3}\vec{S}_1\right], \tag{2.44}$$

where the definition

$$A_2 = \frac{M_2}{M_2 + M_3} \tag{2.45}$$

will be used henceforth. The expression for $\vec{S}_1$ is

$$\vec{S}_1 = \sqrt{\vec{S}_{1x}^2 + \vec{S}_{1y}^2}. \tag{2.46}$$

This leads to

$$\vec{S}_1 = \rho(\cos^2\theta\sin^2\chi + \sin^2\theta\cos^2\chi)^{\frac{1}{2}}, \tag{2.47}$$

which may be rearranged to give

$$\vec{S}_1 = \frac{\rho}{\sqrt{2}}[1 - \cos 2\theta \cos 2\chi)]^{\frac{1}{2}}. \tag{2.48}$$

Combining the expressions for $\vec{s}_1$ and $\vec{S}_1$ gives,

$$\begin{aligned}\vec{S} \cdot \vec{s} = &\rho \cos\theta \sin\theta \times \rho \cos\theta \cos\chi \\ &-\rho \sin\theta \cos\theta \times \rho \sin\theta \sin\chi.\end{aligned} \tag{2.49}$$

Substituting equations 2.42, 2.48 and 2.49 into 2.44 gives

$$\begin{aligned}\left|\vec{X}_1 - \vec{X}_3\right|^2 = \frac{1}{d^2}\left[\frac{\rho^2}{2}[1 - \cos 2\theta \cos 2\chi] - 2A_2\frac{d^2\rho^2}{2}\cos 2\theta \sin 2\chi\right. \\ \left. + A_2^2\frac{d^4\rho}{2}[1 + \cos 2\theta \cos 2\chi]\right],\end{aligned} \tag{2.50}$$

which simplifies to

$$\begin{aligned}\left|\vec{X}_1 - \vec{X}_3\right|^2 = \frac{d^2\rho^2}{2}\left[\frac{1}{d^4}[1 - \cos 2\theta \cos 2\chi] - \frac{2}{d^2}A_2 \cos 2\theta \sin 2\chi\right. \\ \left. + A_2^2[1 + \cos 2\theta \cos 2\chi]\right]\end{aligned} \tag{2.51}$$

This expression does not look very appealing but it is correct. Equations 2.22, 2.23 and 2.24, which are use in the BOUND code, are correct if the three particles have the same mass. When the particles do not have the same mass however the equations are inconsistent. In equations 2.22, 2.23 and 2.24 there are three quantities which depend on the mass d, $A's$ and $\delta's$. We assumed that the δ functions were incorrect, but that the general form of the equations was correct, and tried to derive new expressions for them. This gives the following equation

$$\begin{aligned}&\frac{\rho^2 d^2}{2}\left[\frac{1}{d^4} + A_2^2\right] \times [1 + \cos 2\theta \cos 2(\chi + \delta_2)] = \\ &\frac{1}{d^2}\left[\frac{\rho^2}{2}[1 - \cos 2\theta \cos 2\chi] - 2A_2\frac{d^2\rho^2}{2}\cos 2\theta \sin 2\chi\right. \\ &\left. + A_2^2\frac{d^4\rho}{2}[1 + \cos 2\theta \cos 2\chi]\right].\end{aligned} \tag{2.52}$$

This can be rearranged to

$$\begin{aligned}\left[\frac{1}{d^4} + A_2^2\right]\cos 2(\chi + \delta_2) = &\frac{-1}{d^4}\cos 2\chi \\ &\frac{-2}{d^2}A_2 \sin 2\chi + A_2^2 \cos 2\chi,\end{aligned} \tag{2.53}$$

which can be further rearranged to

$$\left[\frac{1}{d^4} + A_2^2\right] \cos 2\delta_2 \cos 2\chi - \left[\frac{1}{d^4} + A_2^2\right] \sin \delta_2 \sin 2\chi = \left[\frac{-1}{d^4} + A_2^2\right] \cos 2\chi \frac{-2}{d^2} A_2 \sin 2\chi. \tag{2.54}$$

It can be seen that

$$\left[\frac{1}{d^4} + A_2^2\right] \cos 2\delta_2 = \left[\frac{-1}{d^4} + A_2^2\right], \tag{2.55}$$

and

$$\left[\frac{1}{d^4} + A_2^2\right] \sin 2\delta_2 = \frac{2}{d^2} A_2. \tag{2.56}$$

Therefore

$$\cos 2\delta_2 = \frac{-1 + d^4 A_2^2}{1 + d^4 A_2^2} \tag{2.57}$$

and

$$\sin 2\delta_2 = \frac{2d^2 A_2}{1 + d^4 A_2^2}. \tag{2.58}$$

If the assumptions made above about the forms of equations 2.22, 2.23 and 2.24 were correct then

$$\cos 2\delta_2^2 + \sin 2\delta_2^2 = 1 \tag{2.59}$$

must be true. Substituting equations 2.57 and 2.58 into equation 2.59 gives

$$\left(\frac{-1 + d^4 A_2^2}{1 + d^4 A_2^2}\right)^2 + \left(\frac{2d^2 A_2}{1 + d^4 A_2^2}\right)^2 = 1 \tag{2.60}$$

This rearranges to

$$\frac{1 + 2d^4 A_2^2 + d^8 A_2^2}{(1 + d^4 A_2^2)^2} = 1, \tag{2.61}$$

and hence

$$\frac{(1 + d^4 A_2^2)^2}{(1 + d^4 A_2^2)^2} = 1. \tag{2.62}$$

Therefore the equations for the $\cos 2\delta_2$ and $\sin 2\delta_2$ are consistent, and our assumption that the error in equations 2.22, 2.23 and 2.24 was in the δ terms was valid. The final expression used in all the BOUND AB_2 calculations is

$$\begin{aligned} |r_2|^2 &= \frac{\rho^2 d_1^2}{2}\left[\frac{1}{d_1^4} + \left(\frac{M_2}{M_2+M_3}\right)^2\right] \\ &\times \left[1 + \cos 2\theta \cos 2(\chi + \delta_2)\right], \end{aligned} \tag{2.63}$$

where $\cos 2(\chi+\delta_2)$ is expanded in the usual manner and evaluated using equations 2.57 and 2.58. A similar methodology produces an equivalent set of equations for $|r_3|^2$, with the expression

$$\begin{aligned} |r_3|^2 &= \frac{\rho^2 d_1^2}{2}\left[\frac{1}{d_1^4} + \left(\frac{M_3}{M_2+M_3}\right)^2\right] \\ &\times \left[1 + \cos 2\theta \cos 2(\chi - \delta_3)\right]. \end{aligned} \tag{2.64}$$

There were two additional modifications needed to allow calculations of AB_2 rare gas molecules. Firstly I had to alter the BOUND code to incorporate the lower symmetry of AB_2. The A_3 case has 6-fold symmetry whereas in the AB_2 case has only 2-fold symmetry. The first effect of altering the symmetry conditions in the BOUND code is to include more channels for a given $J_{\max}$. The second effect is that the number of matrix elements to be evaluated increases, as previously only one sixth of the matrix elements of equation 2.6 were needed to know the rest. This is because the lower symmetry alters the limits on the integrals over θ and χ, which are used to evaluate the potential energy matrix. In the AB_2 code half of the matrix elements must be evaluated. This makes calculations on an AB_2 much more computationally expensive.

2.5.1 Results of calculations on Ar_2Ne and Ne_2Ar

The results for the calculations of Ar_2Ne and Ne_2Ar are shown in tables 2.10[7] and 2.8[8]. The two potentials used both here and by EH were the Ne-Ne [133], and Ar-Ne [153] HFD-B pair potentials. A comparison of the results obtained from the modified BOUND code with those of Ernesti shows a similar behaviour to the results for the A_3 rare gas molecules. For the more rigid Ar_2Ne system, both methods perform reasonably well, though the BOUND calculations are always a little better. This is especially true for the higher excited states. For the more floppy Ne_2Ar system the results obtained from BOUND are far better. This behaviour is again due to the relative floppiness of the two systems. The basis set method of EH struggles to converge on the energy levels of the more floppy Ne_2Ar. This is because there are not enough basis functions to effectively cover the large amplitude motion of the floppier system. The convergence of the two mixed rare gas systems is shown in tables 2.13[9] and 2.12[10]. Again we see that BOUND has no problem converging on the energy levels of the floppier molecule, unlike the basis set method which becomes less satisfactory as the molecule becomes more floppy.

The modified BOUND code could be used to calculate the bound states of any mixed rare gas trimer, such as He_2Ar or Ar_2He, but for the moment only the Ar_2Ne and Ne_2Ar systems have been investigated.

---

[7]With the following input parameters R_{min} = 3.0 Å, R_{mid} = 6.0 Å, R_{max} = 10.0 Å, h = 0.035 Å, reduced mass = 17.87574286 amu, Ar mass = 39.9623837 amu, Ne mass = 19.992435 amu, Jmax = 66

[8]With the following input parameters R_{min} = 3.0 Å, R_{mid} = 6.0 Å, R_{max} = 10.0 Å, h = 0.035 Å, reduced mass = 14.13479814, amu Ar mass = 39.9623837 amu, Ne mass = 19.992435 amu, Jmax = 66

[9]With the following input perimeters R_{min} = 3.0 Å, R_{mid} = 6.0 Å, R_{max} = 10.0 Å, h = 0.035 Å, reduced mass = 17.87574286 amu, Ar mass = 39.9623837 amu, Ne mass = 19.992435 amu

[10]With the following input parameters R_{min} = 3.0 Å, R_{mid} = 6.0 Å, R_{max} = 10.0 Å, h = 0.035 Å, reduced mass = 14.13479814, amu Ar mass = 39.9623837 amu, Ne mass = 19.992435 amu, Jmax = 66

Energy Level	Energy/cm^{-1}
1	−85.499
2	−72.369
3	−68.566
4	−67.468
5	−65.667
6	−64.130
7	−61.627
8	−58.025
9	−56.440
10	−53.884

Table 2.8: Results of Ne_2Ar (A_1)symmetry in hyperspherical basis set

Energy Level	Energy/cm^{-1}
1	−85.498
2	−72.360
3	−67.573
4	−64.779
5	−61.420
6	−55.948
7	−54.991
8	−51.561
9	−48.743
10	−48.138

Table 2.9: EH results for Ne_2Ar

Energy Level	Energy/cm^{-1}
1	−153.341
2	−133.597
3	−127.562
4	−123.562
5	−120.263
6	−188.991
7	−117.248
8	−115.290
9	−113.427

Table 2.10: Results of Ar_2Ne A_1 symmetry in hyperspherical basis set

Energy Level	Energy/cm^{-1}
1	−153.345
2	−133.608
3	−127.573
4	−123.642
5	−118.664
6	−114.776
7	−110.661
8	−109.028
9	−104.408
10	−102.795

Table 2.11: EH results for Ar_2Ne

λ_{max}	$E_1/\ cm^{-1}$	E_2/cm^{-1}
48	−85.471	−72.323
56	−85.496	−72.363
66	−85.499	−72.369

Table 2.12: Convergence for Ne_2Ar in hyperspherical basis set

λ_{max}	E_1/cm^{-1}	E_2/cm^{-1}
48	−153.090	−133.037
66	−153.341	−133.597
72	−153.343	−133.605

Table 2.13: Convergence for Ar_2Ne in hyperspherical basis set

Chapter 3

Investigating the Eckart Condition

3.1 Rotational Constants

In order to understand why we were interested in investigating the Eckart condition it is necessary to describe previous work carried out by Ernesti and Hutson [20]. High resolution spectroscopy is an important source of information on potential energy surfaces for van der Waals molecules [154, 155]. In the fitting of potential energy functions both vibrational frequencies and rotational constants are important sets of data. It is therefore useful to be able to calculate the rotational constant of a van der Waals molecule for a given potential energy function, and to use the calculations of the rotational constants to adjust the variable parameters of the potential energy function to fit the experimental data. The rotational constants of a molecule may be calculated from perturbation theory using the expectation values of the moments of inertia.

The rotational Hamiltonian of a rigid body can be written as

$$H_{\mathrm{rot}} = \frac{1}{2}\hbar^2 \sum_{qq'} [\mathrm{I}^{-1}]_{qq'} \hat{J}_q \hat{J}'_q, \tag{3.1}$$

where I^{-1} is the inverse of the inertial tensor and $\hat{J}_q$ is the component of the rotational angular momentum along the axis q. In the case of a vibrating molecule the rotational part of the full Hamiltonian retains the form of equation 3.1 provide the axes are chosen to satisfy the Eckart conditions [156, 25, 24], but the inertial

tensor I is replaced by I'. The elements of I' differ from I by small Coriolis terms. In normal co-ordinates the form of I' is actually simpler than I. For molecules that undergo wide amplitude motion, such as van der Waals molecules, normal co-ordinates are not the most convenient co-ordinate system in which to work. As was mention in chapter 2 Jacobi co-ordinates, with the three co-ordinates R, r and θ defining the system is a much more convenient co-ordinate system in which to work. Unfortunately for more general co-ordinate systems the form of I' is no valid.

In work before 1994 rotational constants for van der Waals complexes were often calculated by describing the complex using Jacobi co-ordinates, and calculate the inertial tensor I in a Cartesian axes system in which the Jacobi distance R lies along the z axis [13]. The rotational constants are then found by inverting the inertial tensor and neglecting off-diagonal element in vibrational states. This will be denoted method I from now on. This gives an effective rotational Hamiltonian

$$H_{\text{rot}}^{\text{eff}} = B_x \hat{J}_x^2 + B_y \hat{J}_y^2 + B_z \hat{J}_z^2 + d_{xz}(\hat{J}_z \hat{J}_x + \hat{J}_x \hat{J}_z), \tag{3.2}$$

where the rotation constants are expectation values of expressions involving elements of the inertial tensor and the angle θ.

Ernesti and Hutson pointed out that the method just described did not satisfy the Eckart conditions [24], which will be defined later, because, in the method I atom A is not allowed to move of the z axis. This meant that in physical terms the separation of vibration and rotation was not exact, and leads to a non zero instantaneous angular momentum about the y axis. The fact that the separation of rotation and vibration in the molecule is only approximate means that the degree of vibration in a molecule is important when calculating the rotation constants. If the molecule is executing small amplitude motions, that is so that each atom is moving by a small amount about a reference geometry, then the approximate nature of the separation in method I will not affect the values obtained for the rotational constants. If however the atoms in the molecule are moving by a large amount about their equilibrium geometry then the approximate nature of method I may (and indeed was shown to) lead to an error in the calculated value for the ro-

tational constants. One of the major reasons for studying van der Waals molecules is that they are prototype systems which undergo wide amplitude motion. The fact that they do undergo such large amplitude motion means that they sample a large proportion of the potential energy surface. Therefore when using experimental data to fit a functional form of the potential energy surface any method of calculation used must be able to cope with the large amplitude motions of the system.

Ernesti and Hutson re-derived expressions for B_x, B_y, B_z and d_{xz} for a triatomic system where the A atom is not fixed to the z axis. They were able to show that in calculations on the Ar-CO_2 system the rotational constants calculated with the Eckart axis were significantly more accurate that those calculated by method I.

3.2 Separation of Rotation and Vibrational Motion

In general we want to set up a system that describes the motion on a molecule such that its motion can be split into three components. These components are the translation, vibration and rotation of the molecule. The most convenient co-ordinates are the three co-ordinates of the centre of mass of the molecule, the three Eulerian angles of a rotating system of Cartesian co-ordinates and the Cartesian co-ordinates of the atoms with respect to the rotating co-ordinate system. In a molecule with N atoms there are $3N$ degrees of freedom. Six conditions are needed to define the rotating co-ordinate system: three to locate the origin of the rotating system so that it moves with the centre of mass of the molecule and three to tie the co-ordinate system to the molecule so that they rotate together. This (as is shown below) allows the vibrational and rotational motion of the molecule to be decoupled as far as possible. To do this we define several vectors that will be useful. They are $\vec{R}$ which is a vector between the origin and the centre of mass of the molecule designated O, $\vec{a}_i$ which are a set of vectors that define an equilibrium geometry fixed to the moving axes system, $\vec{r}_i$ which are a set of vectors defining

the instantaneous positions of each atom and $\vec{d}_i$ which are a set of vectors defining the instantaneous displacement of each atom form its equilibrium geometry. If the system of axes at a given moment has an angular velocity ω, and if a vector $\vec{v}_i$ is defined as

$$\vec{v}_i = \dot{\vec{r}}_i, \tag{3.3}$$

then the velocity of the ith atom is

$$\dot{\vec{R}} + \omega \times \vec{r}_i + \vec{v}_i. \tag{3.4}$$

The kinetic energy of the system is therefore give by

$$2T = \dot{\vec{R}}^2 \sum_i m_i + \sum_i m_i(\omega \times \vec{r}_i) \cdot (\omega \times \vec{r}_i) + \sum_i m_i \vec{v}_i^2 \tag{3.5}$$
$$+2\dot{\vec{R}} \cdot \omega \times \sum_i m_i \vec{r}_i + 2\dot{\vec{R}} \cdot \sum_i m_i \vec{v}_i + 2\omega \cdot \sum_i (m_i \vec{r}_i \times \vec{v}_i),$$

where m_i is the mass of the ith atom. Because O is the centre of mass of the molecule at every instance

$$\sum_i m_i \vec{r}_i = 0, \tag{3.6}$$

and it therefore follows that [1]

$$\sum_i m_i \vec{v}_i = 0. \tag{3.7}$$

As has already been stated, the above conditions are not sufficient to define the non-ridged rotating system. To completely define the system the following definition is used

$$\sum_i m_i (a_i \times \vec{v}_i) = 0. \tag{3.8}$$

If $\vec{r}_i$ in equation 3.6 is replaced by $\vec{a}_i + \vec{d}_i$ and the conditions 3.6 and 3.8 applied then 3.6 becomes

$$2T = \dot{\vec{R}}^2 \sum_i m_i + \sum_i m_i(\omega \times \vec{r}_i) \cdot (\omega \times \vec{r}_i) \tag{3.9}$$
$$+ \sum_i m_i \vec{v}_i^2 + 2\omega \cdot \sum_i m_i (\vec{d}_i \times \vec{v}_i).$$

[1] see Wilson, Decius and Cross [156] page 274

The first term in the above equation is the translational energy of the molecule. The second term is rotational energy, and the third term is the vibrational energy. The last term is the Coriolis coupling term, which can be neglected, or added as a small perturbation to the system. The second condition (3.8) can be rewritten as[2]

$$\sum_i m_i(\vec{a}_i \times \vec{d}_i), \tag{3.10}$$

similarly condition 1 can be redefined as

$$\sum_i m_i \vec{d}_i = 0. \tag{3.11}$$

These are the Eckart conditions [24, 157, 158], and the have two main effects. The first is to simplify the form of the kinetic energy expression, as shown above. The second effect is more subtle, and is the focus our investigation. The condition expressed by equation 3.10 is almost equivalent to stating that there must be no angular momentum with respect to translating-rotating co-ordinate system. The reason that condition 3.10 is not the same as saying that there must be no angular moment is because, if we take x_i, y_i and z_i to be the three components of the vector $\vec{r}_i$ then the components of the angular momentum would be

$$\begin{aligned} m_x &= \sum_i^N m_i(y_i\dot{z}_i - z_i\dot{y}_i) \\ m_y &= \sum_i^N m_i(z_i\dot{x}_i - x_i\dot{z}_i) \\ m_z &= \sum_i^N m_i(x_i\dot{y}_i - y_i\dot{x}_i). \end{aligned} \tag{3.12}$$

For small displacements the co-ordinates x_i, y_i and z_i can be replaced by their reference geometry co-ordinates a_i, b_i and c_i this leads to the following expressions for the angular momentum,

$$\begin{aligned} m_x &\cong \sum_i^N m_i(b_i\dot{z}_i - c_i\dot{y}_i) \\ m_y &\cong \sum_i^N m_i(c_i\dot{x}_i - a_i\dot{z}_i) \\ m_z &\cong \sum_i^N m_i(a_i\dot{y}_i - b_i\dot{x}_i). \end{aligned} \tag{3.13}$$

[2]see Wilson, Decius and Cross [156]) page 274 and 13

Using this notation the second Eckart condition 3.10 would be

$$\sum_{i}^{N} m_i(b_i\Delta z_i - c_i\Delta y_i) = 0$$
$$\sum_{i}^{N} m_i(c_i\Delta x_i - a_i\Delta z_i) = 0$$
$$\sum_{i}^{N} m_i(a_i\Delta y_i - b_i\Delta x_i) = 0. \tag{3.14}$$

But it should be noted that

$$\left(\frac{d\Delta x_i}{dt}\right) = \dot{x}_i, \tag{3.15}$$

and therefore equations 3.14 are equivalent to equations 3.13.

3.3 Investigation of Eckart condition

As has already been stated the Eckart conditions embed a set of axes into the rotating system. In doing so they try to set the condition that there is no angular momentum with respect to the rotating axis system. In physical terms this means that if we start with a molecule (ABC) in a 'T shaped' configuration, such that the dimer BC lies parallel to the x axis and the atom A lies on the z axis, then a vibration that moves the A atom from the z axis will cause the dimer BC to rotate, so as to satisfy the second Eckart condition 3.10. To be more specific if the A atom moves into the positive x planes, then the dimer BC will have to rotate in a clockwise manor to meet the second Eckart condition.

Our interest in the Eckart conditions however is not directly related to the calculation of any particular molecular property. We are interested in how the Eckart conditions embed the axes into the rotating molecule system. We are particularly interested in the effect that the second Eckart condition 3.10 has on the embedding of the rotating axes when the molecule is executing large amplitude motions, and specifically in the limit of large amplitude motions where the molecular structure inverts. That is to say when the A atom passed through the middle of the BC dimer.

To be able to see what effect the Eckart conditions are having on the embedding of the rotating axes in the rotating system it is useful to have something to compare them against. We therefore need a second way of embedding the rotating axes. The set of conditions chosen for this purpose is that the off-diagonal moments of the moment of inertia tensor are zero, e.g.

$$\begin{aligned} \sum_i m_i x_i y_i &= 0 \\ \sum_i m_i x_i z_i &= 0 \\ \sum_i m_i y_i z_i &= 0. \end{aligned} \tag{3.16}$$

This will from hence forward be called the instantaneous principle inertial condition. This is equivalent to saying that the embedded axes will lie along the instantaneous principle inertial axes of the molecule. As one set of molecular properties that we might want to calculate is the rotational constants, and therefore the expectation values of the moments of inertia, this set of axes is a natural choice against which to compare the Eckart axes.

We wanted to know what difference the two embedding conditions make to the dynamics of the system. In particular we wanted to investigate the relationship between γ_{EC} (the angle at which the Eckart condition is zero), and γ_{XY} (the angle of the axis at which the inertial tensor is diagonal) for a particular geometry. We want to know how these two quantities differ as the molecule undergoes vibrational motion.

To do this we first wrote a simple program. This program receives a reference geometry, and two distortion vectors. The reference geometry $\vec{a}_i$ is in the form of two interparticle distances $\vec{r}_1$ and $\vec{r}_2$, from which the third interparticle distance $\vec{r}_3$ is calculated assuming the centre of mass is at the origin. Atoms one and two are then moved by the two distortion vectors, and the position of the third atom is then calculated assuming that the centre of mass is unchanged, to give the real geometry, and the vectors $\vec{d}_i$. This is shown in figure 3.1 where the un-primed atoms are the reference geometry, and the primed atoms are the actual geometry formed by distorting the reference geometry.

The primed atoms are then rotated in small steps, from zero degrees to 2π, to give doubly primed atoms. At each step in β the off-diagonal elements of the moment of inertia tensor, and $\sum_i m_i(a_i \times d_i)$, which from hence forth will be called the cross-sum, are calculated. Figure 3.2 shows the primed atoms which are the distorted geometry, and the double primed atoms which are the new geometry formed after the distorted trimer is rotated by an angle β.

The program produces a plot of the value of the $\sum_i m_i(a_i \times d_i)$ and off-diagonal elements of the moment of inertia tensor in the range $0 \rightarrow 2\pi$. We are interested in the points at which the values of these two functions are zero, and forefil the two embedding conditions. These points will be called γ^0_{EC} and γ^0_{XY}. The results of these calculations show that γ_{EC} has a periodicity of π; and that γ_{XY} has a periodicity of $\pi/2$. The two sine functions, γ_{EC} and γ_{XY}, do not have the same phase so we now defined a new quantity γ_{diff}, which is the smallest difference between γ^0_{EC} and γ^0_{XY}. The value of γ_{diff} will tell you about how differently the two co-ordinate systems will treat the same vibrational movement of a molecule.

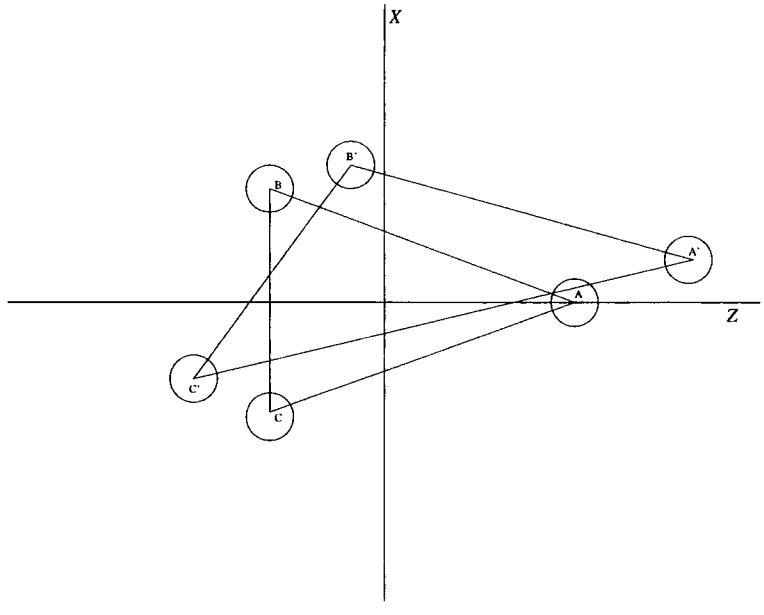

Figure 3.1: Eckart plot 1

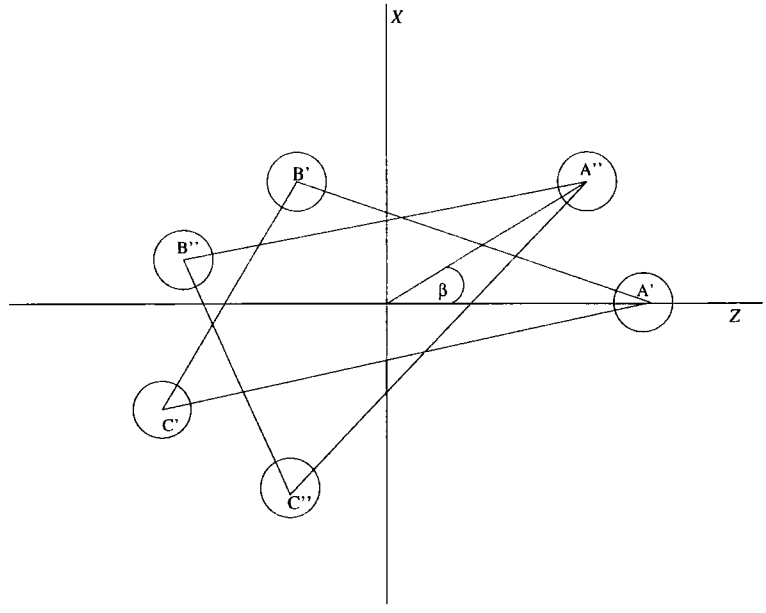

Figure 3.2: Eckart plot 2

The first Eckart program showed the result for only one displacement of the reference geometry. It would be much more useful if we could study a wide range of motion, and its affect on γ_{EC} and γ_{XY}. We could of course just run the simple Eckart program many times to generate the desired effect, but this would be very inefficient. Instead we chose to carry these calculations out in hyperspherical co-ordinates [38], which has the advantage that all molecular geometries can be sampled by scanning over only two co-ordinates. In hyperspherical co-ordinates there are three parameters which describe the geometry of the triatomic molecule, they are ρ, θ, χ. The parameter ρ controls the size of the triangle formed by the three atoms, while the parameters θ and χ control the shape of the molecule. For the calculation ρ is not important, as the size of the trimer does not affect the calculations of γ_{EC} and γ_{XY}. The ranges of χ and θ in hyperspherical are :-

$$\begin{aligned} 0 &\leq \chi < 2\pi \\ 0 &\leq \theta < \pi/4. \end{aligned} \tag{3.17}$$

In the hyperspherical program the co-ordinates of the distorted structure are handled on grid of 101 $\times$ 101 points. At each grid point the program calculates the

interparticle distance use the following formulae, which were derived in chapter 2,

$$\begin{aligned}
|r_1|^2 &= \frac{\rho^2 d_1^2}{2}[1+\cos 2\vartheta \cos 2\chi], \\
|r_2|^2 &= \frac{\rho^2 d_1^2}{2}\left[\frac{1}{d_1^4}+\left(\frac{M_2}{M_2+M_3}\right)^2\right]\times[1+\cos 2\vartheta\cos(2\chi+\delta_2)], \\
|r_3|^2 &= \frac{\rho^2 d_1^2}{2}\left[\frac{1}{d_1^4}+\left(\frac{M_3}{M_2+M_3}\right)^2\right]\times[1+\cos 2\vartheta\cos(2\chi+\delta_3)]. \qquad (3.18)
\end{aligned}$$

The triangle formed by the three interparticle distances is now placed such that atom B is at the origin, and atom A lies on the positive x axis. The centre of mass (R) and the angle (α) are then calculated. The angle α is the angle between a line from R to the atom A, and a line running through R parallel to the x axis. Using R and α the molecule is then moved so that the centre of mass is at the origin and atom one is still on the x axis. The initial values of the cross-sum and zero moment condition are then calculated, and given a parity sign. A γ_{EC} or γ_{xy} value that is greater than zero is given a parity sign of 1, and value that is less that zero is given a parity sign of -1. The program now rotates the molecule by β, as in the first program, and at each value of β the cross-sum and the off-diagonal elements of the moment of inertia tensor are calculated. When the parity of either γ_{EC} or γ_{xy} changes a convergence routine is called, to find the exact value ofγ_{EC} or γ_{xy}. When both γ_{EC} and γ_{xy} have changed parity the program stops. We do not need to know the other point at which γ_{EC} and γ_{xy} are zero in the range $0 \rightarrow 2\pi$ because we know their periodicity. We can therefore calculate the points at which the two functions are zero in the rest of the range; and then find which of these sets of points is closest to each other, and therefore the value of γ_{diff} for that point on the grid. The program calculates the value and difference of γ_{EC} and γ_{xy}, at each grid point.

3.4 Results and Conclusions

One of the main problems encountered during this work on the Eckart condition is trying to understand and interpret the results of the computer program.

The computer program calculates the angle between the two embedded axes systems, denoted γ_{diff}. The best method of displaying the results of the program was found to be to draw the three atoms and then to show the two axis systems imposed on top of the molecular geometry. The Eckart axes are shown as a set of solid lines and the moment of instantaneous principle inertial axes are shown as a set of dashed lines. The two sets of axes have different ranges, as has been previously explained. The value of γ_{EC} can range from $0 \rightarrow \pi$, whereas the value of γ_{XY} can range from $0 \rightarrow \pi/2$. The diagrams show the molecular configuration and the two sets of axes at intervals in the hyperspherical angles θ and χ. The step sizes in the two hyperspherical angles are $\pi/10$ and $\pi/8$ for χ and θ respectively, where the range of θ is $0 \rightarrow \pi/4$, and that of χ is $0 \rightarrow 2\pi$.

Due to the symmetry of the hyperspherical co-ordinate system the positions of atoms for a given value of θ and a range of χ values are related to each other. For example for $\theta = 0°$ and $\chi = \pi/8$ the molecular configuration is linear, with the A atom near to the B atom. For $\theta = 0°$ and $\chi = \frac{15}{8}\pi$ the molecule is again linear, but this time the A atom is near to the C atom. These two structures are related to each other by a 180° rotation about the middle to the BC bond. This is a specific example of a general property, that the structures found for a given value of θ are symmetric about $\chi = \pi$ within a rotation. The result of this symmetry is that we only have to study either $\chi = 0 \rightarrow \pi$ or $\chi = \pi \rightarrow 2\pi$. I shall only discuss the plots for $\chi = \pi \rightarrow 2\pi$, but have included the plots for $\chi = 0 \rightarrow \frac{7}{8}\pi$ for completeness. It should be noted that due to the way the plots are drawn the molecule is always pointing the same way, so that related structures give the same picture, as well as the same result for γ_{diff}.

The plots have the A atom represented by a filled-in circle, with the B and C atoms represented as open circles. They are arranged so that each column represents a given value of θ, and each row represents a given value of χ.

When we first started plotting the result from the hyperspherical Eckart program we found the smallest γ_{diff} for each point on a 101×101 grid. The results were displayed as a contour map. The contour plots showed that γ_{diff} was not only

symmetric about $\chi = \pi$, but that in the intervals $\chi = 0 \rightarrow \pi$ or $\pi \rightarrow 2\pi$ γ_{diff} was symmetric about $\pi/2$ and $\frac{3}{2}\pi$ respectively. However the plots on pages 57 to 66 do not show this symmetry. The reason for this is that we store the first values of γ_{EC} and γ_{xy} found, and not necessarily the values of γ_{EC} and γ_{xy} that give the smallest γ_{diff}. Due to the periodicity of the two functions the first two values found may not be the two values of γ_{EC} and γ_{xy} that give the smallest γ_{diff}. If there were not an arrow to define the orientation of the two axes then the symmetry of γ_{diff} about $\chi = \frac{3}{2}\pi$ would be shown in the plots. Therefore to see the value of γ_{diff} the two structures reflected about $\chi = \frac{3}{2}\pi$ must both be considered. In order to calculate the cross sum we have to specify a reference geometry. We chose a 'T shaped' reference geometry, with the A atom sitting on the Z axis. This structure was chosen because the geometry of neutral rare gas trimers is fundamentally triangular. The choice of the reference geometry is in some sense arbitrary as any geometry could be chosen as the reference geometry, and the Eckart conditions could be implemented. However the Eckart condition assumes the displacements from the reference geometry are small, and therefore the more unrealistic the reference geometry the poorer the results of any calculation should be. The results for all figures are for a reference geometry that is an equilateral triangle. If we had chosen a linear reference geometry it would have altered the result of each individual geometry but the overall pattern of results would have been unchanged.

One problem with only having the two hyperspherical co-ordinates to describe the complete motion of the system is that some changes in co-ordinates can represent unphysical motions. A good example of this is shown in the first column of figure 3.3 where $\theta = 0°$ and $\chi = \pi \rightarrow \frac{3}{2}\pi$. The A atom starts in the middle of the BC bond and moves towards and through the B atom, into a linear B-C-A configuration.

3.4.1 Ar_3

For a set of θ and χ values the geometry of the trimer is determined by the three masses, i.e. equation 3.3. Therefore if the masses of the three atoms are simply

scaled it will not affect the geometries that you find for system, and will not therefore effect the value of γ_{EC} or γ_{xy} for a given geometry. We therefore expect that the results for an A_3 trimer should be the same. This is indeed what we see for the three trimer, Ar_3, Ne_3 and He_3, that we investigated.

The first and most striking point to note is that when the molecular configuration is T shaped γ_{diff} is zero. This is due to the fact that the reference geometry is also T shaped and because the zero moment of inertia condition will always chose to lie along a centre of symmetry. This can be seen by examining the $\chi = \pi$ row of figure 3.3, where γ_{diff} is zero for all θ values except zero. For $\theta = 0$, the γ_{xy} is zero as it points along a centre of symmetry, but γ_{EC} is now ninety degrees.

One other feature that is quite clear from the results is that as the molecule geometry moves further away from that of the reference geometry γ_{diff} increases. This is due to the fact that the two sets of conditions have different priorities for embedding the rotating axes. The instantaneous principle inertial condition simply tries for each molecular configuration to embed the axes so that the off-diagonal moments of inertia are zero, which can be thought of as trying to find the best axes to 'balance' each configuration. The Eckart condition however is not trying to 'balance' each new molecular configuration, but is instead trying to embed the axes such that with respect to some predetermined geometry there is no instantaneous angular momentum about The Y axis.

As well as looking at how the two embedding systems differ, we were also interested in looking at the way the Eckart axes behave as the molecule undergoes large amplitude motions. We were particularly interested in what happens to the Eckart axes as the A atom moves in-between the BC dimer, to form a linear triatomic molecule.

As the A atom moves in closer to the BC dimer, such as in the $\chi = \pi$ row, the Eckart axes do not alter, but at linearity the Eckart axes flip by ninety degrees. As the A atom passes through the BC dimer and forms the inverted structure, the Eckart axes flip back and point along the same direction as the instantaneous principle inertial axes. In the case of the $\chi = \pi$ row the molecular geometries

are symmetric, with the A atom passing through the middle of the BC dimer. The behaviour of the Eckart axes is however qualitatively similar for molecular configurations where the A atom does not pass through the middle of the BC dimer. The Eckart axes do flip at the linear configuration, but as can be see in figure 3.3 Eckart axis (γ_{EC}) and the instantaneous principle inertial axes (γ_{XY}) are non zero for the non-linear configurations. This means that the Eckart axes rotate more smoothly, than they did in the $\chi = \pi$ row, as we move across a given row.

3.4.2 AB_2 rare gas trimers

As well as studying the A_3 cases we have also studied some AB_2 cases, to illuminate what happens when the masses of the three particles are not the same. We have studied the two limiting cases of a heavy BC dimer and a light A atom, and a light BC dimer and a heavy A atom. In this and all subsequent mixed trimers the reference geometry is an equilateral triangle.

He_2Ar

There are some similarities in the Eckart axes for He_2Ar and for Ar_3. For instance the $\chi = \pi$ row is the same. Yet again we see that as the actual geometry moves further away from the reference geometry the two axis systems move further apart. However one of the most notable differences between the two systems is that γ_{diff} for any given geometry is less than that found for the Ar_3 system.

Another point to notice, and one that has already been stated previously, is that the ratio of the masses affects the position of atoms for a given θ and χ. In the He_2Ar system this is clearly shown by the position of the A atom for the $\theta = 0$ column in figure 3.7 compared to the same column in the Ar_3 system shown in figure 3.3. This makes a direct comparison of the sets of results more difficult. It is however possible to see the general trends described above showing through.

The different trimer geometries for a given θ and χ, and the subtle changes in γ_{EC} amd γ_{XY} for similar structures is clearly shown by a study of the $\theta = 0$ $\chi = 1.3\pi$ structure for the He_2Ar system (figure 3.7) and the $\theta = 0$ $\chi = 1.2\pi$

structure from the Ar_3 (figure 3.3). The structures are both linear and they both have the A atom inside the BC dimer. The value of γ_{xy} is still zero. However the Eckart axes have clearly not rotated as much as in the Ar_3 system.

Ar_2He

For Ar_2He we see that the different ratio of masses means that the structures for a given θ and χ are very different. This is shown by the $\theta = 0$, $\chi = \pi$ and 2π structures which are linear CAB structures in the x axis, and not the z axis. This does not affect γ_{xy} which is still zero, but γ_{EC} is now 180°. In previous systems γ_{EC} was 90°. This difference is explained by the fact that for symmetric linear molecules the Eckart condition forces the embedded axes to be at right-angles to the linear molecule. Therefore when the linear molecule lies along the x axis the Eckart axis lies along the $-Z$ axis.

We again see that γ_{diff} is smaller for most configuration that it was for the Ar_3 system. Indeed for many of the molecular configurations it appears that both sets of axes follow the heavier Ar_2 dimer. This is not to surprising as dimer is twenty times the mass of the He atom.

He_2Ne and Ar_2Ne systems

The final two A_2B systems that we studied were He_2Ne and Ar_2Ne. They were chosen as intermediate cases to the light BC-heavy A and heavy BC-light A systems respectively. In both systems, see figures 3.7 and 3.12, we see that the extreme geometry changes for a given θ and χ found in the He_2Ar and Ar_2He systems do not occur. For both of these two intermediate systems the molecular configuration for a given θ and χ is much more like that for the Ar_3. This similarity is also shown in the two embedded axis systems.

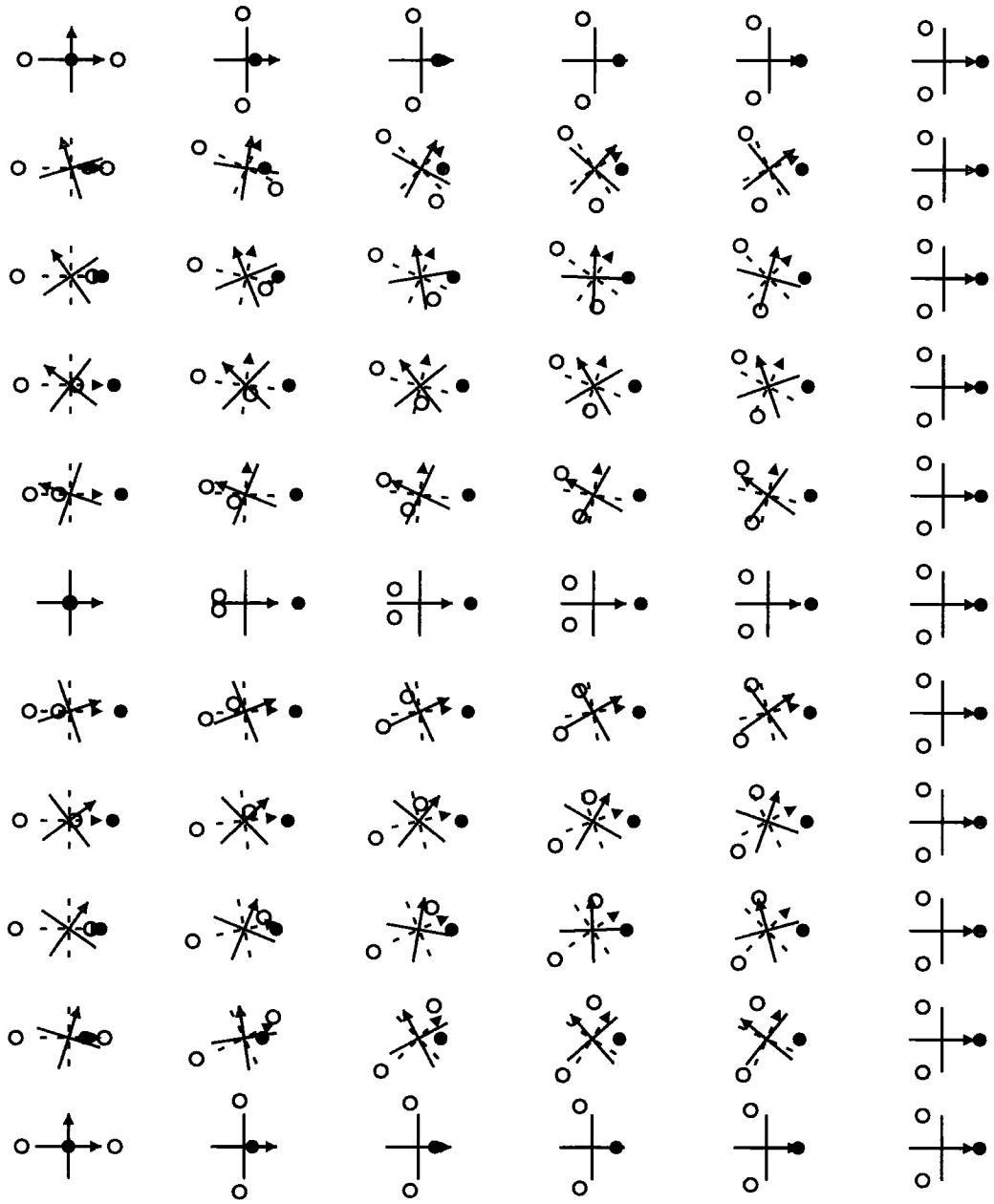

Figure 3.3: Eckart plot for Ar_3 $\chi = \pi \rightarrow 2\pi$

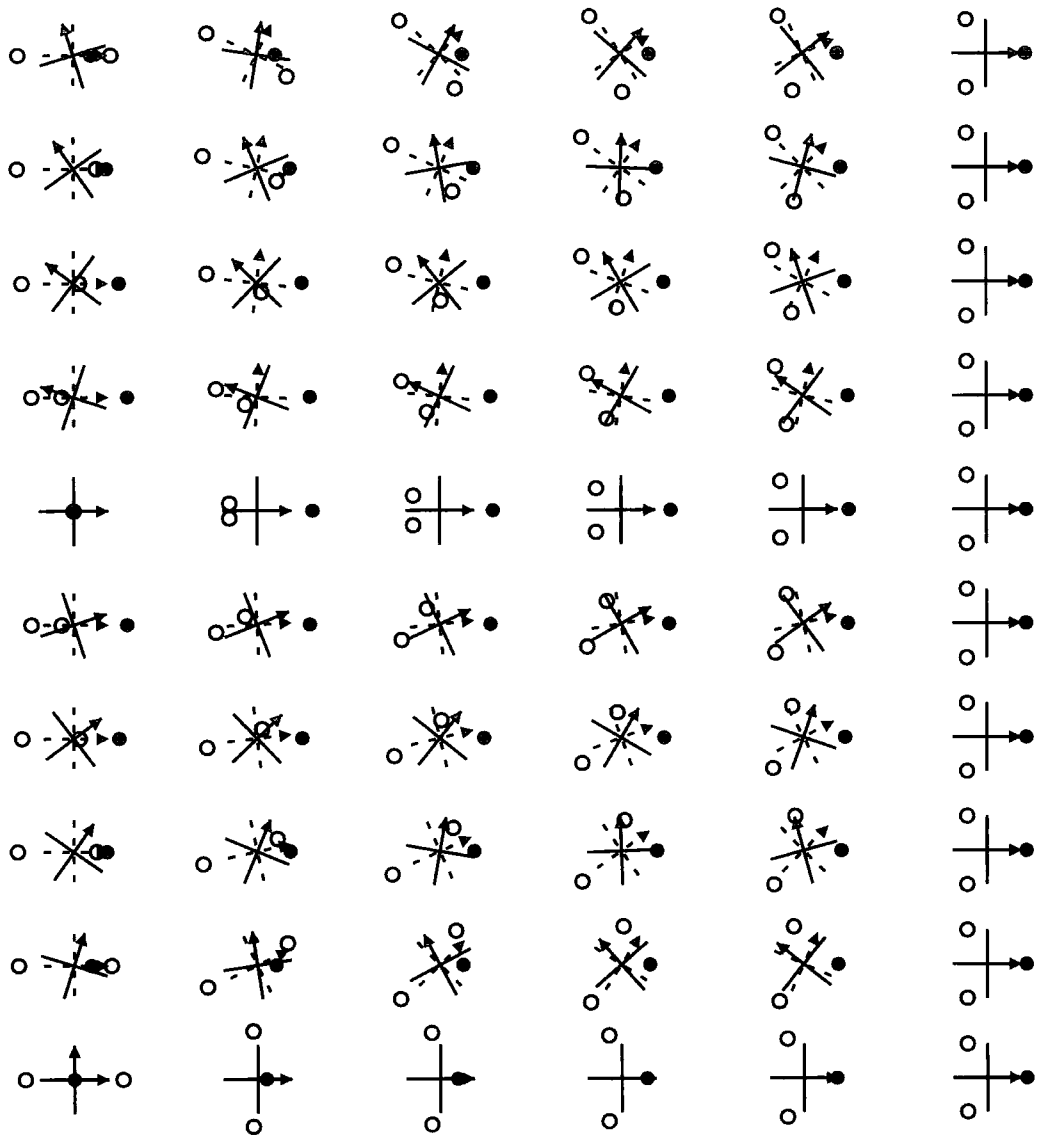

Figure 3.4: Eckart plot for Ar_3 $\chi = 0 \rightarrow 0.875\pi$

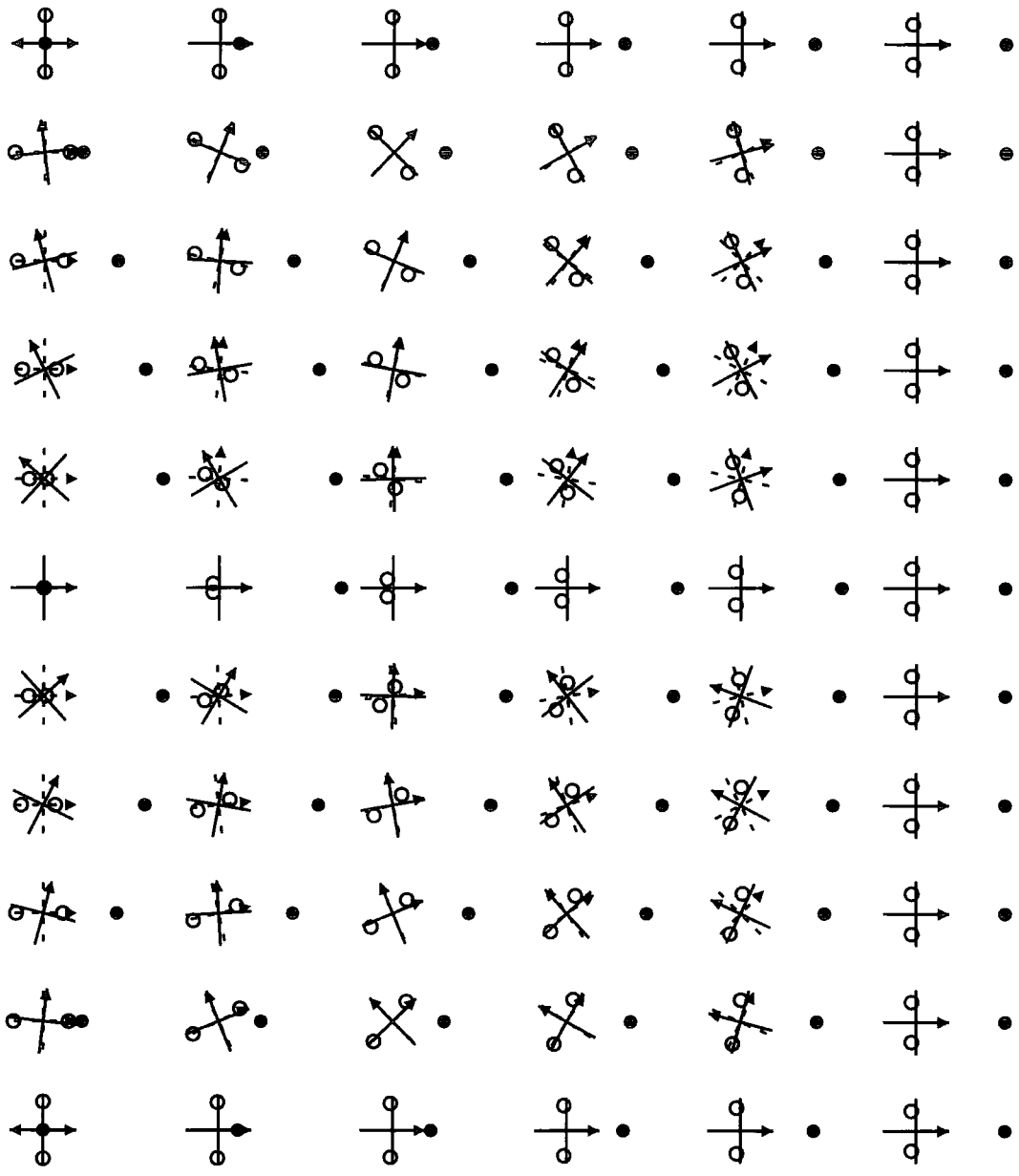

Figure 3.5: Eckart plot for Ar_2He $\chi = \pi \rightarrow 2\pi$

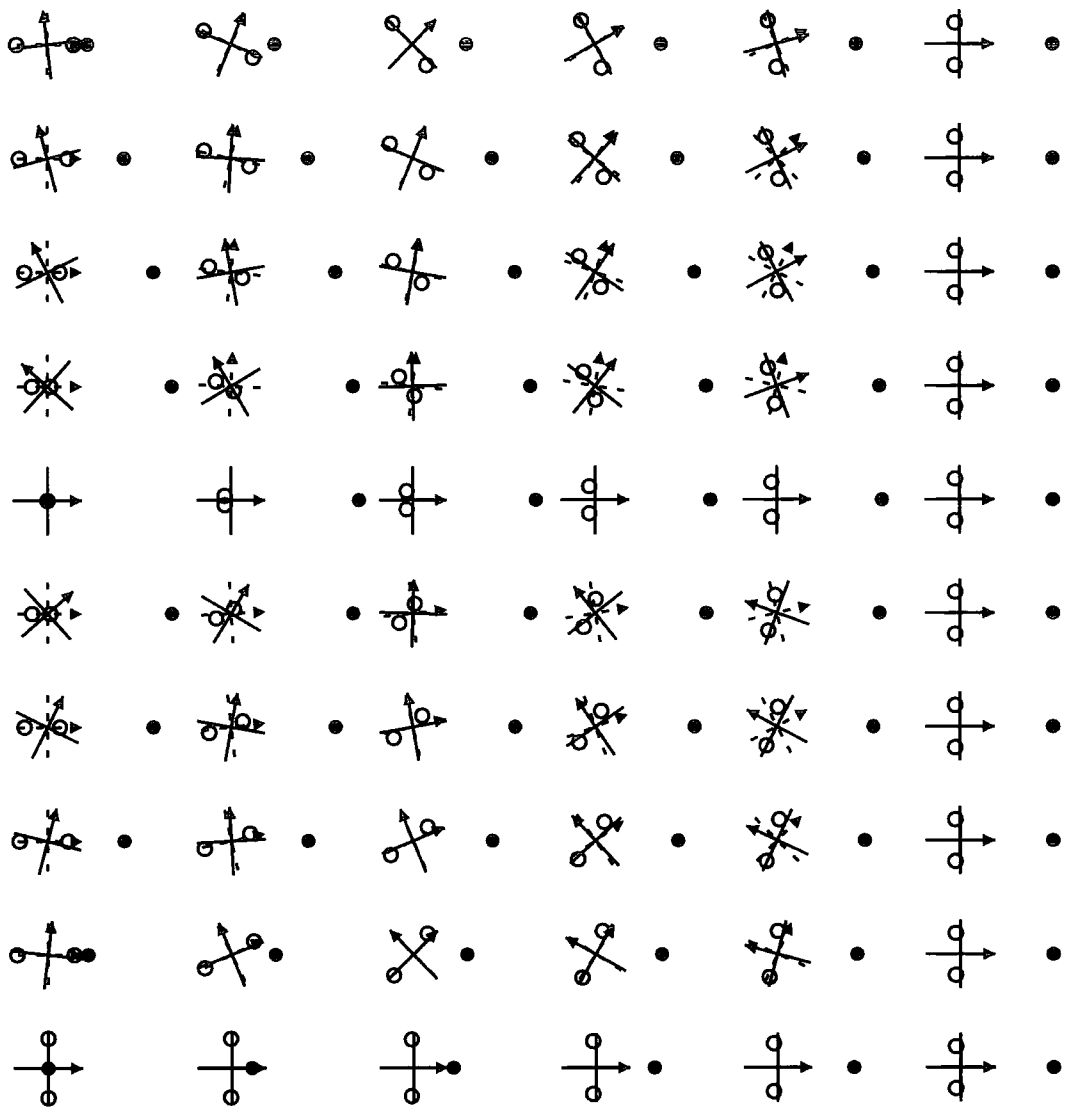

Figure 3.6: Eckart plot for Ar_2He $\chi = 0 \rightarrow 0.875\pi$

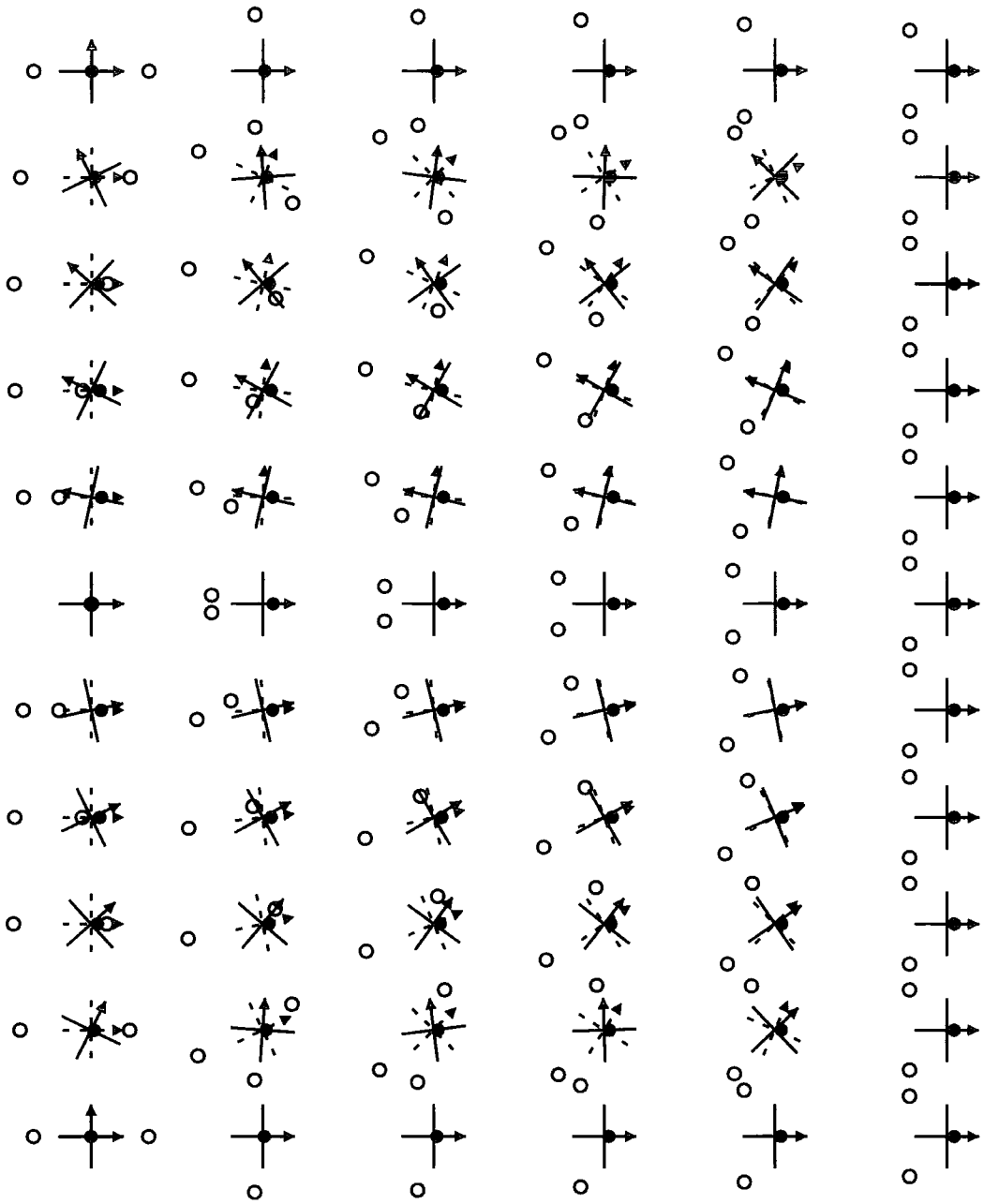

Figure 3.7: Eckart plot for He_2Ar $\chi = \pi \rightarrow 2\pi$

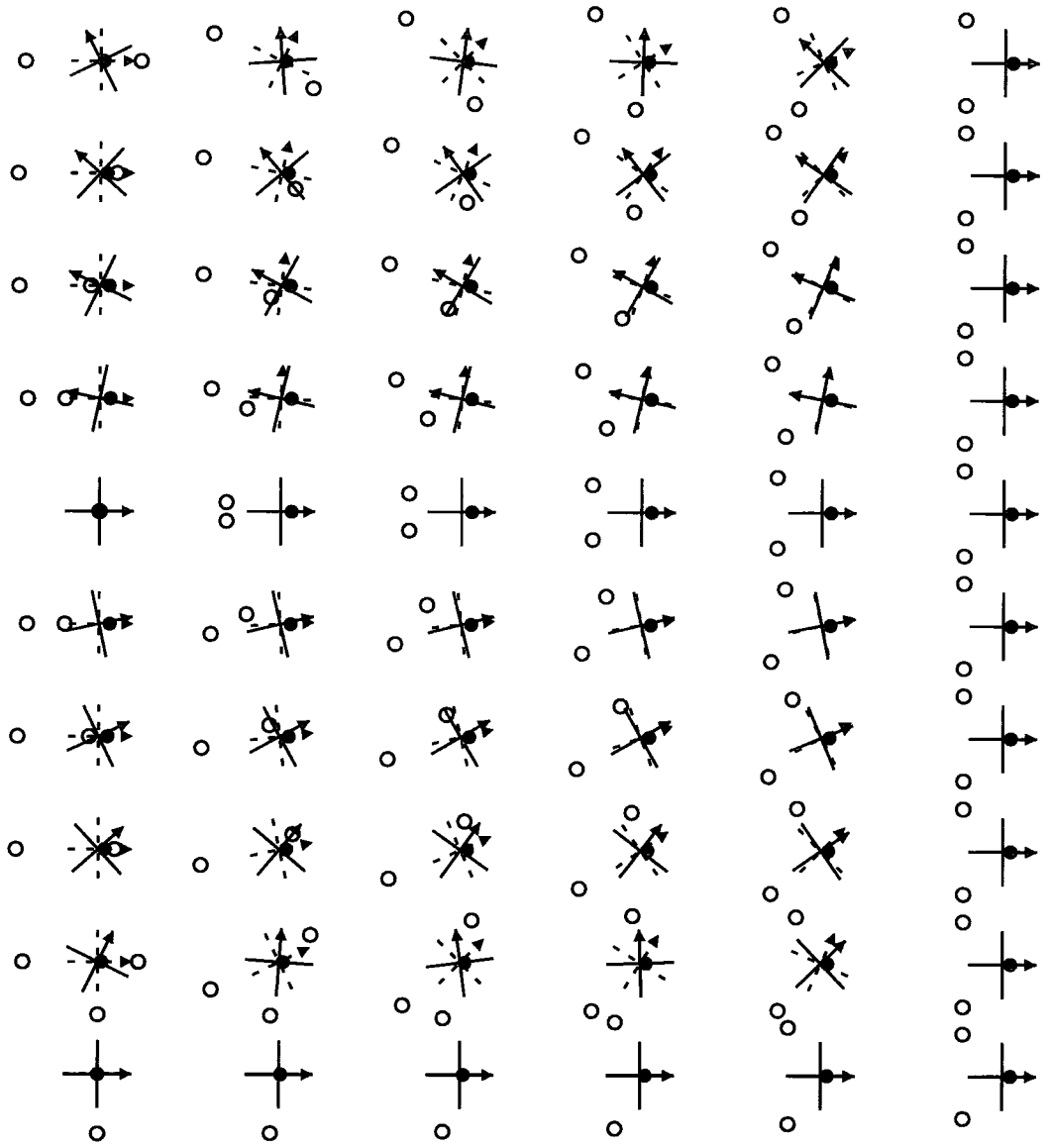

Figure 3.8: Eckart plot for He_2Ar $\chi = 0 \rightarrow 0.875\pi$

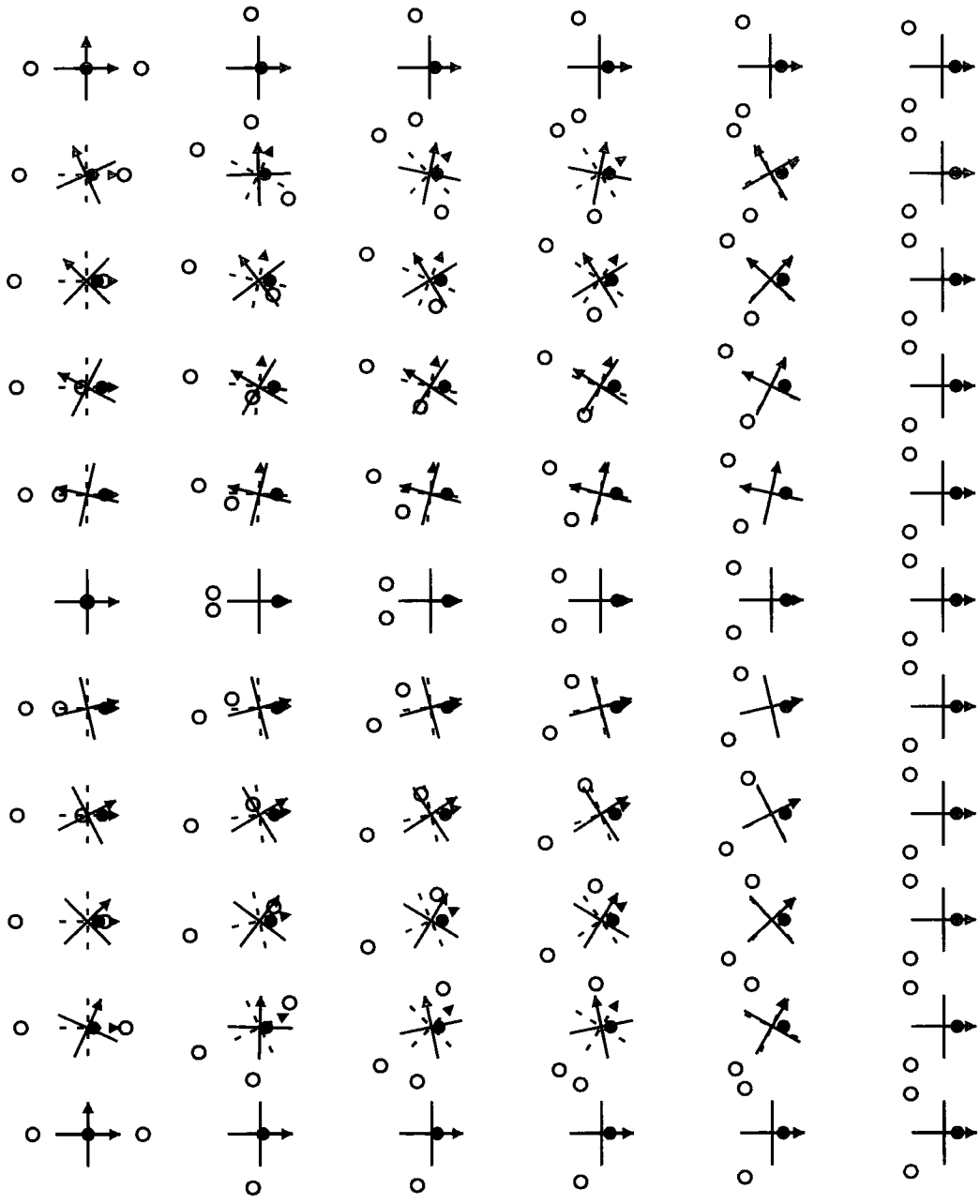

Figure 3.9: Eckart plot for He_2Ne $\chi = \pi \rightarrow 2\pi$

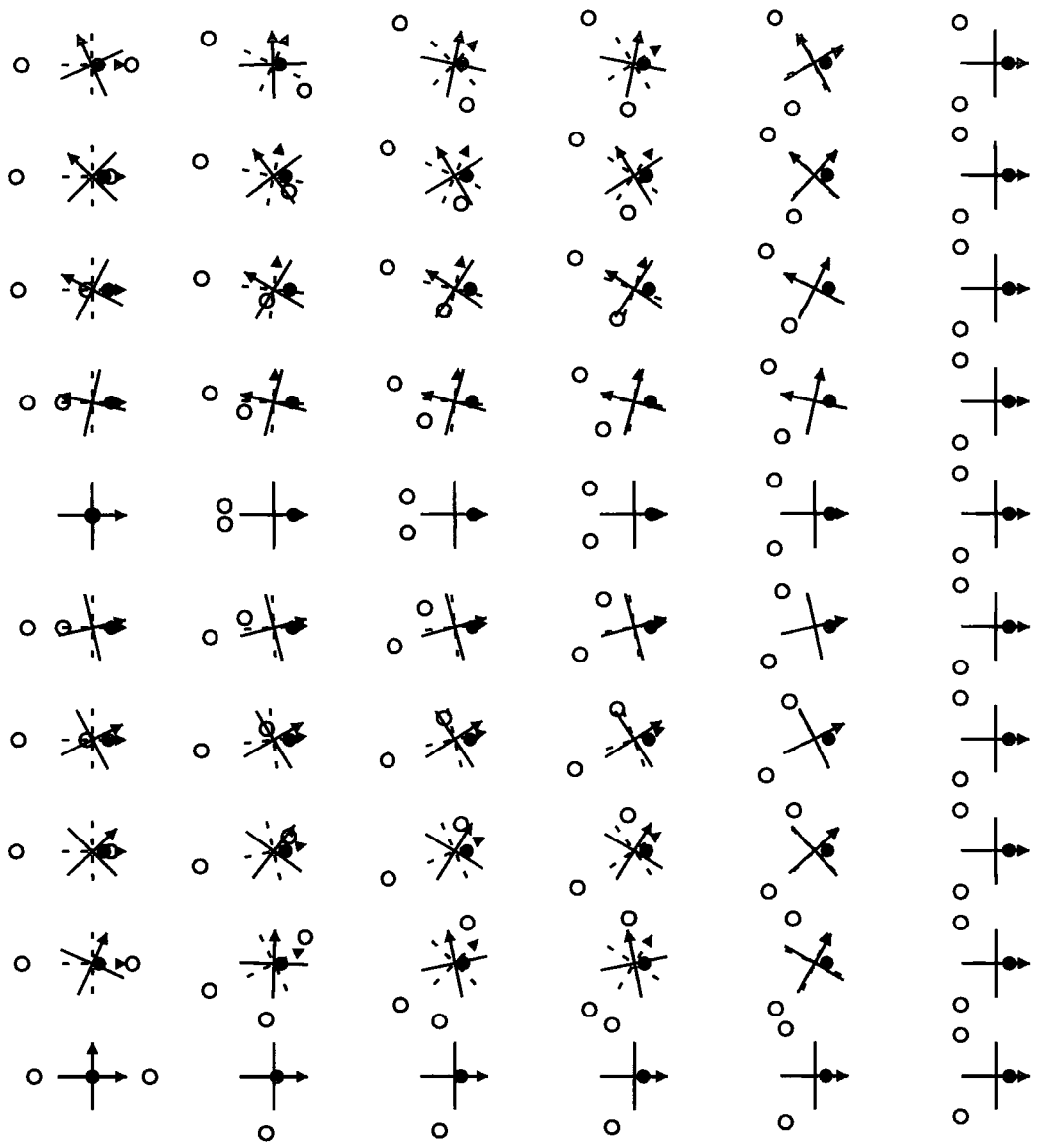

Figure 3.10: Eckart plot for He_2Ne $\chi = 0 \rightarrow 0.875\pi$

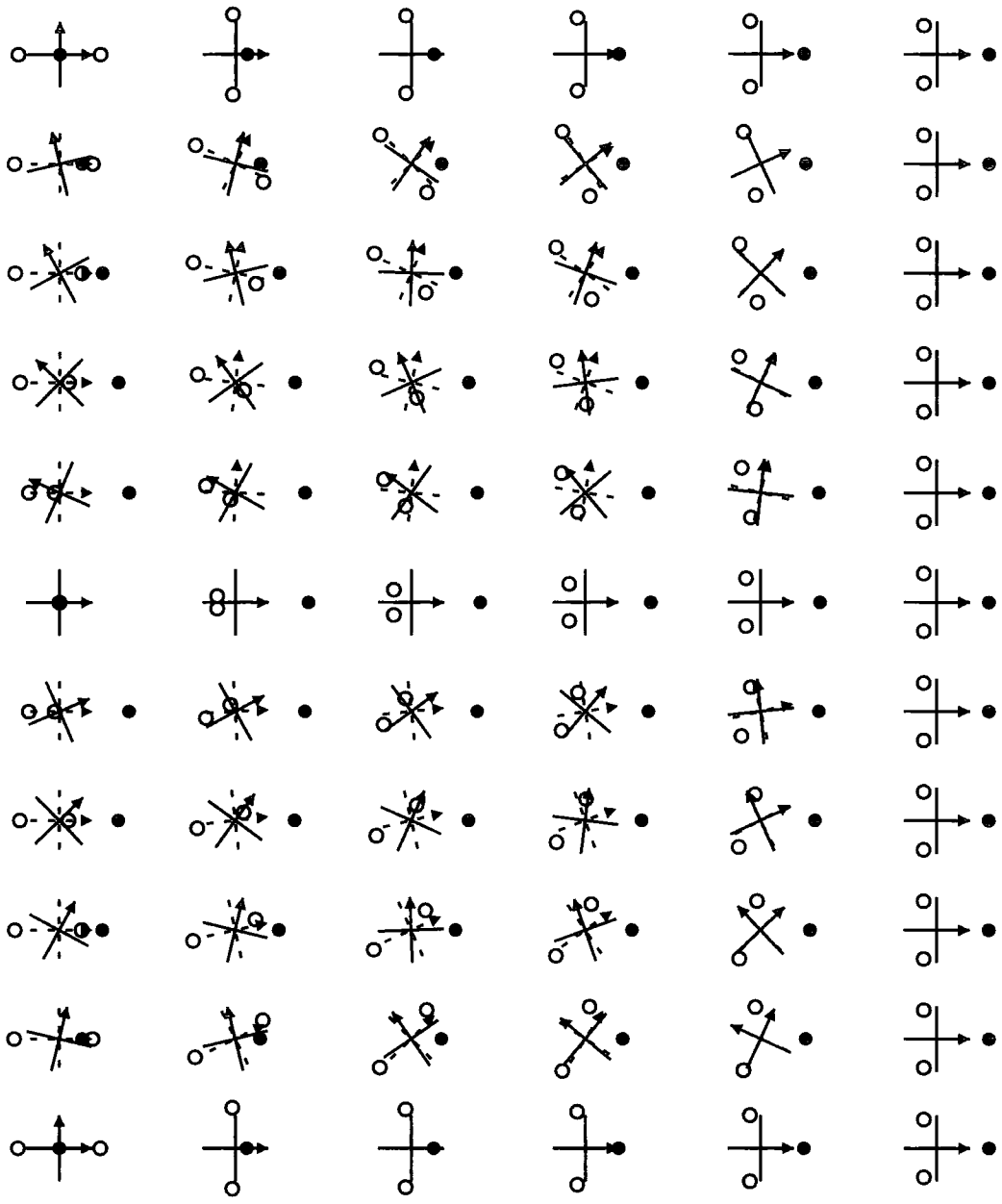

Figure 3.11: Eckart plot for Ar_2Ne $\chi = \pi \rightarrow 2\pi$

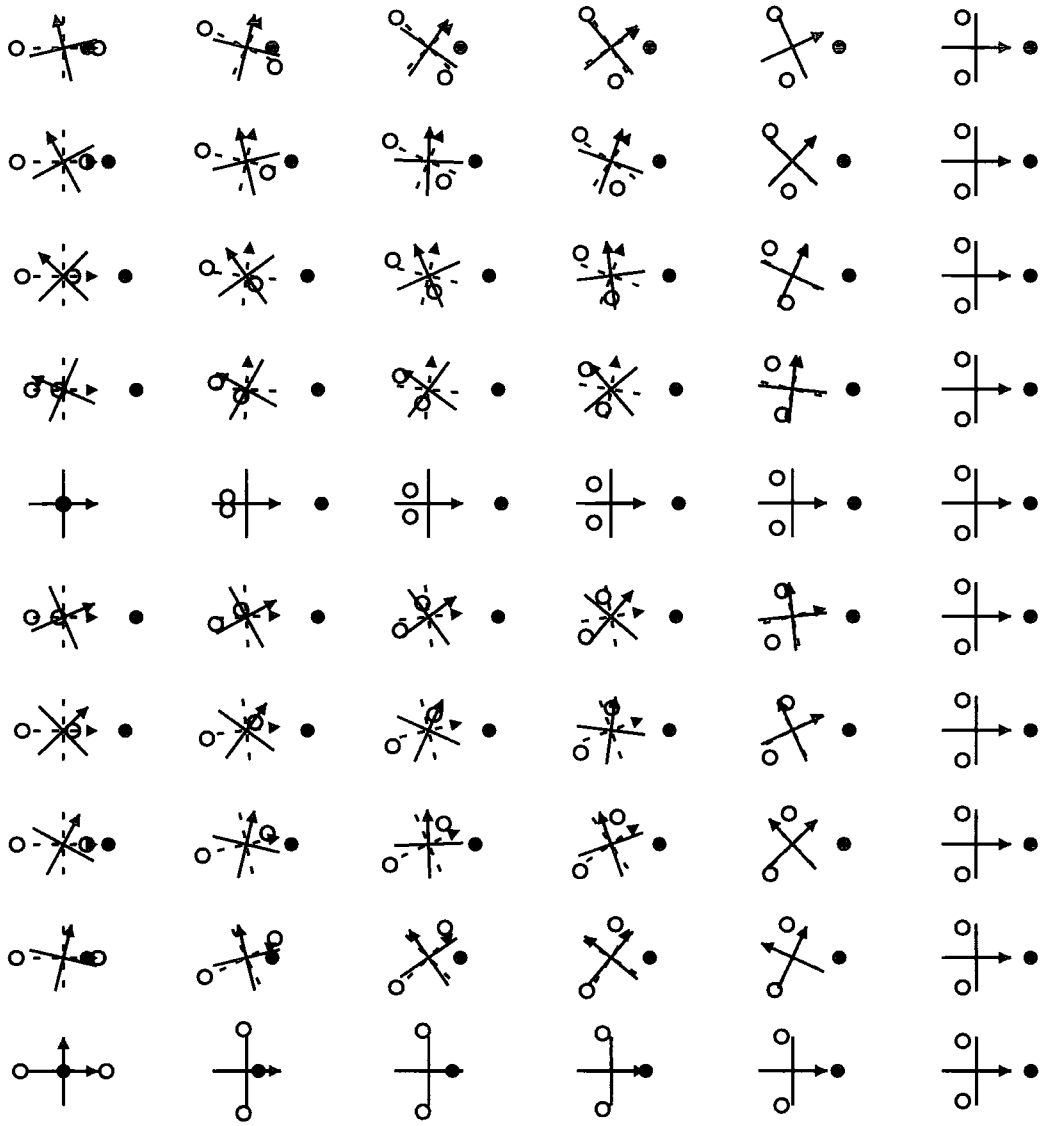

Figure 3.12: Eckart plot for Ar_2Ne $\chi = 0 \rightarrow 0.875\pi$

Chapter 4

The Ar_nN_2 system

4.1 Studying the Ar_nN_2 system

This chapter deals with clusters of the type Ar_nN_2. This work follows on from the work by Bačić et al. [101, 159, 160, 161] on Ar_nHF, and Sperhac et al. [95] on Ar_nCO_2, and more recently [91] Ar_nHCl. Bačić et al. used simulated annealing to search for the minima of a potential energy surface of Ar_nHF. They then calculated the total energy of the system by reducing the problem to five dimensional one, by treating the HF dimer as a quantum object interacting with the static potential of the rare gas cluster. By performing separate calculations of potential energy structures for HF $\nu = 0$ and 1, they were able to calculate the red shift for each system. Their results were in quite good agreement with experiment [159], considering the inherent approximations in the calculation. Sperhac et al studied Ar_nCO_2 by constructing potential energy surface, and then searching for the global minimum using a gradient based searching technique.

The potential energy surface for Ar_nN_2 used here is made by summing over the Ar-N_2 and Ar-Ar interactions in a pairwise additive manner,

$$V_n^{\text{tot}} = \sum_{i=1}^{n} V_{\text{ArN}_2}(R_i\theta_i) + \sum_{i<j}^{n} V_{\text{Ar}_i\text{Ar}_j}(r_{ij}) \tag{4.1}$$

The Ar-N_2 potential energy is a function of two variables, the distance R from the Ar atom to the centre of mass of the N_2 molecule, and the angle θ formed

between the N_2 bond and the vector of length R between the centre of mass of the N_2 and the Ar atom. The minimum of the Ar-N_2 potential is at $\theta = 90^0$, which is described as a 'T shaped' configuration. The Ar-Ar potential is of a simpler form, and only depends on R, the distance between the two Ar atoms. We use simulated annealing in the present work, because for complicated N dimensional surfaces it has proved to be very robust in dealing with the problem of local minima [162, 101, 49, 50, 109].

The Ar-Ar potential [163] (which is of the HFD-C form) is given by

$$V(r) = \varepsilon V^*(x), \tag{4.2}$$

where

$$\begin{aligned} V(x) &= A^* x^\gamma \exp(-\alpha^* x) \\ &- F(x) \sum_{j=0}^{2} c_{2j+6}/x^{2j+6}. \end{aligned} \tag{4.3}$$

The function $F(x)$ is defined as

$$F(x) = \begin{cases} \exp\left[-\left(\frac{D}{x} - 1\right)^2\right] & \text{for } x < D \\ 1 & \text{for } x \geq D \end{cases},$$

where

$$x = r/r_m \tag{4.4}$$

The Ar-N_2 interaction potential is the exchange Coulomb potential [164] of Dham et al., which is written as,

$$E_{\text{int}} = F'(R) E_{\text{HL}}^{(1)} + \Delta E_{\text{c}}. \tag{4.5}$$

Where $E_{\text{HL}}^{(1)}$ is the first-order Heitler-London interaction energy, which can be evaluated using SCF wave functions for the isolated species and then fitted to a functional form. The non-first-order Coulombic interaction ΔE_{C} is modelled by individually damped, overall-corrected, multipole terms in the dispersion energy for the dimer AB. The term ΔE_c term is given by the expression:

$$\Delta E_c = -\left[\sum_{n=3}^{5} C_{2n}(\theta) R^{-2n} f_{2n}(R,\theta)\right] G_{10}(R,\theta). \tag{4.6}$$

The θ dependent functions are defined as:

$$C_{2n}(\theta) = \sum_{l=0}^{n-2} C_{2n}^{2l} P_{2l}(\cos\theta), \tag{4.7}$$

$$f_{2n}(R,\theta) = [1 - \exp\{-A_n S(\theta)R - B_n(S(\theta)R)^2 - D_n(S(\theta)R)^3\}]^{2n} \tag{4.8}$$

and

$$G_{10}(R,\theta) = 1 + 41.34\exp\{-0.8588 S(\theta)R\}, \tag{4.9}$$

where $S(\theta)$ is given by

$$S(\theta) = 7.82/R_{\rm m}(\theta). \tag{4.10}$$

The expression for $R_{\rm m}(\theta)$ is

$$R_{\rm m}(\theta) = \bar{R}_{\rm m}\left(1 + \sum_{i=1}^{n_{\max}} \alpha_{2i} P_{2i}(\cos\theta)\right), \tag{4.11}$$

where $\bar{R}_{\rm m}$ and the α_{2i} are fitted parameters of the potential.
The Heitler-London repulsion term is given by

$$E_{\rm HL}^{(1)} = \exp\left[-R\sum_{i=0}^{2} b_i Z^i\right] \sum_{i=0}^{3} \beta_{2l} P_{2l}(\cos\theta), \tag{4.12}$$

where Z is given by

$$Z = (R - R_0)/(R + R_0)\ , \tag{4.13}$$

where $R_0 = 7.45\ a_0$. The function $F(R)$, from equation 4.5, is replaced in the final version of the potential is replaced with the expression $F' + \Delta F'$, where F' is defined as

$$F' \equiv F'(\theta) = \sum_{l=0}^{l_{\max}} c_{2l} P_{2l}(\cos\theta), \tag{4.14}$$

and the $\Delta F'$ function is

$$\begin{aligned} \Delta F' &= \left[\sum_{l=1}^{3} d_{2l}(\cos\theta)\right] \\ &\times \exp\left[-4.5\times 10^5 \left(\frac{R - R_m(\theta)}{R + R_m(\theta)}\right)^4\right]. \end{aligned} \tag{4.15}$$

The $\Delta F'$ term is highly localised around $R = R_m$ as a function of θ.

4.2 Discussion and Results for the Ar_nN_2 System

In the Ar_nHF system the highly anisotropic nature of the Ar-HF potential energy surface [165] dominates the system [101]. The Ar-HF potential has a deep minimum about the linear Ar-H-F configuration with a second minimum approximately 100 cm^{-1} above the linear Ar-H-F minimum, which has the HF rotated by 180°. This means that the HF molecule always tries to orientate itself so that the hydrogen atom is 'pointing' at as many Ar atoms as possible.

The Ar_nCO_2 system is very different. In the Ar_nCO_2 the first 5 Ar atoms cluster equatorially around the carbon atom, and the next ten Ar atoms cluster around the two oxygen atoms. This leads to many structures with almost identical energies for $n > 5$, as the Ar atoms can add sequentially to either end of the CO_2 molecule. The large number of nearly equivalent structures makes finding the global minimum very difficult. This is not as much of a problem as it first appears though because all that is physically happening is that Ar atoms are sticking to the two oxygen atoms, and the order in which the argon atoms stick to the existing cluster gives rise to clusters with slightly different energies. When the cluster has grown to fifteen atoms, with five around each of the three atoms in CO_2, the next two Ar atoms cap the top and bottom of the $Ar_{15}CO_2$ structure to give the first full solvation shell [95].

The reason for our interest in the Ar_nN_2 system was that it offered an important prototype system that has not been studied. In the case of ArHF the atom-diatom interaction has strongly anisotropic attraction, whereas that for $ArCO_2$ [166][1] has a strongly anisotropic repulsive core. The ArN_2 surface lies somewhere in between these two, and should therefore provide interesting insight into to the effects of the atom-diatom potential energy surface on the clustering around mildly anisotropic diatoms. The Ar_nN_2 system also has a weaker rare gas-molecule interaction than the systems studied previously systems studied. It should thus give a useful insight into the effects of the solvent-solvent interactions in the solvation process.

[1] see [8] for further information on Ar-CO_2 potentials

In all the following discussions the structures of each Ar_nN_2 system $V_{n,m}$, where n is the number of Ar atoms in the cluster and m designates that it is the mth minimum of the system. So $V_{4,1}$ is the global minimum of the Ar_4N_2 system and $V_{4,2}$ is the first low-lying minimum. One other point of notation is that we use the term "low-lying minima" to mean all low-energy minima other than the global minimum. All references in the following discussion to Ar_nHF structures are taken from the Bačić [101] study of the system.

4.2.1 Potentials

The potential energy functions used in the next two chapters are shown below.

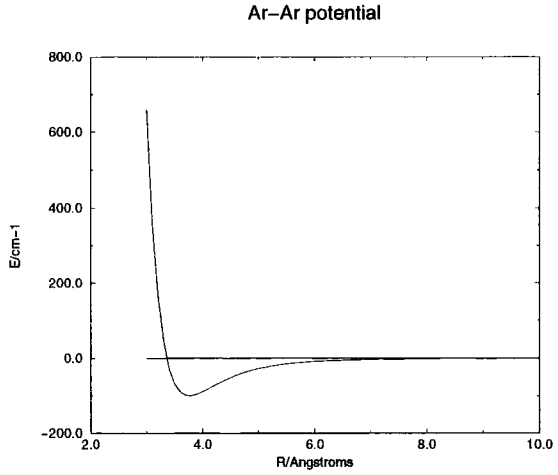

Figure 4.1: Ar-Ar pair potential (in cm^{-1})

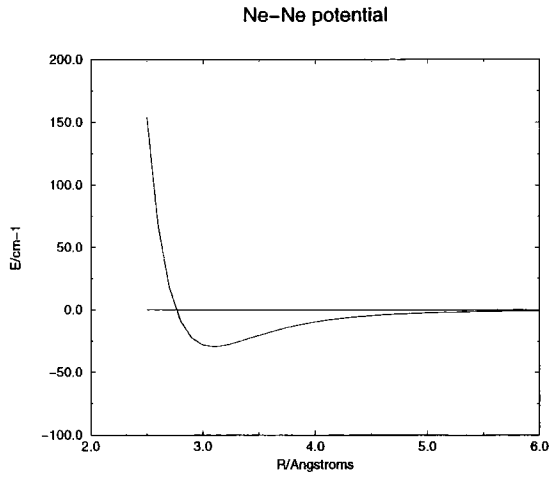

Figure 4.2: Ne-Ne pair potential (in cm^{-1})

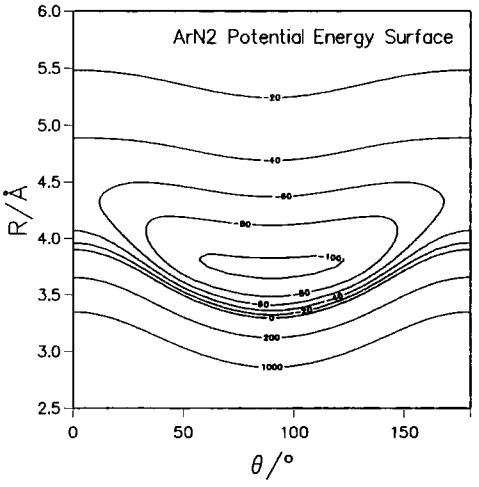

Figure 4.3: Ar-N_2 potential energy surface (in cm^{-1})

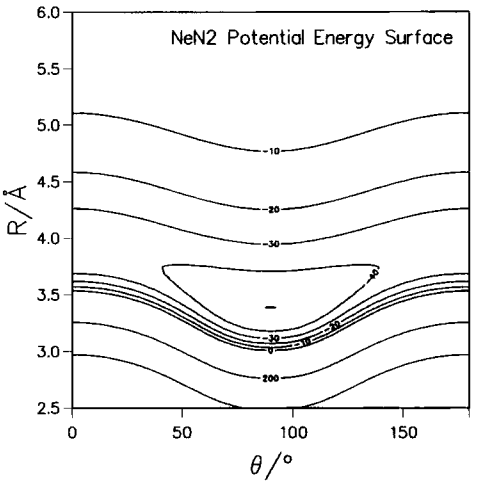

Figure 4.4: Ne-N_2 potential energy surface (in cm^{-1})

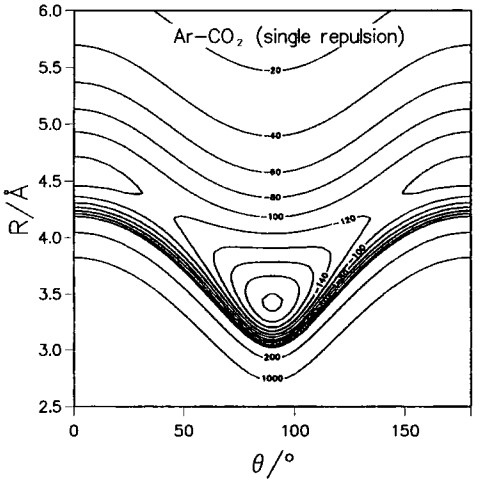

Figure 4.5: Ar-CO_2 potential energy surface (in cm^{-1})

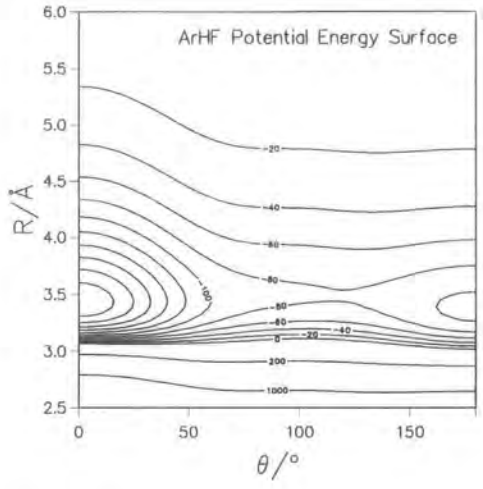

Figure 4.6: Ar-HF potential energy surface (in cm^{-1})

4.2.2 Ar_2N_2

For Ar_2N_2 the two Ar atoms sit equatorially around of the N_2 diatomic. This configuration keeps the Ar atoms in the 'T shape' position relative to the N_2, thus maximising the Ar-N_2 interactions, while allowing the Ar atoms to be separated by their equilibrium distance.

Figure 4.7: Ar_2N_2 $V_{2,1}$ structure

4.2.3 Ar_3N_2

For Ar_3N_2 the lowest-energy structure is a triangle of Ar atoms, with the N_2 molecule lying parallel to the plane of the triangle. This behaviour is different to that of the Ar_3CO_2 system, where the Ar atoms cluster equatorially around the carbon atom. This does not happen in Ar_3CO_2 because the potential energy surface of Ar-N_2 is less anisotropic than that of $ArCO_2$.

The Ar_3N_2 structure is very similar to the $V_{3,1}$ Ar_nHF structure, except that the N_2 lies parallel with the argon triangle, whereas in the Ar_nHF system the HF point at the centre of the triangle. This difference is due to the difference in topology, i.e. the ArHF surface is more anisotropic than that of ArN_2, of the two rare gas-molecule potential energy surfaces. The Ar-HF potential energy surface has a deep minimum about the linear Ar-H-F configuration, whereas the sole minimum in Ar-N_2 potential energy surface is about the 'T-shaped' configuration.

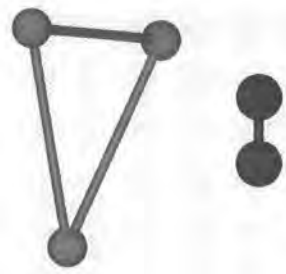

Figure 4.8: Ar_3N_2 $V_{3,1}$ structure

4.2.4 Ar_4N_2

For Ar_4N_2 the $V_{4,1}$ structure is a C_{2v} envelope structure. The $V_{4,2}$ structure is a C_{3v} pyramid. This is interesting because, these two structures were also found in the Ar_4HF. However in Ar_4HF the pyramid structure was found to be the global minimum, and the envelope structure was the first low-lying minimum. The difference in the relative ordering of the Ar cage structures between the two systems is due to the difference in the topology of the two atom-diatom potential

energy surfaces. In the Ar_4N_2 case, the relative isotropy of the potential energy surface leads to a stabilisation of the envelope structure, which allows the N_2 dimer to interact with all the Ar atoms.

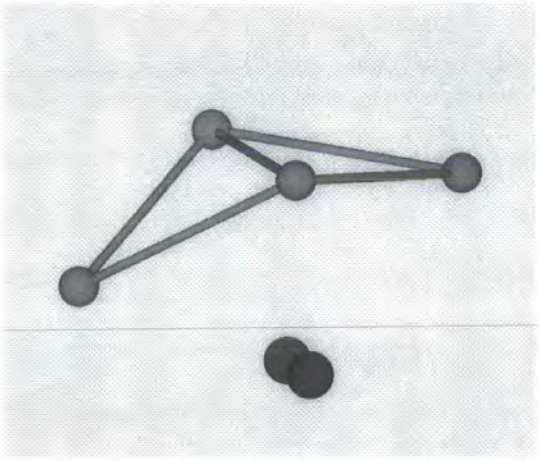

Figure 4.9: Ar_4N_2 $V_{4,1}$ structure

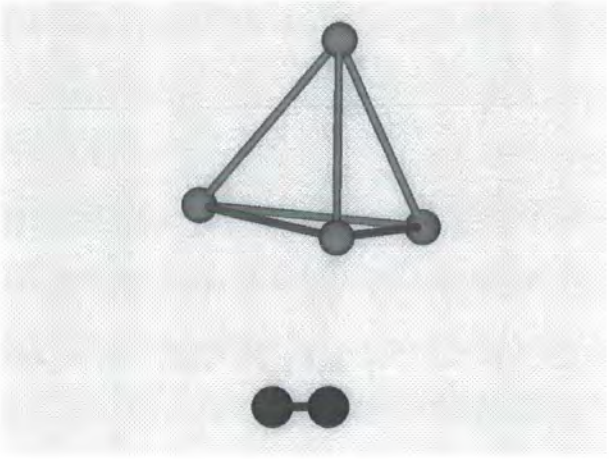

Figure 4.10: Ar_4N_2 $V_{4,2}$ structure

4.2.5 Ar_5N_2

As in the Ar_4N_2 system, we find many of the Ar cage structures for Ar_5N_2 are the same as for Ar_5HF; the relative ordering however is different. Again this

is due to the difference in the two atom-diatom potential energy surfaces. The other significant difference is that the global minimum is a completely different structure to those found in the Ar_5HF system. The global minimum is a pyramid with four Ar atoms in the base, and the N_2 molecule lying parallel to the base of the pyramid. It should be noted that when we describe something as above or below we mean with reference to the top or bottom of the printed figure. So using figure 4.11 for an example, if something is described as 'above' the four atoms in the base of the pyramid it appears further towards the top of the page than the ring of atoms; conversely if something is describe as 'below' the ring it appears towards the bottom of the page. The $V_{5,2}$ structure is a pentagon with one of the vertices missing, and the fifth Ar atom sitting above the four atoms in the base. This Ar cage structure sits above the N_2, with the N_2 directly below the top capping Ar atom. This structure allows the N_2 to interact with all five Ar atoms. In doing so, though, it reduces the Ar-Ar interaction in comparison to the $V_{5,1}$ structure. The $V_{5,3}$ structure is a $V_{4,1}$ structure with a capping Ar atom, which forms a pyramid. The $V_{5,4}$ structure is a pyramid structure, with one of the faces of the pyramid capped. The interesting point about these low-lying minima is that they are the same structures found for Ar_5HF ($V_{5,1-3}$). However in Ar_nN_2 system their positions are reversed. This shows yet again the effect the different potential energy surface on the clusters formed.

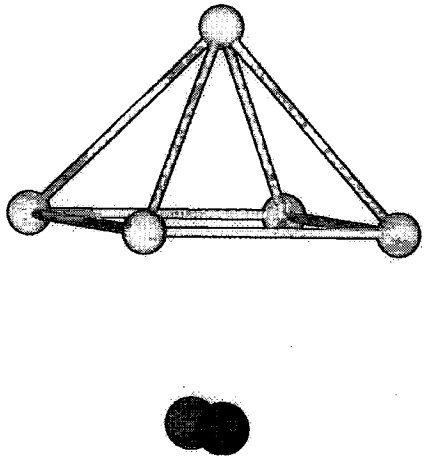

Figure 4.11: Ar_5N_2 $V_{5,1}$ structure

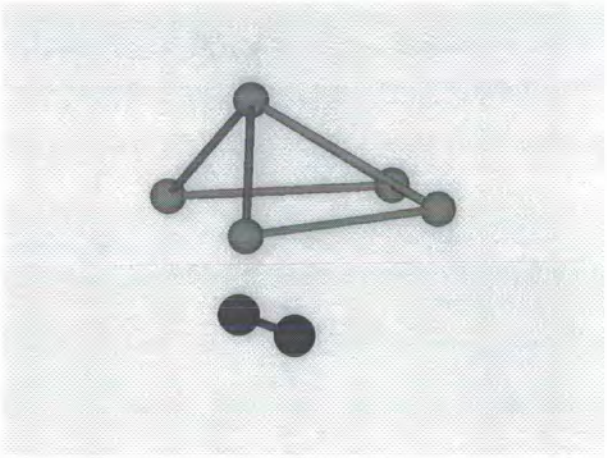

Figure 4.12: Ar_5N_2 $V_{5,2}$ structure

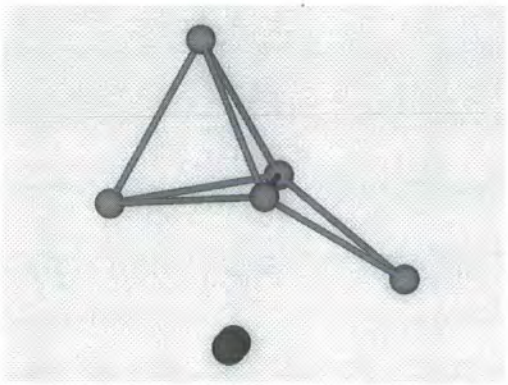

Figure 4.13: Ar_5N_2 $V_{5,3}$ structure

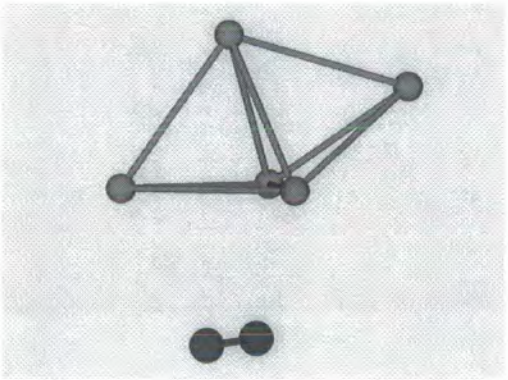

Figure 4.14: Ar_5N_2 $V_{5,4}$ structure

4.2.6 Ar_6N_2

The global minimum is a bipyramidal structure, which can be seen to arise from capping the two top faces of the $V_{4,1}$ envelope structure. The first-low-lying minimum is a capped pentagon structure, with the sixth atom capping the C_{5v} axis above the ring of atoms. Interestingly the first two minima are the same as found in Ar_6HF. This similarity between the two systems is unusual, as the previous Ar_nN_2 structure were usually different from those of the corresponding Ar_nHF system. It results from the fact that the pentagon structure allows fewer Ar-Ar interactions, and neither dimer interacts strongly enough with the argon cage to overcome the inherent unfavourability of the capped pentagon structure. Bačić et al. only discuss these two structures for Ar_6HF, as the next lowest minimum is 100 cm^{-1} above the global minimum. In the Ar_6N_2 system, however, there are several low-lying minima due to the relative isotropy of the Ar-N_2 potential energy surface, and the similarity in the Ar-Ar and Ar-N_2 interaction strengths. The $V_{6,3}$ structure is a face-capped four-atom-based pyramid $V_{5,1}$ structure. The $V_{6,4}$ structure is a $V_{5,2}$ structure with an Ar atom capping one of the top faces, and forming a pyramid with the three Ar atoms in the structure below it. It actually caps the completed 'back' side of the part completed pentagon ring, because this part of the ring is most ridgely bound part of the argon substructure. This means that the argon atoms hold each other closer to their equilibrium distance, which leads to the capping atom interacting slightly more strongly with the three atoms it interacts with. The $V_{6,5}$ structure is like the $V_{6,4}$ structure in that it is a derivative of the $V_{5,2}$ structure. In this case though the capping atom sits below the $V_{5,2}$ structure and interacting with the N_2 in a 'T shaped' configuration. This forms a semi-circular cage structure around the nitrogen dimer. There are other structures based on capped versions of the $V_{5,2}$ structure, but they were out side the energy range of interest. The $V_{6,6}$ structure is a pyramid with two faces capped to form pyramids themselves.

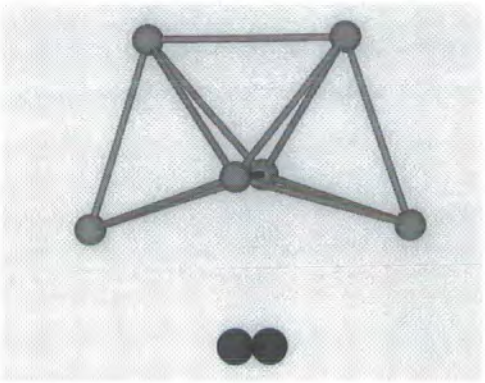

Figure 4.15: Ar_6N_2 $V_{6,1}$ structure

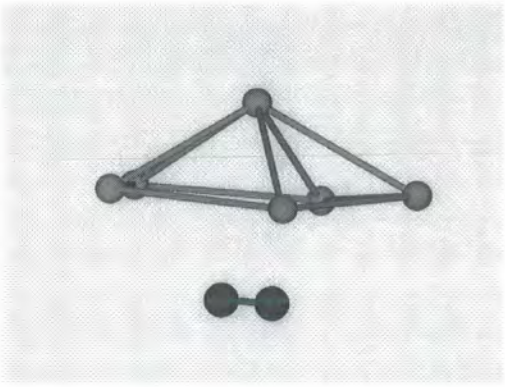

Figure 4.16: Ar_6N_2 $V_{6,2}$ structure

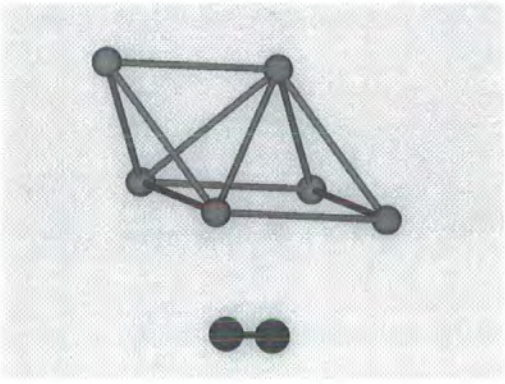

Figure 4.17: Ar_6N_2 $V_{6,3}$ structure

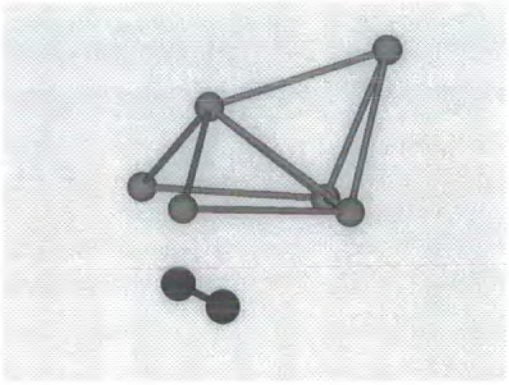

Figure 4.18: Ar_6N_2 $V_{6,4}$ structure

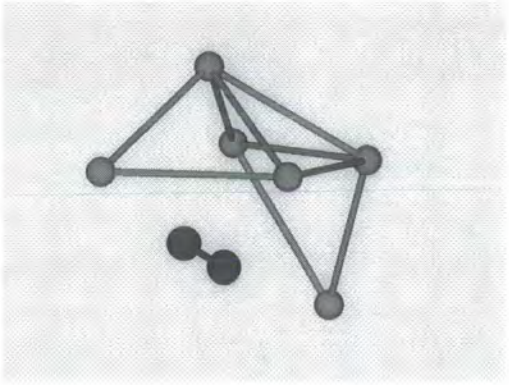

Figure 4.19: Ar_6N_2 $V_{6,5}$ structure

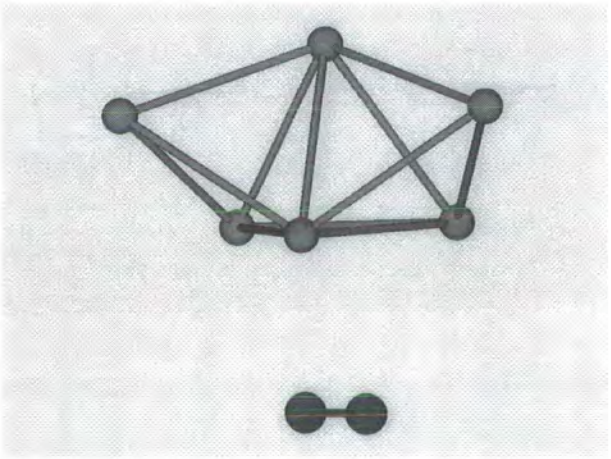

Figure 4.20: Ar_6N_2 $V_{6,6}$ structure

4.2.7 Ar_7N_2

The structures for $V_{7,1}$ and $V_{7,2}$ are both based on the bipyramidal $V_{6,1}$ structure. The global minimum has the seventh Ar atom added in below the Ar_6 structure, interacting with the N_2 in a 'T shaped' manner, and forms a second envelope ($V_{4,1}$) structure around the N_2. The first low-lying minimum has the seventh Ar atom capping one of the upper face of the bipyramidal structure. As can be seen from table 4.1, these two structures are very close in energy with ΔE approximately 1 cm^{-1}. That $V_{7,1}$ and $V_{7,2}$ are so similar to each other, in terms of both energies and structures, means that a cluster can easily convert between the two structures. The next low-lying minimum $V_{7,3}$ is interesting, because it does not appear in the Ar_7HF system. The $V_{7,3}$ structure is based on the four-atom-based pyramid, $V_{5,1}$, structure with one of the extra Ar atoms added below the base, interacting with the N_2 in a 'T-shaped' manner. The remaining argon atom sits on the side face of the $V_{5,1}$ structure, and above the argon atom that is interacting with the N_2. These two capping atoms in effect forms a second slightly distorted $V_{5,1}$ structure. Yet again the relative stability of this structure in comparison to its Ar_7HF counterpart illustrates the dramatic effect of the different atom-diatom potential energy surface. The $V_{7,4}$ structure is the pentagonal structure of $V_{6,2}$, with the seventh Ar atom added below the argon cage to form an envelope structure with three of the Ar atoms on the base of the pentagon subunit. It is interesting to note that the structures of this system show how finely balanced it is. There is a very small difference in energy between adding the last so that it interacts solely with the argon cage, or with both the cage and the N_2 molecule.

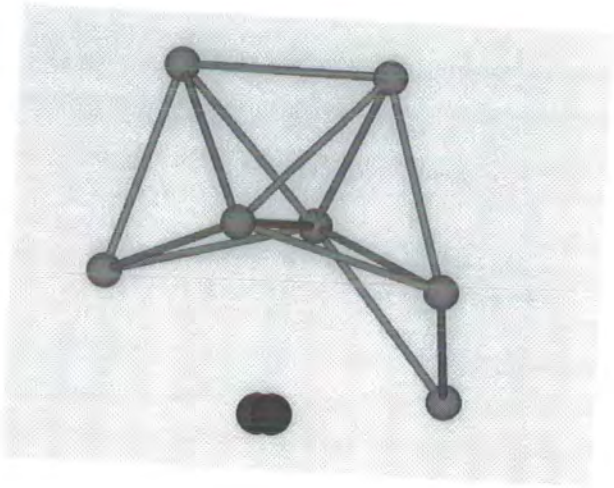

Figure 4.21: Ar_7N_2 $V_{7,1}$ structure

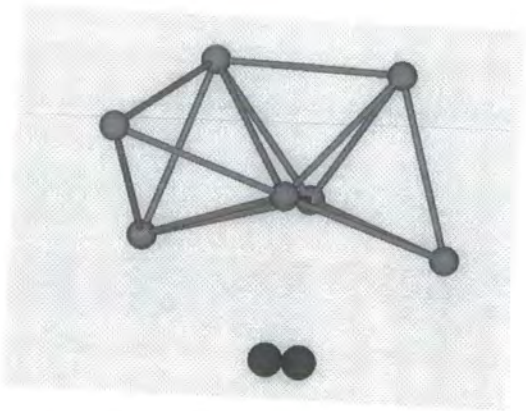

Figure 4.22: Ar_7N_2 $V_{7,2}$ structure

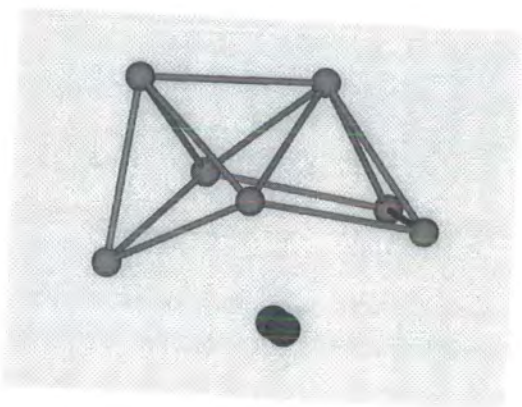

Figure 4.23: Ar_7N_2 $V_{7,3}$ structure

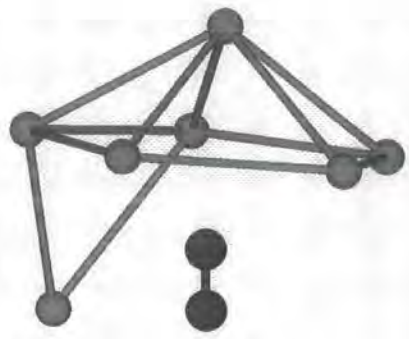

Figure 4.24: Ar_7N_2 $V_{7,4}$ structure

4.2.8 Ar_8N_2

The global minimum, $V_{8,1}$, is a new structure, that can be thought of as an extension of the $V_{5,2}$ structures. As we shall see later, it is the first example of a structure that will come to dominate the high n clusters. It is the precursor to a series of pure Ar_n structures which we will see as the size of the clusters increases. It has four atoms in a part formed pentagon base, that are capped by a single Ar atom sitting above them on the C_{5v} axis of the part formed pentagon. There are then three more Ar atoms which lie above the first capping atom, and parallel to the four atoms in the base. The four atoms in the base however do not form a square, and is best thought of as having a structure of a pentagon base with one of the atoms removed. This means that two of the Ar are splayed out, and thus allow the N_2 to get nearer the middle argon atom. In fact the distance of the middle argon atom to the centre of mass of the N_2 is 3.513 Å, which is almost exactly the equilibrium distance of the Ar-N_2 potential. The structure of $V_{8,1}$ clearly indicates that we have a finely balanced interplay between the Ar-Ar interaction and the Ar-N_2 interaction. The balance between these two interactions will become more important in determining the ordering of structures as n increases.

The global minimum is $\approx$ 1 cm^{-1} below $V_{8,2}$, and $\approx$ 2 cm^{-1} below $V_{8,3}$.

This is very different behaviour to that of the Ar_8HF system, or indeed any of the Ar_nHF systems, where the gap between the global minimum and the first few low-lying minima was always larger. The closeness of minima in the Ar_nN_2 systems makes it harder to search the potential energy surface. As the surface becomes flatter and more subtle, it becomes easier for a simulated annealing search to pass through a minimum without staying in it. This problem is overcome by using a large number of starting positions. The simulated annealing can be supplemented by carefully chosen searches of the potential energy surface using a gradient-based search method to make sure that certain structures that might be the global minimum or a low-lying minimum have not been missed by the simulated annealing searches.

The first two low-lying minima have the same Ar_6 bicapped bipyramidal structure, with the two capping-atoms capping adjacent face on one side of the bipyramidal Ar_6 substructure, and are separated by $\Delta E = 0.7$ cm^{-1}. The difference between the two structures is that in $V_{8,2}$ the N_2 molecule lies on a line with the bicapped end of the Ar_8 cluster; whereas in $V_{8,3}$ the N_2 molecule is rotated by about 90°. The effect of this, and the reason for the difference in the energy of the two structures, is that the N_2 dimer to get slightly closer to the underside of the Ar cluster in the $V_{8,2}$ structure, thus increasing the Ar-N_2 interaction slightly. This situation does not occur in the Ar-HF system, because of the more anisotropic nature of the Ar-HF interaction. The $V_{8,4}$ structure is a bicapped $V_{6,2}$, i.e. a bicapped pentagon structure, where the capping atoms cap adjacent faces of the $V_{6,2}$ structure. The $V_{8,5}$ structure has the same Ar_6 pentagon-based pyramid structure as the $V_{8,4}$ structure, but with the two capping atoms moved beneath the Ar_6 structure. This structure can be thought of as the beginnings of an icosahedral cage.

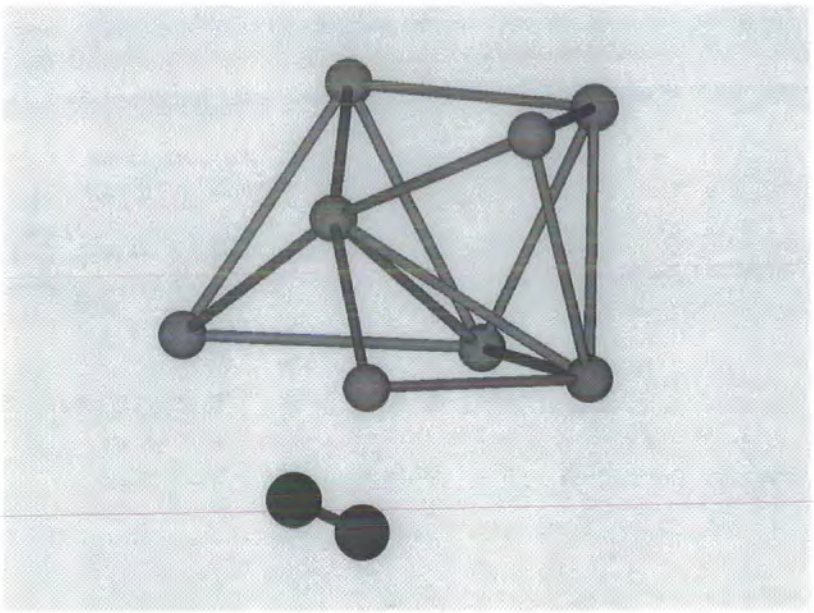

Figure 4.25: Ar_8N_2 $V_{8,1}$ structure

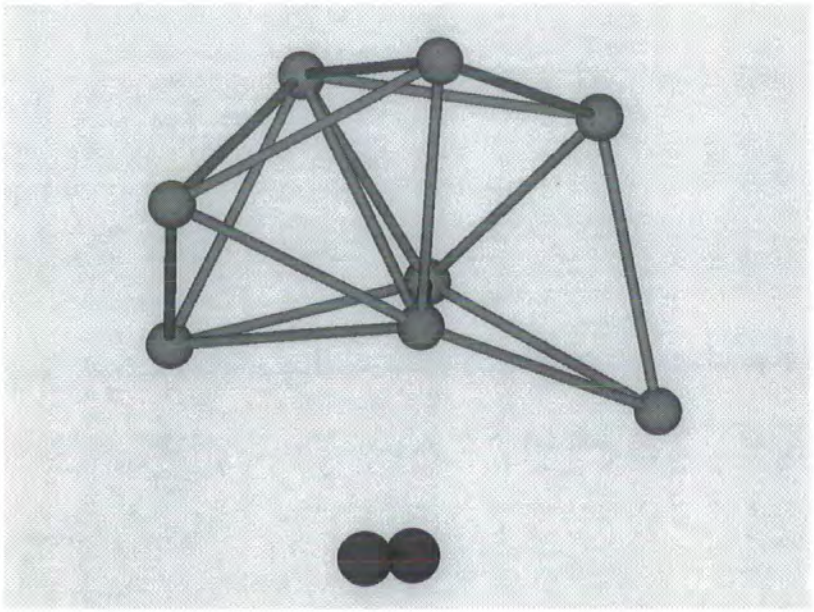

Figure 4.26: Ar_8N_2 $V_{8,2}$ structure

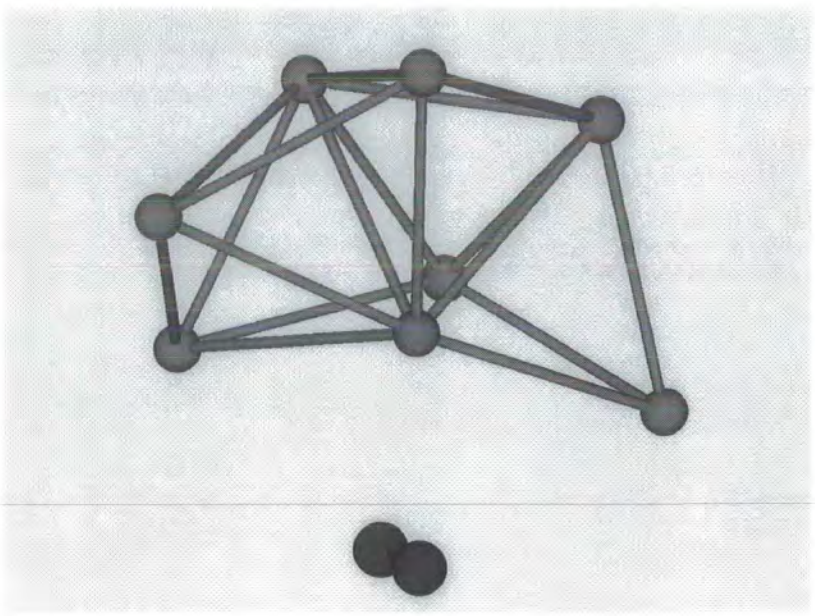

Figure 4.27: Ar_8N_2 $V_{8,3}$ structure

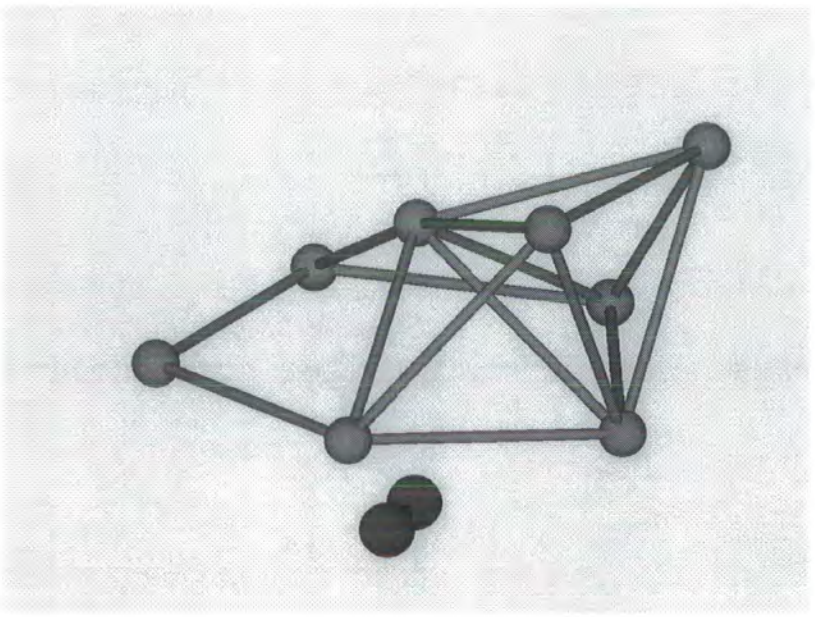

Figure 4.28: Ar_8N_2 $V_{8,4}$ structure

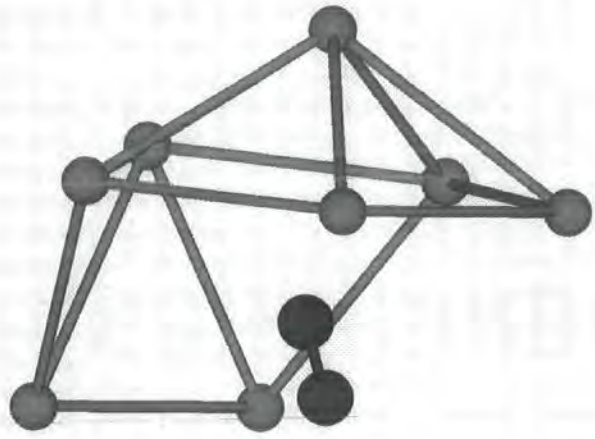

Figure 4.29: Ar_8N_2 $V_{8,5}$ structure

4.2.9 Ar_9N_2

In the Ar_nHF system, $n = 9$ is the point at which the lowest energy structure first has the HF inside a part-formed Ar icosahedral cage. In the Ar_nN_2 system however this does not happen. Yet again we find several structures that are similar in energy, due to the small difference between the interaction strengths of Ar-Ar and Ar-N_2 potentials. The global minimum is a capped version of the Ar_8N_2 global minimum, with the capping Ar atom sitting above the atom which is in-between the two rings of atoms in the $V_{8,1}$ structure. This structure shows clearly that the Ar-Ar interaction is coming to dominate the high n structures, because from the $V_{8,1}$ structure it can be see that an alternative structure would have the top Ar atom down in the four-atom base of the $V_{8,1}$ Ar structure. However this alternative structure is found to be energetically less favourable. What we are really seeing here is that the Ar-Ar interaction is stronger than that for Ar-N_2 except when θ is close to 90°, 'T shaped'. As there are only a few sites were the Ar atom is in a 'T shaped' configuration this means the Ar must choose between an Ar-Ar interaction or a non 'T shaped' Ar-N_2 interaction, and thus the Ar atom adds

to the Ar cage rather than sitting somewhere around the N_2. Taking this into account we should expect to see the global minimum of the higher n clusters look more and more like the structures found for pure Ar_n cages. The first low-lying minimum has all three Ar atoms capping faces on one side of the $V_{6,1}$ Ar_6 subunit. The $V_{9,3}$ structure has the same Ar structure as that of the global minimum, but this time the N_2 lies across the σ_v symmetry plane of the Ar cage instead of along it. This structure will be discussed in more detail later. The $V_{9,4}$ structure is a tricapped version of the $V_{6,2}$ pentagon based structure with three Ar atoms capping adjacent faces of the pentagonal pyramid, which was previously described above as a possible alternative for the global minimum. The $V_{9,5}$ structure is a part-formed icosahedron, which is the minimum energy structure for Ar_9HF.

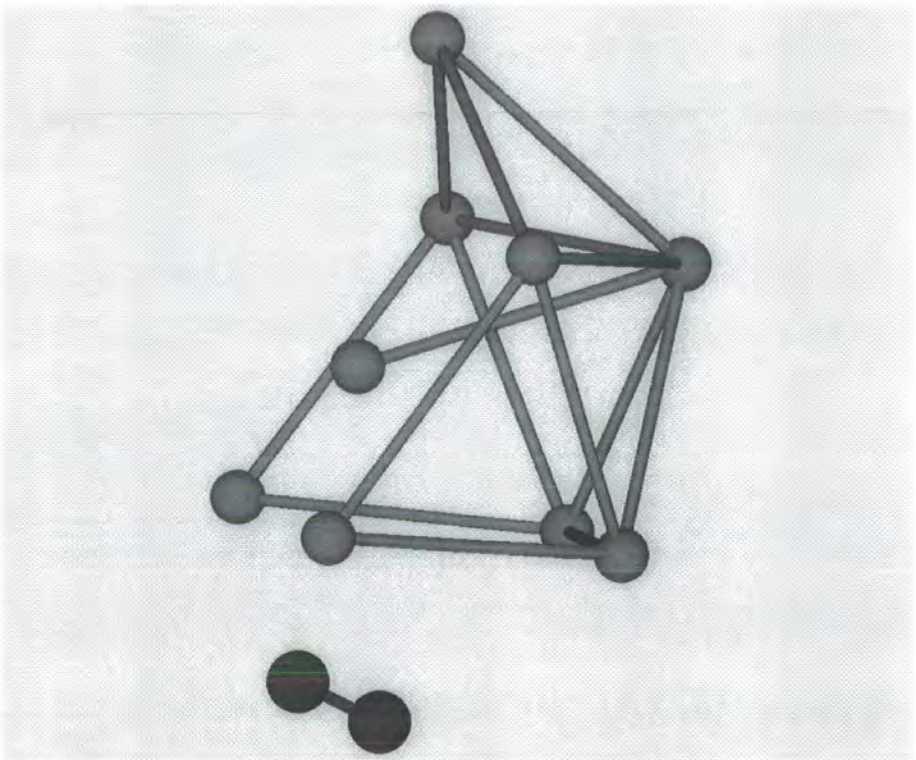

Figure 4.30: Ar_9N_2 $V_{9,1}$ structure

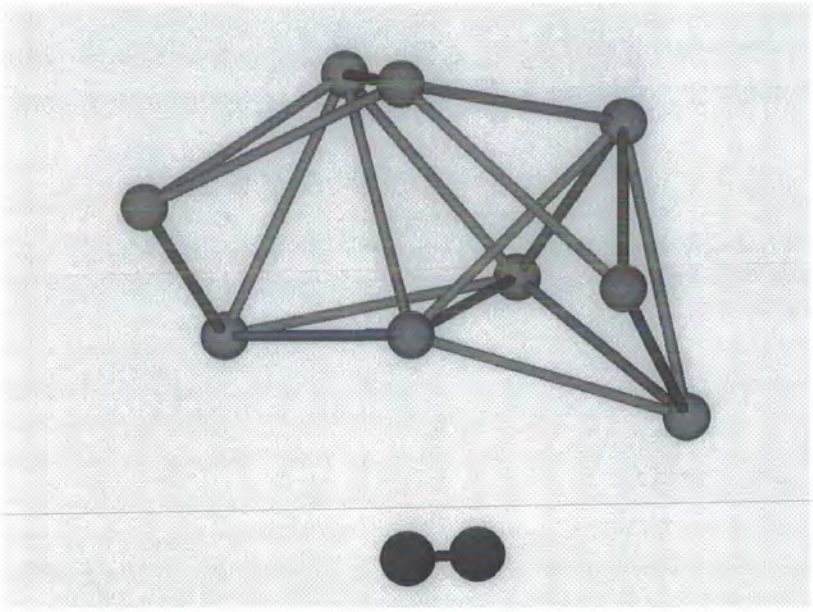

Figure 4.31: Ar_9N_2 $V_{9,2}$ structure

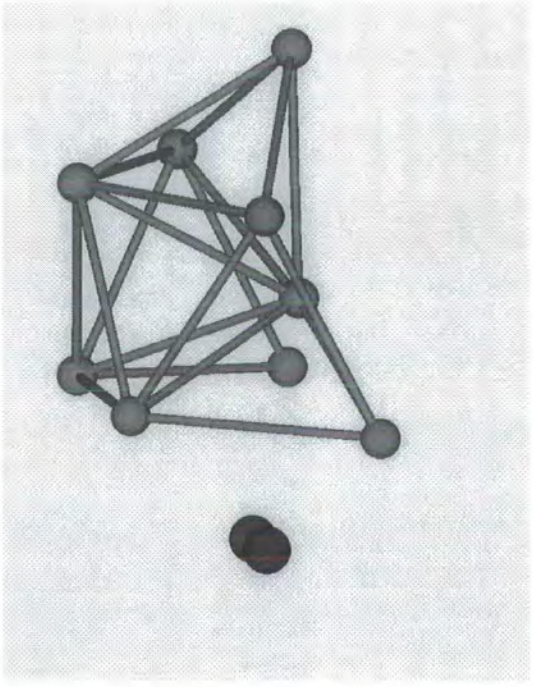

Figure 4.32: Ar_9N_2 $V_{9,3}$ structure

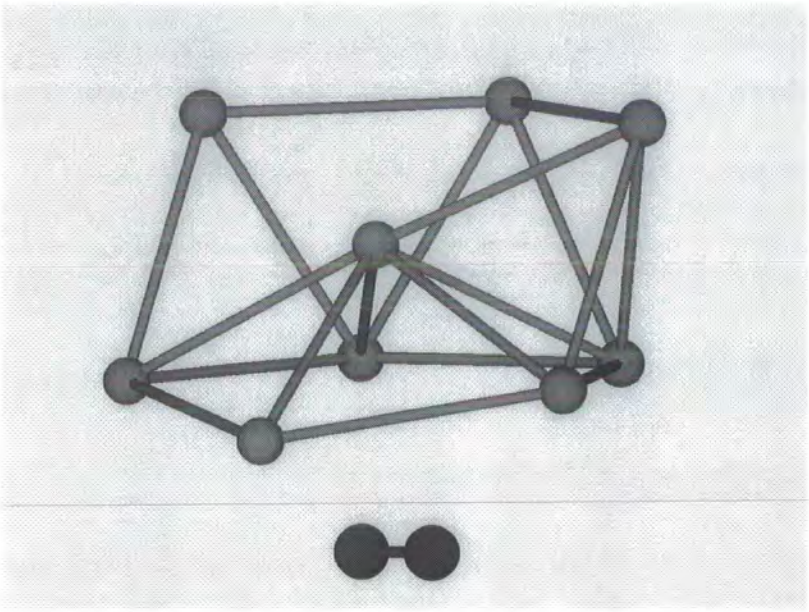

Figure 4.33: Ar_9N_2 $V_{9,4}$ structure

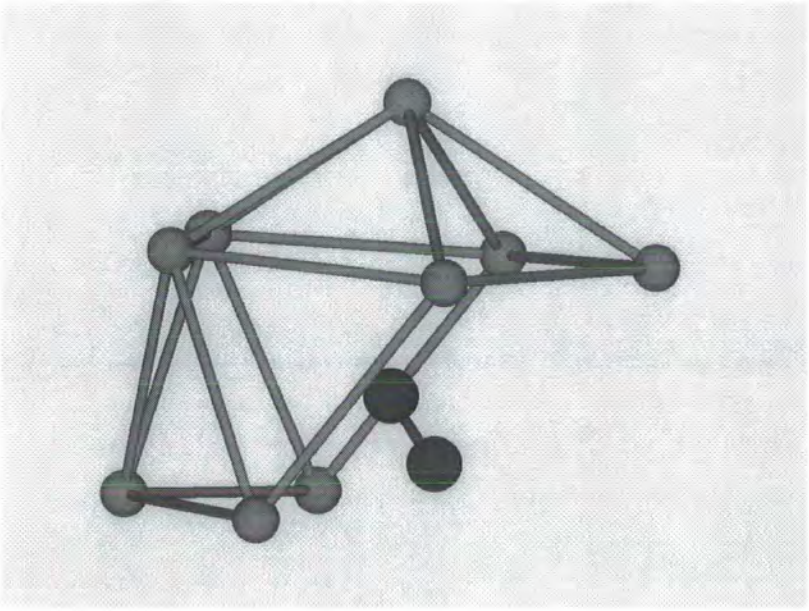

Figure 4.34: Ar_9N_2 $V_{9,5}$ structure

4.2.10 $Ar_{10}N_2$

In the $V_{10,1}$ structure the Ar cage is like that of the $V_{9,1}$ structure with the tenth Ar atom adding to the upper ring of argon atoms, and the N_2 under the Ar cage. Again we could imagine the tenth atom moving down into the lower layer of Ar atoms, which lies above the N_2, but again the Ar-Ar interaction is too strong. We will see later that the pentagon structure is again higher in energy. The $V_{10,2}$ and $V_{10,3}$ structures are based on the six atom pentagonal pyramid $V_{6,2}$ structure. The $V_{10,2}$ structure has three Ar atoms capping adjacent to each other, with the forth Ar atom sitting above the top atom of the pentagonal pyramid. The $V_{10,3}$ structure is simpler, with the four remaining Ar atoms capping the four adjacent faces of the Ar_6 subunit. The $V_{10,4}$ structure is the part-formed icosahedral cage, which was the minimum energy structure for $Ar_{10}HF$. As we can see from the above discussions the behaviour of the Ar_nN_2 system is very different from that of the Ar_nHF system, in which for $n > 9$ the minimum-energy structure is a part-formed icosahedral cage. The reason for this difference is that the maximum Ar-HF interaction is approximately twice that of Ar-Ar whereas the maximum Ar-N_2 interaction is approximately the same as that of the Ar-Ar; if the Ar-N_2 is not near the 'T shape' configuration the Ar-N_2 interaction is weaker than that of Ar-Ar. This means that in Ar_nHF structures which preferentially maximises the Ar-HF interaction are energetically favoured, over those which preferentially maximise the Ar-Ar interaction. This leads to the icosahedral cage (and other cage) structures having the lowest energy. In the Ar_nN_2 system this is not true as there is no one interaction that is predominant.

Interestingly, although the Ar-Ar interaction can clearly be seen as the dominant interaction, the structures are still not those of the equivalent pure Ar_n system. This is an illustration that we are dealing with a very finely balanced system, with a potential energy surface that is much more complicated.

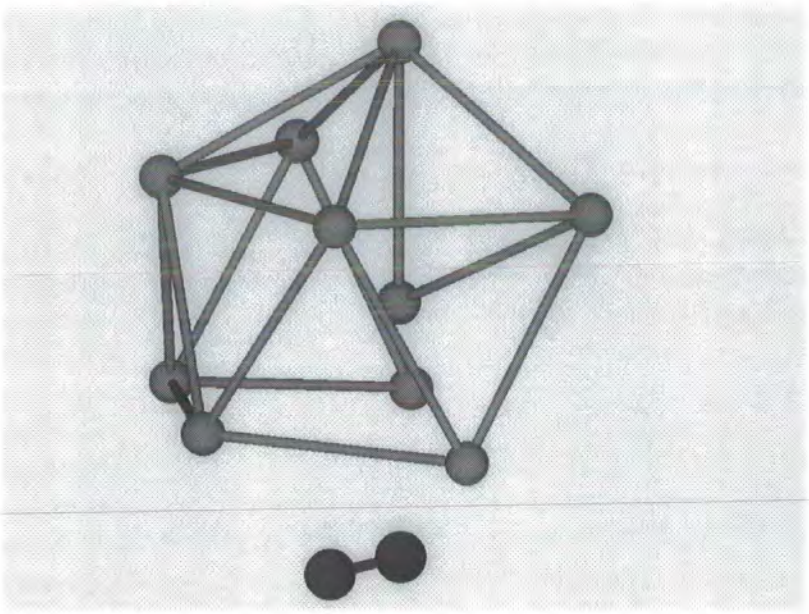

Figure 4.35: $Ar_{10}N_2$ $V_{10,1}$ structure

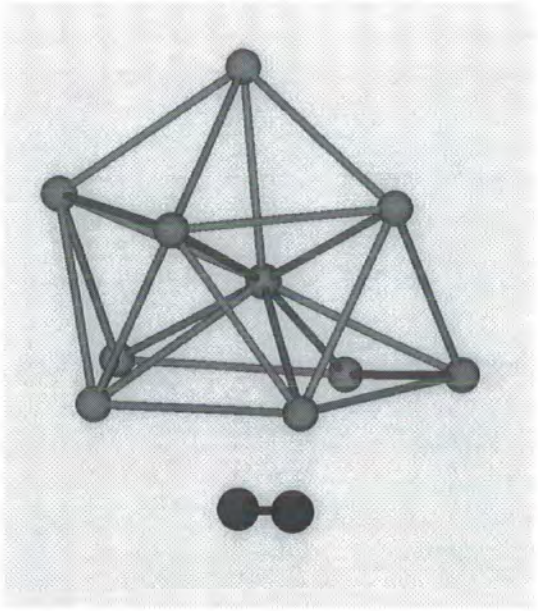

Figure 4.36: $Ar_{10}N_2$ $V_{10,2}$ structure

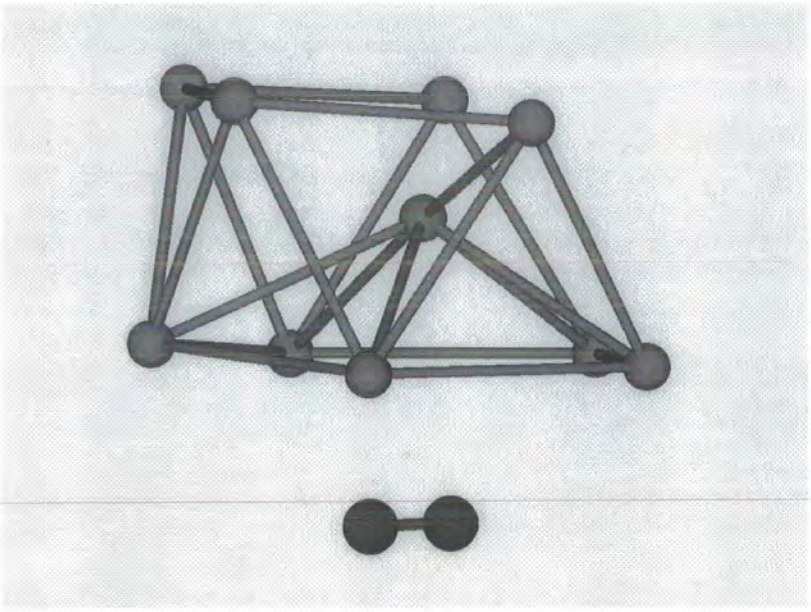

Figure 4.37: $Ar_{10}N_2$ $V_{10,3}$ structure

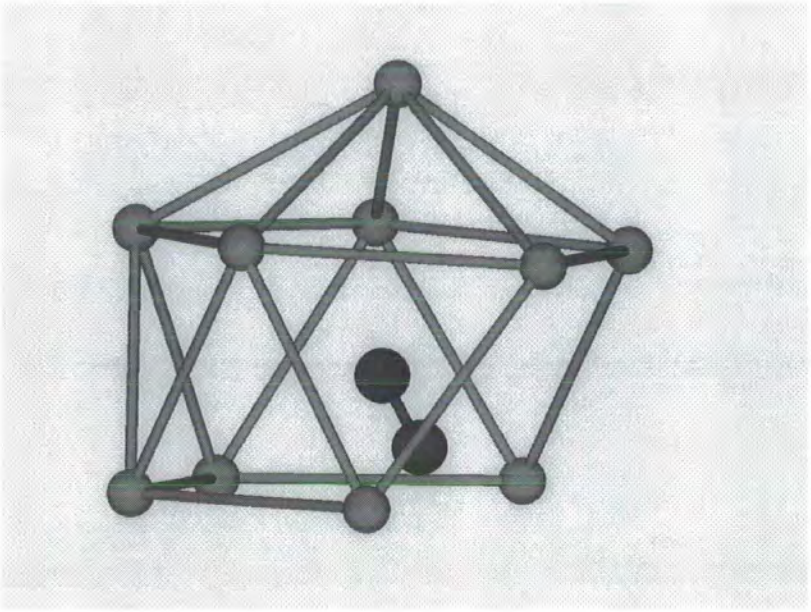

Figure 4.38: $Ar_{10}N_2$ $V_{10,4}$ structure

4.2.11 $Ar_{11}N_2$

The global minimum structure for $Ar_{11}N_2$ is similar to the pure Ar_{11} minimum structure, with the N_2 sitting underneath the Ar cage. This structure obviously follows on from the $V_{9,1}$ and $V_{10,1}$ structures. The structure of the first low-lying minimum has the same argon cage as the global minimum, and the N_2 still sits under the Ar cage. The difference in the two structures is due the orientation of the N_2 with respect to the Ar cage. In the global minimum the N_2 lies parallel to the σ_v plane of the Ar_{11} cage, and will be denoted the $\parallel$ structure. In the first low-lying minimum the N_2 lies across the σ_v plane, and will be denoted the $\perp$ structure. The difference in energy between these two configurations is due to the fact that the $\parallel$ structure allows the N_2 to interact more favourably with the Ar atoms in the base ring, because the N_2 can interact in a near 'T shaped' manner with the two Ar atoms at the open end of the lower ring. The N_2 can also interact more strongly with the Ar atom in-between the two Ar rings in the $\parallel$ structure that in the $\perp$ structure, as the N_2 can get slightly nearer to the middle Ar atom in the $\parallel$ structure. This is clearly shown by the values of the Ar-N_2 interaction energy in the two structures. The Ar-N_2 interaction energy for the $\parallel$ structure is -530 cm^{-1}, compared to -505 cm^{-1}. This is actually larger that the energy difference between the two structures. The difference is made up by the fact that the Ar-Ar interactions for the two structures are -3175 cm^{-1} for the $\parallel$ structure, and -3189 cm^{-1} for the $\perp$ structure. This is very interesting, because it means that in the $\parallel$ structure the Ar cage is distorted slightly to maximise the Ar-N_2 interaction. This is quite unusual as distorting the cage reduces the Ar-Ar interaction, yet as we have already seen the Ar-Ar interaction is dominating the larger Ar_nN_2 clusters. This clearly shows that the Ar_nN_2 system is a far more subtle system that Ar_nHF system. The structures are determined by a balance of competing forces. In the main the Ar-Ar interaction is the dominant force determining the structures of the Ar_nN_2 system, but it is far from being a one sided race.

An interesting question to ask is why we did not see the $\parallel$ and $\perp$ structures in

the $Ar_{10}N_2$ or Ar_8N_2 systems, which both have Ar cages which could support these structures. To understand why this is so we have to think about what happens when we find a structure. In finding a structure we search a potential energy surface looking for minima in the surface. When we find a well in the potential energy surface we find the bottom of the well and the associated structure. We have found two structures that are very similar to each other. This means that we have two wells in the local parameter space. The fact that the search routine becomes trapped in the $\perp$ structure well and does not escape to find the $\parallel$ structure well means that the there is no downhill path connecting the two wells. In the $Ar_{10}N_2$ and Ar_8N_2 systems we appear not to have a second well in which to become trapped.

This effect was studied further by starting from the $V_{11,2}$ structure, and removing one atom in the top ring to give a $Ar_{10}N_2$ version of the $V_{11,2}$ structure. We then used a gradient-based technique to find the local minimum. We found that the search routine travelled in parameter space to the $V_{10,1}$ structure. A similar investigation of the Ar_8N_2 system showed the same result, with the search returning to the $V_{8,1}$ structure. This suggests that in these systems there is no second minimum. It is very surprising that the Ar_8N_2 and $Ar_{10}N_2$ systems have such different behaviour to the Ar_9N_2 and $Ar_{11}N_2$ systems.

The $V_{11,3}$ structure has a $V_{6,2}$ capped pentagon substructure with four Ar atoms capping the upper faces of the $V_{6,2}$ structure, and the eleventh Ar atom sitting above the top atom of the pentagonal pyramid. The $V_{11,4}$ structure has the same $V_{6,2}$ substructure, but this time all the five upper faces are capped. The $V_{11,5}$ structure is that of the part-completed icosahedral cage, which was the global minimum for $Ar_{11}HF$.

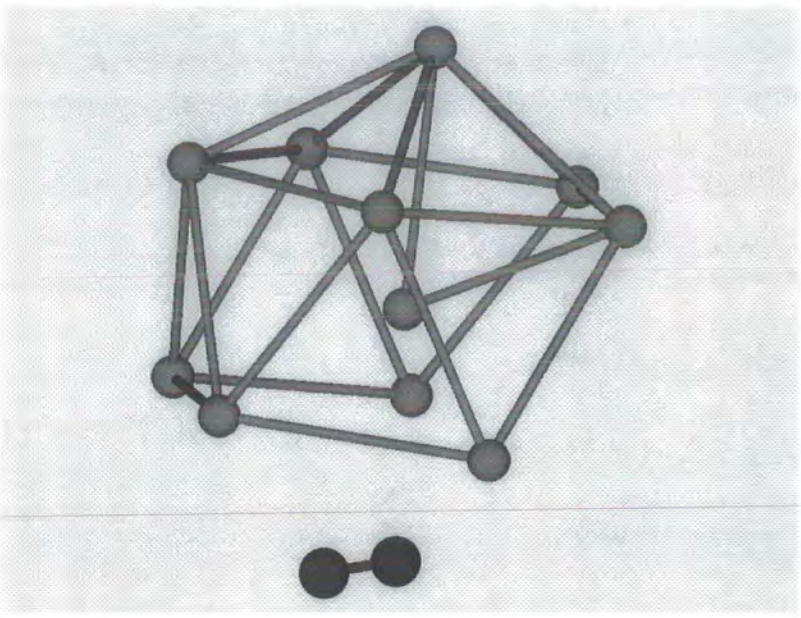

Figure 4.39: $Ar_{11}N_2$ $V_{11,1}$ structure

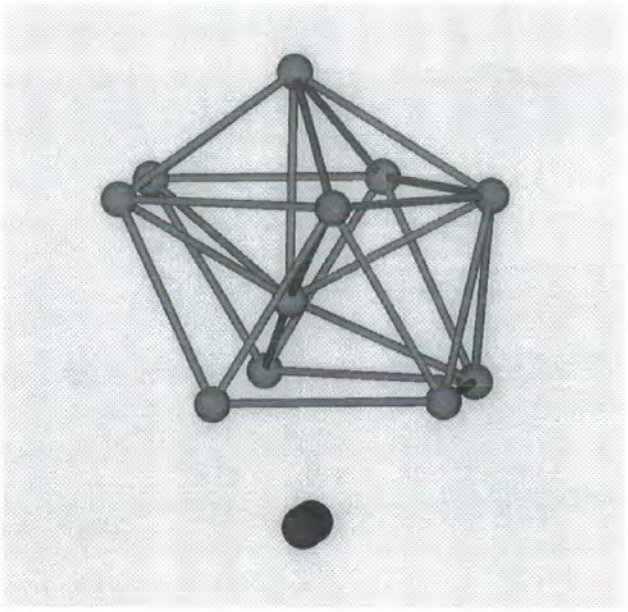

Figure 4.40: $Ar_{11}N_2$ $V_{11,2}$ structure

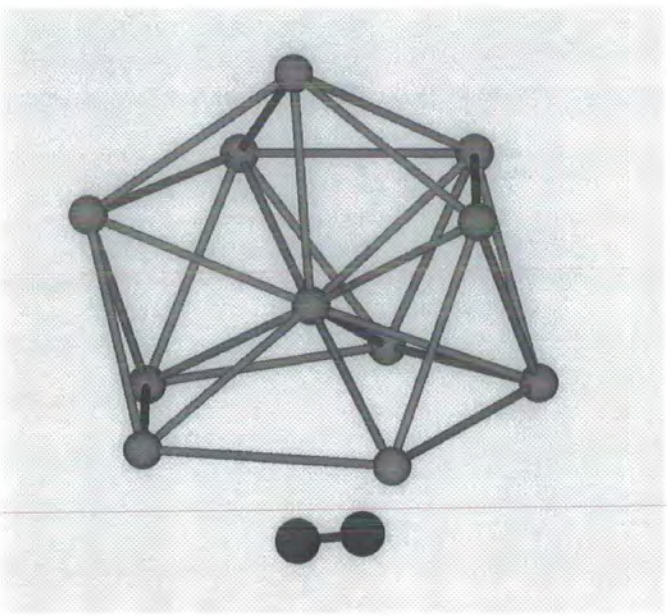

Figure 4.41: $Ar_{11}N_2$ $V_{11,3}$ structure

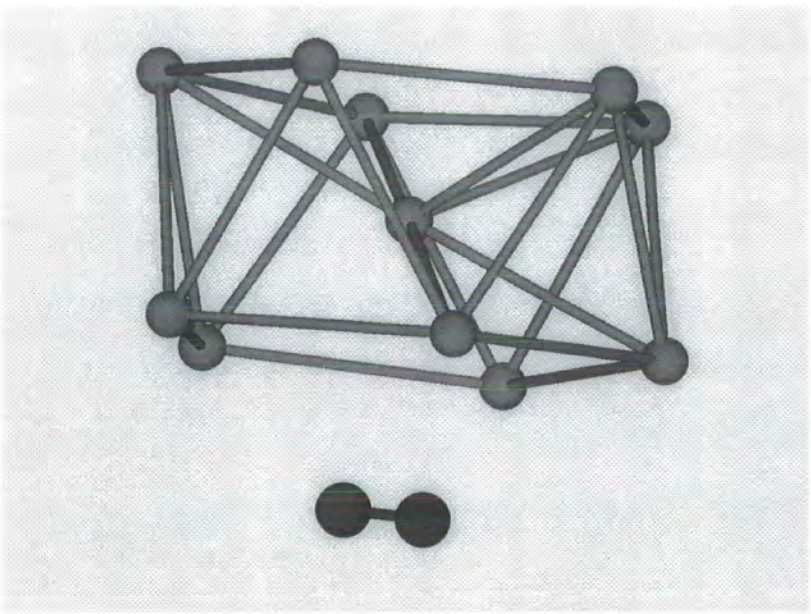

Figure 4.42: $Ar_{11}N_2$ $V_{11,4}$ structure

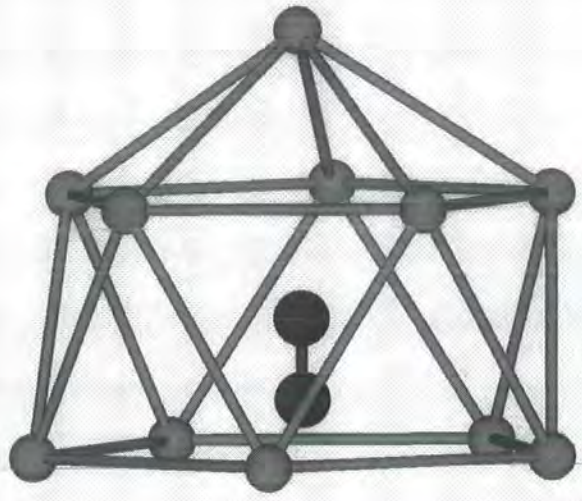

Figure 4.43: $Ar_{11}N_2$ $V_{11,5}$ structure

4.2.12 $Ar_{12}N_2$

In the $Ar_{12}N_2$ system, we continue to see the dominance of the Ar-Ar interaction over the Ar-N_2 interaction. The minimum energy structure has a pure Ar_{12} cage, with the N_2 sitting underneath the Ar structure. The next minimum is 250 cm^{-1} above the global minimum. The reason for this is that the next few minima are based on the pure Ar_{11} structure, with the twelfth Ar atom capping the Ar_{11} structure. This leads to all the low-lying minima being energetically very unfavoured compared to the global minimum; additionally because the low-lying minima are capped pure Ar_{11} structure they are close in energy. Ar_{11} has an inversion centre; this means that there are 3 sites (on the top of the cage) and 4 sites (around the middle of the cage) that are not related by rotation to each other. This lead to structures that are slightly different in energy. For the three top capped structures the difference in the energy comes from the Ar cage, and not from the Ar-N_2 interaction. For the four sites around the middle of the Ar_{11} structure the difference in energy is a mixture of the two interactions. The trend in the energies for the capped structures, both on the top and in the middle, can be rationalised

by looking at the Ar_{11} cage. The pure Ar_{11} structure has one Ar atom missing from the bottom five membered ring of the pure Ar_{12} structure. This leads to capped structures at the closed part of the ring being lower in energy because the Ar atoms around the closed end of the ring are more likely to be confined close to their equilibrium distances. In addition the Ar_{11} based structures that are capped on the top have a smaller Ar-N_2 interaction than structures capped around the middle. These two trends explain the ordering of the minima found. The completed icosahedral cage structure was also found, in the same energy range as the capped Ar_{11} structures. This again shows the difference between the Ar_nN_2 system and the Ar_nHF system, in which the icosahedral cage was the global minimum.

There is one final structure that I have not mentioned yet. This structure also has the pure Ar_{11} structure as its base, but with the twelfth atom below the Ar_{11} structure, and interacting with the N_2 near the 'T shaped' geometry, which is energetically most favoured.

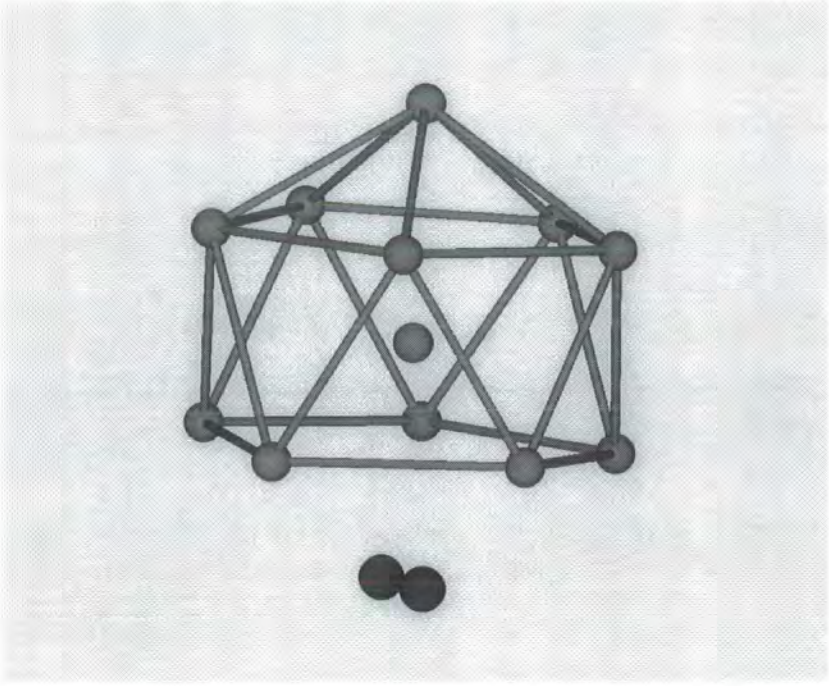

Figure 4.44: $Ar_{12}N_2$ $V_{12,1}$ structure

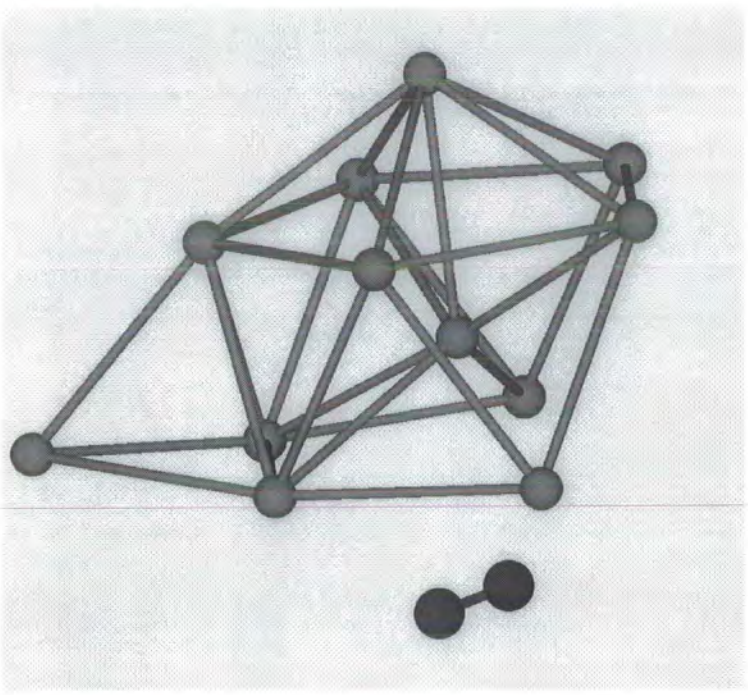

Figure 4.45: $Ar_{12}N_2$ $V_{12,2}$ structure

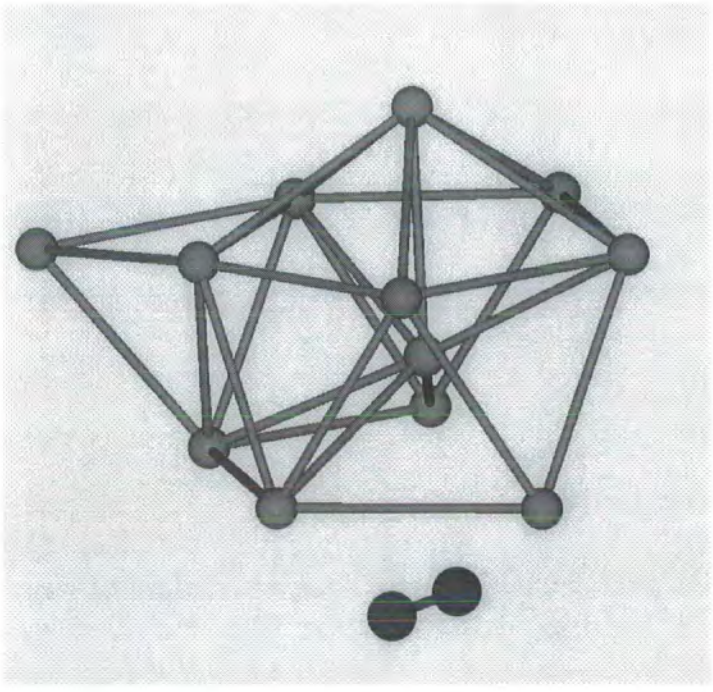

Figure 4.46: $Ar_{12}N_2$ $V_{12,3}$ structure

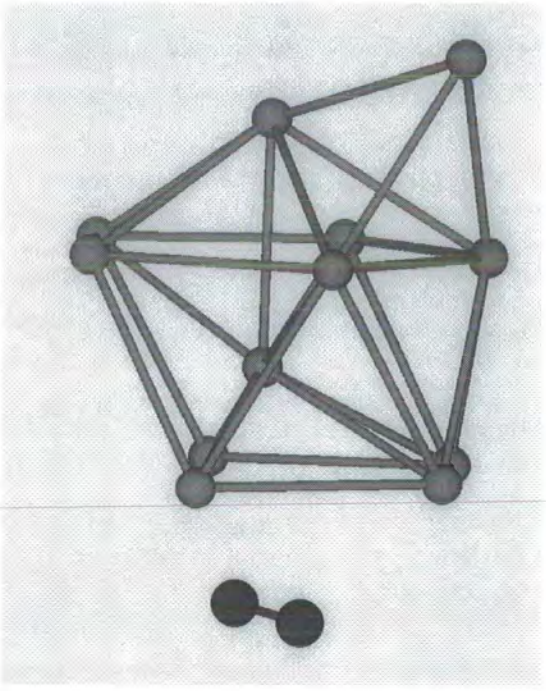

Figure 4.47: $Ar_{12}N_2$ $V_{12,4}$ structure

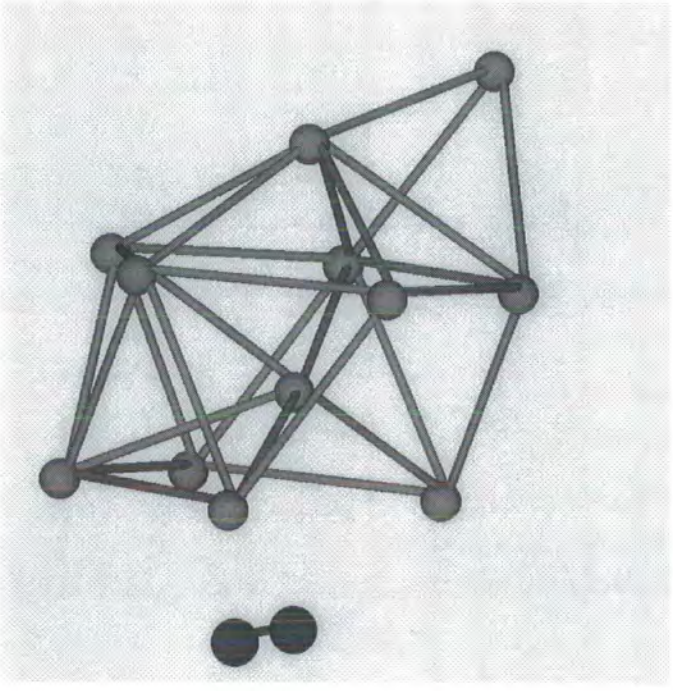

Figure 4.48: $Ar_{12}N_2$ $V_{12,5}$ structure

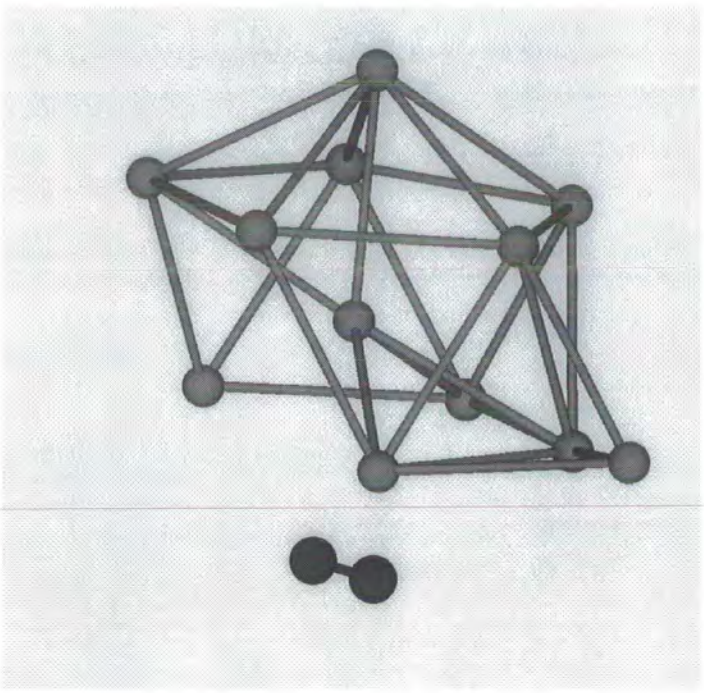

Figure 4.49: $Ar_{12}N_2$ $V_{12,6}$ structure

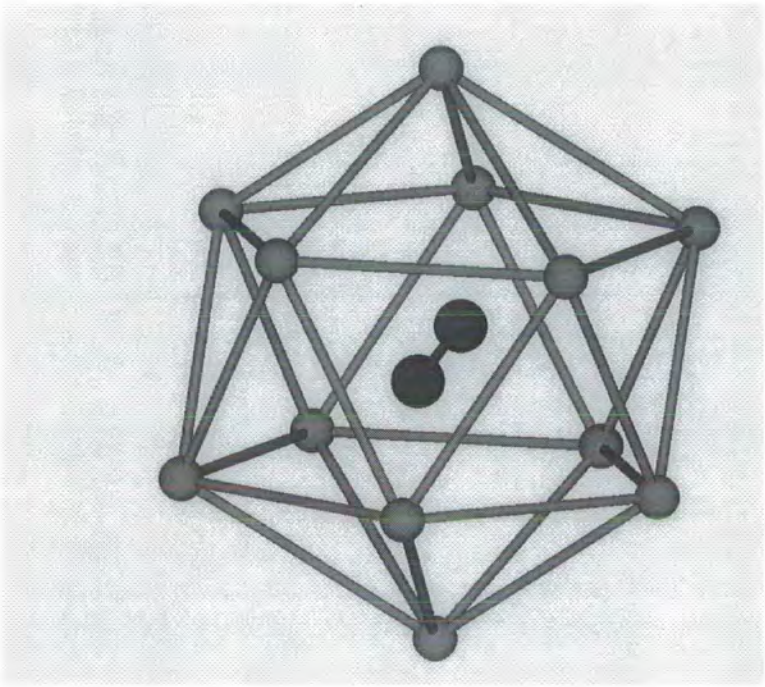

Figure 4.50: $Ar_{12}N_2$ $V_{12,7}$ structure

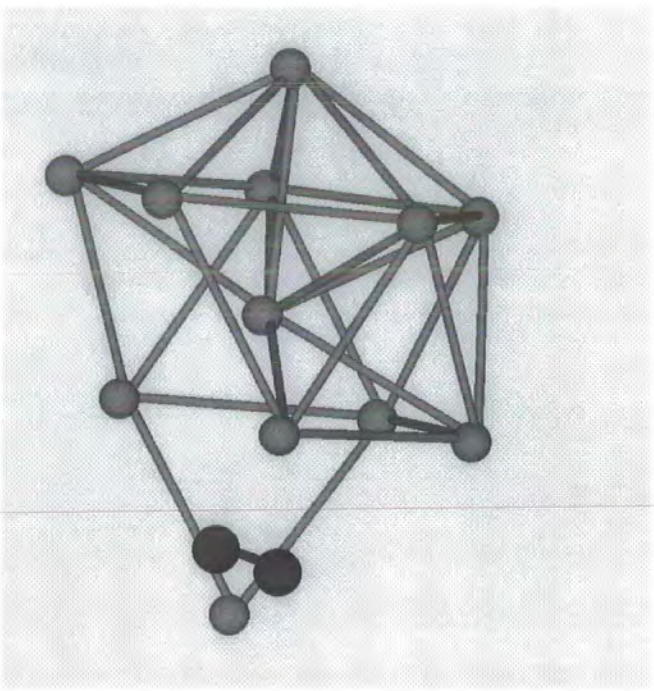

Figure 4.51: $Ar_{12}N_2$ $V_{12,8}$ structure

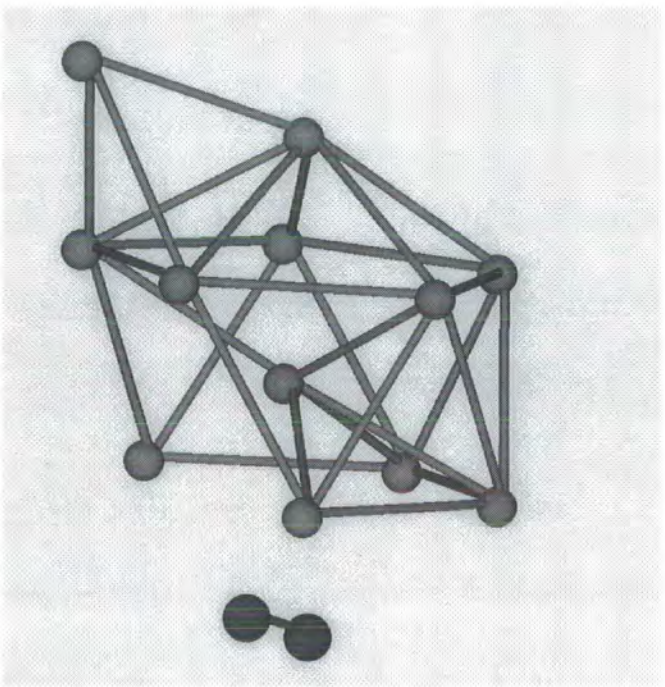

Figure 4.52: $Ar_{12}N_2$ $V_{12,9}$ structure

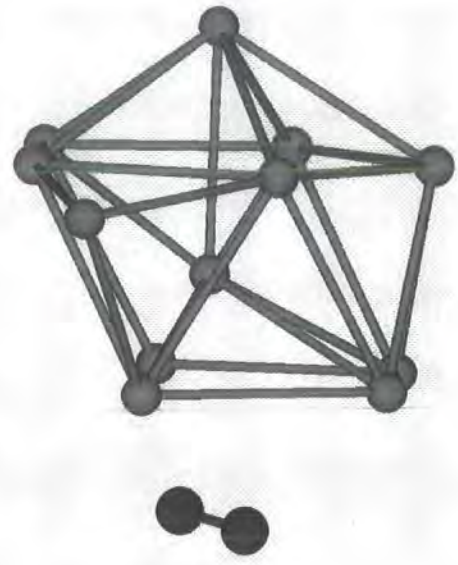

Figure 4.53: $Ar_{12}N_2$ $V_{12,10}$ structure

4.2.13 Ar_nN_2 where $n > 12$

From our studies so far we have seen that the Ar_nN_2 system is much more subtle and open-ended than the Ar_nHF system. In Ar_nHF the strong Ar-HF interaction dominates the system. This means that Ar_nHF quickly forms a first solvation shell, i.e. at n=12. After the first solvation shell the extra Ar atoms just add to the outside of the cage, and have little effect on the system other than to make it bigger. For example they do not much affect the red shift, which is a measure of the interaction of the argon cage with the HF, and for which the calculated value at n=12 is very close to the experimental value for the bulk red shift. In the Ar_nN_2 system this is not the case, and we have not completed the first solvation shell at n=12. Indeed it does not look as if we are even close to the first solvation shell, as the global minimum for $Ar_{12}N_2$ is a pure Ar_{12} structure with the N_2 sitting under the Ar cage.

The question now becomes what does the first solvation shell for the Ar_nN_2

system look like? We cannot know for sure as we have not done any calculations above n=12. We can however use our understanding gained from the study of the Ar_nN_2 system up to n=12 to take an educated guess at the probable structure of the first solvation shell. The first obvious possibility is a stretched version of the icosahedral cage, where a second ring of five Ar atoms is put in-between the two five-members of the twelve atom icosahedral cage. This would form a tube-like cage. This structure is unlikely to be the global minimum as adding the extra ring of the Ar atom will only force the other two rings further apart. It would also make many of the Ar-N_2 interactions less 'T shaped' which is also energetically unfavoured.

Our calculations have shown that the icosahedral cage is not the global minimum of the $Ar_{12}N_2$ system, and we have just suggested that the tube structure is unlikely to be a global minimum. The question now is, is there another micro cluster structure which might be a global minimum of its Ar_nN_2 system.

For a structure to be the global minimum it most have all the atoms interacting at close to their equilibrium distance. The structure will also preferentially maximise the dominant interaction. Given that the Ar-Ar interaction is dominant, and that changing the interatomic distance by more than a few tenths of an angstrom from the equilibrium distance is energetically unfavoured, it seems highly unlikely that there is a finite size micro-cluster which can maximise the Ar-Ar interaction, and still have room inside the argon structure for the N_2 without radically disturbing that structure. We therefore conclude that there is no finite sized micro-cluster which can enclose the N_2 molecule and is also the global minimum of its particular Ar_nN_2 system. The global minimum for larger Ar_nN_2 clusters, i.e. $n > 12$, are therefore expected to be similar to the pure Ar_n structures, with the N_2 molecule interacting with an external face of the Ar structure.

We have suggested that micro-cluster solvation structures are highly unlikely, but as yet we have not mentioned bulk phase structures. These could be calculated by classical dynamics simulations using periodic boundary conditions. Such simulations might find structures which are stable, but do not correspond to any

micro-cluster structure.

4.3 Conclusions

When we started the investigation of the Ar_nN_2 system there were two previous studies of similar systems. They were the Ar_nHF [101] and Ar_nCO_2 [91] systems. There was however little know about the structures of the Ar_nN_2 system [167]. In Ar_nHF the first solvation shell had been found at n=12, and a red shift calculated for the $V_{12,1}$ structure. The value of the calculated red shift was in rough agreement with the experimental bulk red shift. This strongly suggested that the solvation structure found was indeed the basic solvation structure for all Ar_nHF systems with n greater than 12, and that all the extra atoms added to the outside of the icosahedral argon cage. In the Ar_nCO_2 system the structures for each value of n were not thoroughly investigated, but the salient points of the system behaviour were found. These were that the first five argon atoms clustered around the carbon atom, and that the first solvation shell was formed at n=17. The first solvation shell had five argon atoms around each of the atoms in CO_2, and one argon atom capping the top and bottom of this structure. The red shift for the solvation structure was estimated by experimentally determining a constant of proportionality for the red shift produced by each argon atom as a percentage of its interaction strength. This method also gave rough agreement with the experimental bulk red shift.

We were particularly interested in comparisons between the Ar_nN_2 and Ar_nHF systems. This was because they are both diatomic molecules with argon clustering around them. This meant that the results from our study of the Ar_nN_2 system would show how the balance between the rare gas-rare gas and rare gas-molecule interactions, as well as the topology of the potential energy surface, affects the structures formed. One reason for looking at these simpler rare gas-molecule systems is that they provide excellent prototype systems on which to test our understanding of more complex chemical events. The Ar_nN_2 system was a type of

prototype system that had not as yet been investigated. The Ar_nHF system is a prototype for systems where the interaction of the solvent and the solute is highly directional, and the strength of the solvent-solute interaction is greater than that of the solvent-solvent interaction. Ar_nHF is a prototype for solvation of highly polar molecules and hydrogen-bonded solvation systems.

In the case of the Ar_nCO_2 system the Ar-C interaction energy is approximately 200 cm^{-1} and the Ar-O interaction energy is approximately 110 cm^{-1} [166]. This makes the Ar_nCO_2 a prototype for linear systems with several interaction sites of varying strengths. The Ar_nN_2 system is a prototype for solvent-solute systems where there is a much closer balance of interactions. The more isotropic nature of the Ar-N_2 interaction is an important feature, as many chemical interactions are not as anisotropic as that modelled by Ar-HF.

4.3.1 $Ar_{2-6}N_2$

The structures belonging to the small Ar_nN_2 clusters are interesting because they show a lot of similarities between the Ar_nN_2 and Ar_nHF systems. In particular the structures formed by the Ar_n cage are similar. In the early ($n = 2 - 4$) part of this series of systems, the argon structures are exactly the same as those found in the equivalent Ar_nHF system. The reason for this is that for a small number of argon atoms there are few simple configurations that allow all the atoms to interact with each other. If we take three argon atoms, for example, they can either form a triangle or a line of atoms. The triangle structure will always be energetically more favoured as it allows all argon atoms to interact with each other. However, even though the argon substructures are the same the Ar_nN_2 structures are not the same as their Ar_nHF counterparts. In the Ar_nN_2 system the N_2 lies flat to the Ar_n structure, whereas in the Ar_nHF system the HF points at the face of the Ar_n structure. This is due to the different topologies of the two rage gas-molecule potential energy surfaces.

As the value of n increases the number of different possible arrangements of the argon cage increases and the subtle effects of the relative magnitudes of the

rare gas-rare gas and rare gas-molecule interaction energies and the topology of the rare gas-molecule potential energy surface start to show through.

One of the many manifestations of the difference of the two systems is that as n increases the energy difference between successive structures is small for the Ar_nN_2 systems, but relatively large for the Ar_nHF systems. This means that the number of structures that need to be described increases. In the Ar_5N_2 system we see another significant sign that the long-term behaviour of the two systems is going to diverge. The global minimum is a completely new structure. It has four argon atoms forming the square base of a pyramid, with the N_2 lying flat under the base of the pyramid. This structure is not found in the Ar_nHF system because the HF dimer would have to point at the centre of the base of the pyramid. This is energetically very unfavourable due to the highly anisotropic nature of the Ar-HF interaction. In the Ar_nN_2 system however the opposite is true due to the more isotropic nature of the Ar-N_2 interaction. In the Ar_nHF system the $V_{5,1}$ structure is a capped envelope structure. This structure has a smaller Ar-Ar interaction energy than the equivalent $V_{5,1}^{Ar_nN_2}$ structure. This means that the effect of the stronger and more anisotropic Ar-HF interaction is to force the system to maximise the Ar-HF interaction at the expense of the Ar-Ar interaction.

4.3.2 $Ar_{7-12}N_2$

In the Ar_7N_2 system we found $V_{7,3}$ to be a bi-capped version of the $V_{5,1}$ structure. This structure is also not found in the Ar_nHF system. The two capping atoms form a second $V_{5,1}$ structure. This structure is clearly a product of the more isotropic nature of the Ar-N_2 potential energy function. Just as the $V_{5,1}$ structure illustrated the difference between the Ar_nN_2 and Ar_nHF systems, so does the $V_{7,3}$ structure.

From Ar_7N_2 onwards the similarities with the Ar_nHF system become less obvious. We do find some argon cage structure in common between the two systems. In particular we find the icosahedral cage structure and its part-formed precursors. The relative stability of these structures in the two systems is however very

different. Whereas for $n \geq 9$ in the Ar_nHF system the icosahedral cage or its precursor is the global minimum, in the Ar_nN_2 system such structures are never the global minimum. In some cases, most notably $Ar_{12}N_2$, the icosahedral cage is substantially less stable than other structures. The reason for this difference in behaviour is that the icosahedral cage structures maximise the rare gas-molecule interaction at the expense of the rare gas-rare gas interactions.

The corollary to the discussion of icosahedral cages in the previous paragraph is that the structures found in the $Ar_{7-12}N_2$ systems are determined more by the Ar-Ar interaction than the Ar-N_2 interaction. This is indeed just what we see. The global minimum for the $Ar_{7-12}N_2$ systems are structures which maximise Ar-Ar interactions. There are many examples of structures that come from adding an argon atom to a $Ar_{n-1}N_2$ structure and in all cases the energetically more favoured structure is the one that adds the argon atom to the Ar_{n-1} cage, rather that adding it to the cluster so that it could interact with the argon cage and the N_2. It is not just the global minimum that shows the dominance of the Ar-Ar interaction. Many of the low-lying minima clearly show the Ar-Ar dominance in determining structures. This is particularly well shown in the case of the $Ar_{12}N_2$ system, where many of the low-lying minima are based on capped versions of the $Ar_{11}N_2$ global minimum structure. Other examples of the dominance of the Ar-Ar interaction are the capped ($V_{6,1}$) pentagon structures that are found in the $Ar_{7-11}N_2$ systems. Structures such as $V_{9,1}$,which has argon atoms capping the argon atoms that cap the $V_{6,2}$ pentagon structure, show quite clearly that the Ar-Ar interaction is dominant in Ar_nN_2. In this range of Ar_nN_2 structures the energy difference between the neighbouring structures is less than found for the Ar_nHF system, as was true for the $Ar_{2-6}N_2$ structures. However in the $Ar_{6-12}N_2$ systems the gap between adjacent structures is even smaller. For example in Ar_7N_2 and $Ar_{11}N_2$ the gap can be as small as 1 cm^{-1}, or less. In addition to this, the relatively isotropic nature of the Ar-N_2 interaction leads to structures where the N_2 and a given argon cage can interact in more than one configuration. Again the Ar_7N_2 and $Ar_{11}N_2$ systems provide good examples of such structure.

In the Ar_nN_2 system as the number of argon atoms increases we see that the Ar-Ar interaction comes to dominate the structures of the system more and more. The reason for this behaviour is the fact that the Ar-N_2 interaction is weaker than the Ar-Ar interaction for all but 'T shaped' interactions. The dominance of the Ar-Ar interaction means that as the number of argon atoms in the cluster increases the structures of the system become more like the structures found for the pure argon clusters. This trend leads to the $V_{12,1}$ and $V_{11,1}$ structures, which are pure argon cages with the N_2 sitting underneath the argon cage. There is further evidence for the dominance of the Ar-Ar interaction on the Ar_nN_2 system in the $Ar_{12}N_2$ structures. Most of the low-lying minima that are describe in the text above for the $Ar_{12}N_2$ system are based on the $V_{11,1}$ structures. The last argon atom is added to the outside of the pure Ar_{11} structure. The fact that the low-lying minima are based on pure Ar_{11} structure rather that any other type of structure show the basic stability of the Ar_{11} structure.

Though it is undoubtedly true that the Ar-Ar interactions are dominant in determining the structures of the Ar_nN_2 system, it is not however true that the effect of the Ar-N_2 interact can be ignored. The structures found are determined by a balance of forces. The effects of the Ar-N_2 interaction are more subtle, and less obvious, but the evidence for their effects on determining the structures is clear to see. Examples of the effect of the Ar-N_2 interaction are the parallel and perpendicular structures in the $Ar_{11}N_2$ structure. In the case of the parallel structure the Ar-N_2 interaction is maximised at the expense of the Ar-Ar interaction. In addition to this the very existence of the parallel and perpendicular structures is due to the nature of the Ar-N_2 interaction. If the rare gas-molecule interaction was too anisotropic the molecule would not be able to lie under the argon cage; on the other hand if the rare gas-molecule interaction was too isotropic the two wells would not exist. This last point is illustrated in the Ne_nN_2 system described in the next chapter.

Another point arising from our work on the Ar_nN_2 system is that, because the system is more finely balanced, the surface that has to be searched is more

complicated. This point is shown very clearly in the $Ar_{12}N_2$ system, where the low-lying minima are capped versions of the $V_{11,1}$ structure. The fact that these structures are based on the same eleven-atom argon cage actually makes it difficult to find all the structure by simulated annealing. The problem is that, with so many structures that are so close in energy, the simulated annealing search can actually pass through a minimum. In this particular case we can overcome the problem because we know what structures we should find due to the symmetry of the $V_{11,1}$ structure. The point of this explanation, though, is to show that as the Ar_nN_2 system gets larger it becomes more and more likely that a local minimum in the energy range of interest may be missed. As previously stated this problem can be overcome by starting from many different starting positions. This policy has a limited life though, and as the systems we are trying to search get larger the more likely this policy is to fail. In a system where there is a single dominant interaction, such as in Ar_nHF, it is less likely for this problem to arise.

n	$V_{n,1}$ /cm^{-1}	$V_{n,2}$ /cm^{-1}	$V_{n,3}$ /cm^{-1}	$V_{n,4}$ /cm^{-1}	$V_{n,5}$ /cm^{-1}	$V_{n,6}$ /cm^{-1}
2	−304.566					
3	−603.22					
4	−912.164	−908.986				
5	−1254.057	−1225.030	−1224.067	−1222.407		
6	−1634.591	−1596.788	−1567.990	−1543.707	−1541.277	−1540.990
7	−1956.907	−1955.688	−1924.558	−1907.191		
8	−2373.195	−2372.212	−2371.466	−2336.40	−2329.024	
9	−2788.664	−2788.261	−2754.746	−2749.368		
10	−3206.484	−3178.606	−3167.379	−3157.585		
11	−3694.282	−3675.946	−3669.557	−3606.495		
12	−4293.965	−4038.508	−4036.706	−4036.676	−4036.614	4026.721

Table 4.1: results for Ar_nN_2

Chapter 5

The Ne_nN_2 system

5.1 Ne_nN_2

We have seen that the Ar_nN_2 system will not form a solvated structure easily until we reach very large values of n. This has been rationalised by considering the competing interactions of Ar-Ar and Ar-N_2. To test these arguments we now investigate a system where the cage interactions are weaker than those of the cage-diatom. Since we want to stay within the rare gas-N_2 type of system, the system that best suits our needs is the Ne_nN_2 system.

The maximum Ne-Ne interaction is only ≈ 29 cm^{-1}, whereas the maximum Ar-Ar interaction is ≈ 99 cm^{-1}. The Ne-N_2 potential energy surface is more isotropic than that for Ar-N_2, although it still has a 'T shaped' minimum. The 'T shaped' interaction of Ne-N_2 is much stronger than the Ne-Ne interaction, with a well depth of ≈ 50 cm^{-1}. Even when the Ne atom interacts linearly with the N_2, $\theta = 0°$, the interaction strength is ≈ 39 cm^{-1}, which is greater than the maximum Ne-Ne interaction. This should mean that the Ne-N_2 interaction will play a greater role in determining the structures of the Ne_nN_2 that the Ar-N_2 interaction did for Ar_nN_2. The Ne-Ne potential [133] that we used (which is of the HFD-B form) is

$$V(r) = \varepsilon V^*(x) \tag{5.1}$$

where

$$V^*(x) = A^* \exp(-\alpha^* x + \beta^* x^2) - F(x) \sum_{j=0}^{2} c_{2j+6}/x^{2j+6}, \tag{5.2}$$

with

$$F(x) = \begin{cases} \exp\left[-\left(\frac{D}{x} - 1\right)^2\right] & \text{for } x < D \\ 1 & \text{for } x \geq D \end{cases},$$

where

$$x = r/r_m \tag{5.3}$$

The Ne-N_2 potential [168] is

$$V(R,\theta) = V_0(R) + V_2(R)P_2(\cos\theta) + V_4(R)P_4(\cos\theta), \tag{5.4}$$

where the three radial components are related to the potential at the three geometries with $\theta = 0°, 45°$ and $90°$, and are given by

$$V_0 = \frac{1}{105}[7V(R,0°) + 56V(R,45°) + 42V(R,90°)], \tag{5.5}$$

$$V_2 = \frac{2}{105}[25V(R,0°) + 20V(R,45°) + 45V(R,90°)], \tag{5.6}$$

$$V_4 = \frac{16}{105}[3V(R,0°) + 6V(R,45°) + 3V(R,90°)]. \tag{5.7}$$

The three potentials $V(R,0°)$, $V(R,45°)$ and $V(R,90°)$ are each generated from a Tang-Toennies potential [169], shown below, which incorporates available dispersion coefficients, and damps the asymptotica dispersion series using a universal damping function. This is then added to a simple Born-Mayer repulsion term:

$$\begin{aligned} V(R,\theta) &= A(\theta)\exp[-b(\theta)R] \\ &- \sum_{n\geq 3}\left(1 - \sum_{k=0}^{2n}\frac{[b(\theta)R]^k}{k!} \times [-b_(\theta)R]\right)\frac{C_{2n}(\theta)}{R^{2n}}. \end{aligned} \tag{5.8}$$

The angular dependence of the dispersion coefficients is defined by

$$C_{2n}(\theta) = C_{2n}[1 + \Theta_{2n}^2 P_2(\cos\theta) + \Theta_{2n}^4 P_4(\cos\theta) + \cdots]. \tag{5.9}$$

The isotropic C_{2n} and anisotropic $\Theta_{2n}^{(i)}$ coefficients are obtained from perturbation theory. The $C_{2n}(\theta)$ coefficients for $2n > 10$ are calculated from the recursion relationship,

$$C_{2n}(\theta) = \left(\frac{C_{2n-2}(\theta)}{C_{2n-4}(\theta)}\right)^3 C_{2n-6}(\theta). \tag{5.10}$$

5.2 Results of Simulated Annealing for Ne_nN_2

5.2.1 Ne_1N_2 and Ne_2N_2

Both Ne-N_2 and Ne_2N_2 have the Ne atoms placed equatorially about the N_2 bond. This is as expected, as the minimum for the Ne-N_2 potential energy surface is 'T shaped'.

Figure 5.1: Ne_2N_2 $V_{2,1}$ structure

5.2.2 Ne_3N_2

The global minimum is the same as that found for Ar_3N_2. It has the three Ne atoms forming a triangle which lies parallel to the N_2. In $V_{3,2}$ though we see the first differences between the two rare gas systems. The first low-lying minimum has the three atoms lying equatotially about the centre of the N_2. In this configuration the Ne atoms all interact in a 'T shaped' manner and maximise the Ne-N_2 interaction, at the expense of the Ne-Ne interaction. This structure

is the first evidence that the Ne atoms might indeed cluster round the N_2 and eventually form a icosahedral cage.

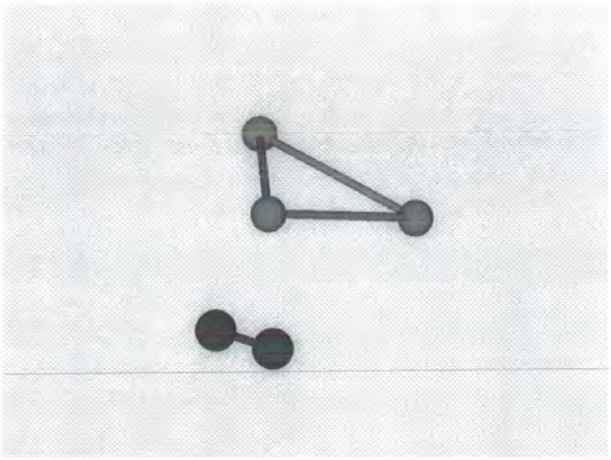

Figure 5.2: Ne_3N_2 $V_{3,1}$ structure

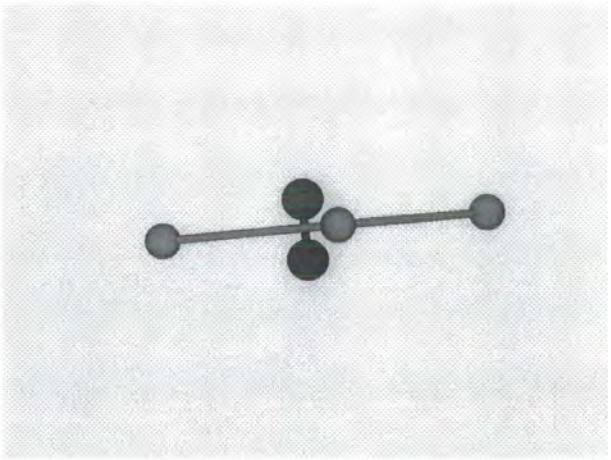

Figure 5.3: Ne_3N_2 $V_{3,2}$ structure

5.2.3 Ne_4N_2

The $V_{4,1}$ and $V_{4,2}$ structures are the same as found the Ar_4N_2 system. The global minimum is the envelope structure, and the first low-lying minimum is the pyramid structure. The next low-lying minimum, $V_{4,3}$, has the four Ne atoms

about the middle of the N_2 bond, and is obviously a continuation of the $V_{3,2}$ structure. The four atoms do not form a square about the N_2, but instead form a pentagon structure where the fifth atom is missing. This again shows that the Ne-N_2 interaction plays a greater role in determining the structures and their relative ordering in the Ne_nN_2 system than the Ar-N_2 interaction did in the Ar_nN_2 system.

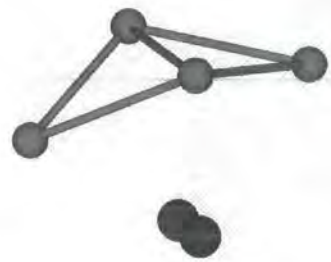

Figure 5.4: Ne_4N_2 $V_{4,1}$ structure

Figure 5.5: Ne_4N_2 $V_{4,2}$ structure

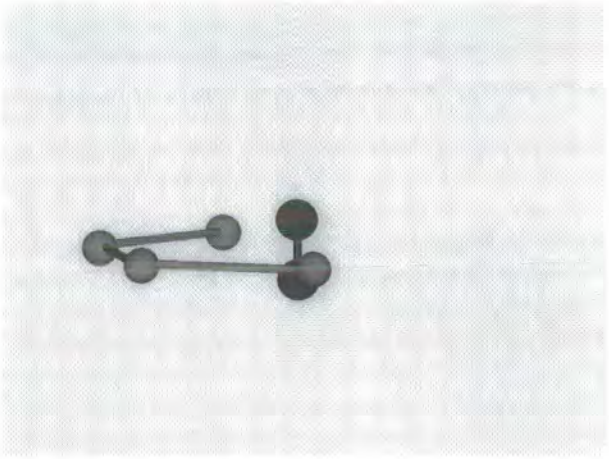

Figure 5.6: Ne_4N_2 $V_{4,3}$ structure

5.2.4 Ne_5N_2

The structures found for Ne_5N_2 are the same as those found for the Ar_5N_2 system, i.e. a pyramid with four atoms in the base, a capped part-formed pentagon, a capped envelope and a capped $V_{4,1}$ structure. They also have the same energetic ordering as for Ar_5N_2. We do not see a pentagon structure encasing the nitrogen molecule, as might have been expected, because the Ne atoms would have to be too close to the N_2 to be at their equilibrium distance from one another.

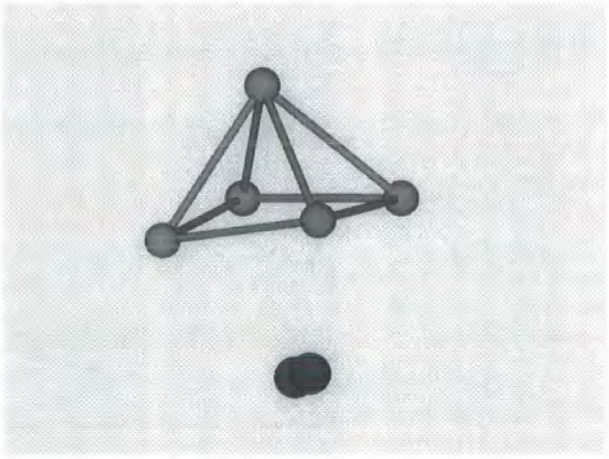

Figure 5.7: Ne_5N_2 $V_{5,1}$ structure

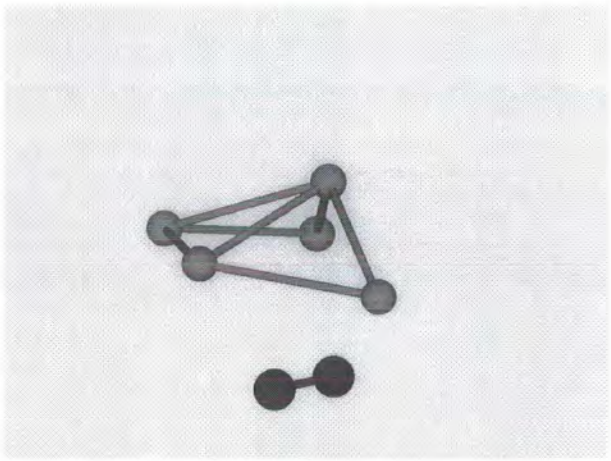

Figure 5.8: Ne_5N_2 $V_{5,2}$ structure

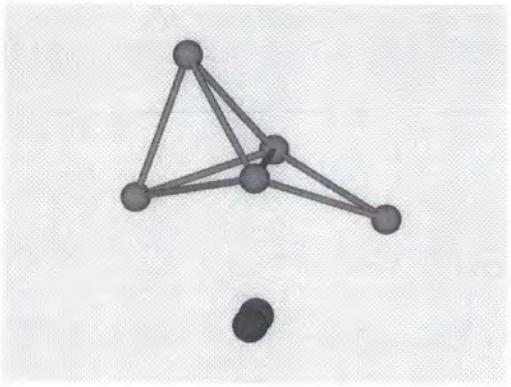

Figure 5.9: Ne_5N_2 $V_{5,3}$ structure

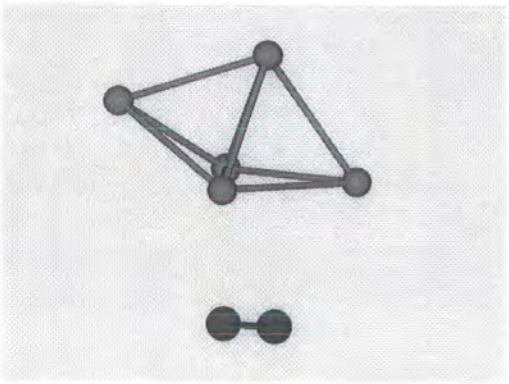

Figure 5.10: Ne_5N_2 $V_{5,4}$ structure

5.2.5 Ne_6N_2

The global minimum is a capped pentagon structure, with the N_2 sitting under the pentagon. The first low-lying minimum is a bicapped envelope structure. The next four structures are capped versions of the same basic capped part-formed pentagon $V_{5,2}$ structure. The capping atoms then either sit above or below the basic structure. In both cases the capping atom can sit at the back, or the adjacent side face of the basic Ne structure. The ordering of the $V_{6,2}$ and $V_{6,1}$ structures has swapped between the Ar_6N_2 and Ne_6N_2 systems. This is again due to greater dominance of the Ne-N_2 interaction, which decreases the stability of the bipyramidal structure. The higher-energy structures, $V_{6,3}$ and $V_{6,4}$, are those where the Ne atom sits level with the N_2, because the Ne-N_2 interaction is stronger than the Ne-Ne interaction. In the $V_{6,4}$ structure the N_2 molecule has rotated round so that it avoids interacting in a linear manner with the sixth atom. It is worth noting that the bi-capped pyramid $V_{6,6}$ structure of Ar_6N_2 is now outside the energy range of interest, because of the weaker rare gas-rare gas interactions.

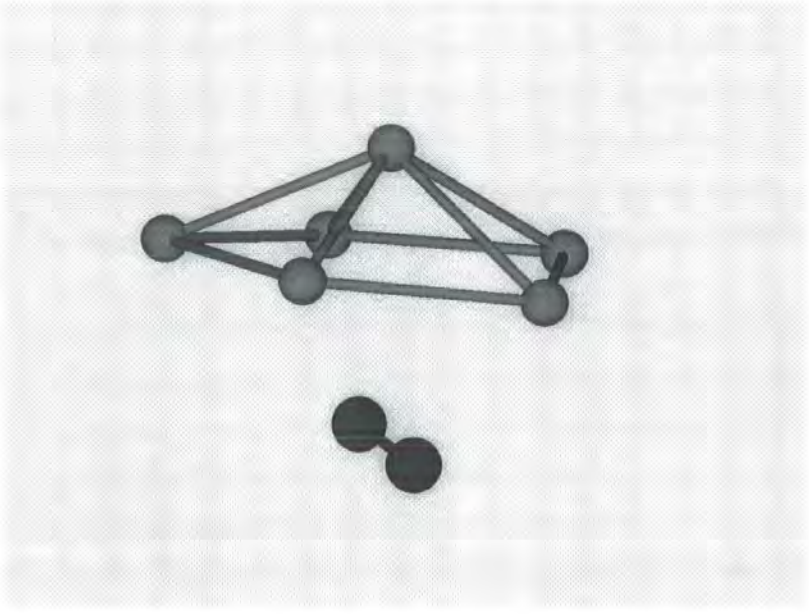

Figure 5.11: Ne_6N_2 $V_{6,1}$ structure

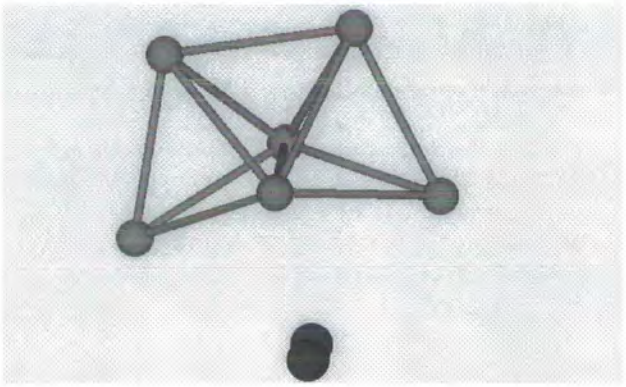

Figure 5.12: Ne_6N_2 $V_{6,2}$ structure

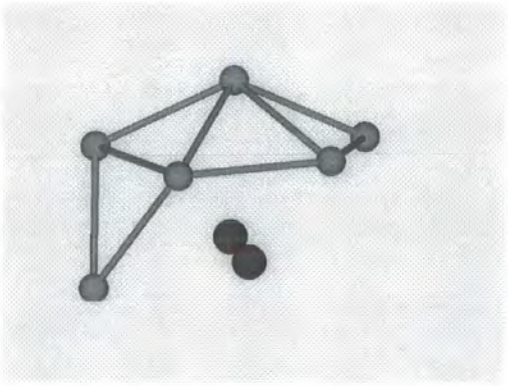

Figure 5.13: Ne_6N_2 $V_{6,3}$ structure

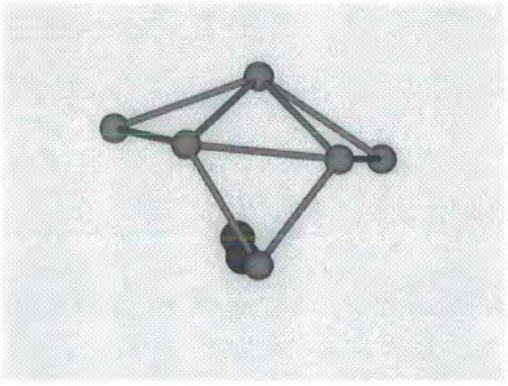

Figure 5.14: Ne_6N_2 $V_{6,4}$ structure

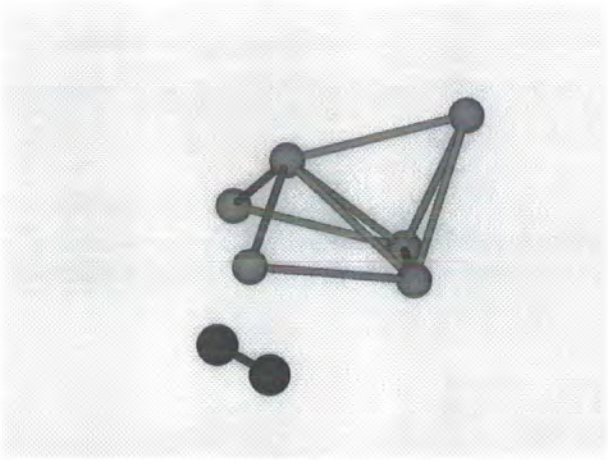

Figure 5.15: Ne_6N_2 $V_{6,5}$ structure

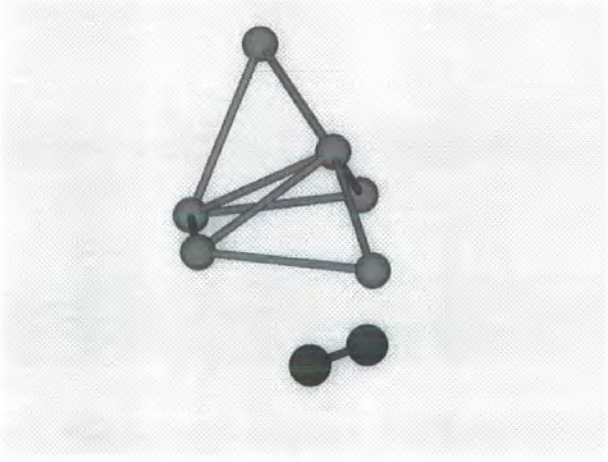

Figure 5.16: Ne_6N_2 $V_{6,6}$ structure

5.2.6 Ne_7N_2

The $V_{7,1}$ and $V_{7,2}$ structures are capped versions of the $V_{6,1}$ and $V_{6,2}$ structures respectively. In both cases the capping atom lies below the cage structure and interacts with the N_2. This is in marked contrast to the Ar_7N_2 system where both the $V_{7,1}$ and $V_{7,2}$ structures are capped bipyramidal structures. The next low-lying structure is something that we do not at all see in the Ar_nN_2 system. It

is a part-formed icosahedral cage. It is possible to argued that the $V_{7,1}$ structure could be described as a part-formed icosahedral cage. This is not untrue, but the $V_{7,3}$ structure has two Ne atoms lying next to the N_2 and with a θ value close to 90°. In this sense the $V_{7,3}$ structure is a cage structure, whereas the $V_{7,1}$ structure is a Ne cluster sitting on top of the N_2. The $V_{7,4}$ and $V_{7,5}$ structures are based on the same Ar_6 sub-units as $V_{7,1}$ and $V_{7,2}$, but with the Ne atoms that interacted with the N_2 now capping the basic Ne pentagon structure. These last two structures are the same as the $V_{7,2}$ and $V_{7,4}$ structures for the Ar_7N_2 system. The fact that they are now less stable is due entirely to the weaker cage interactions.

More generally it can be seen that all the Ne_7N_2 structures show the dominance of the Ne-N_2 interaction over that of the Ne-Ne interaction. One of the clearest examples of this may be seen by comparing the $V_{7,3}$ structures of the two rare gas-N_2 systems. Both structures are less symmetric and less tightly packed than their neighbouring structures ($V_{7,2}$ and $V_{7,4}$). Both owe their relatively high stability to the dominance of one of the interactions. In the Ar system the strong rare gas-rare gas interaction allows the Ar atom to attach to the side of the square pyramid structure. This clearly shows that the Ar-Ar interaction dominates the large Ar_nN_2 systems. In the Ne system the opposite is true, and it is the rare gas-N_2 interaction that is the dominant interaction. This is maximised in the part-formed cage and leads to the relatively high stability of the cage structure for Ne_7N_2.

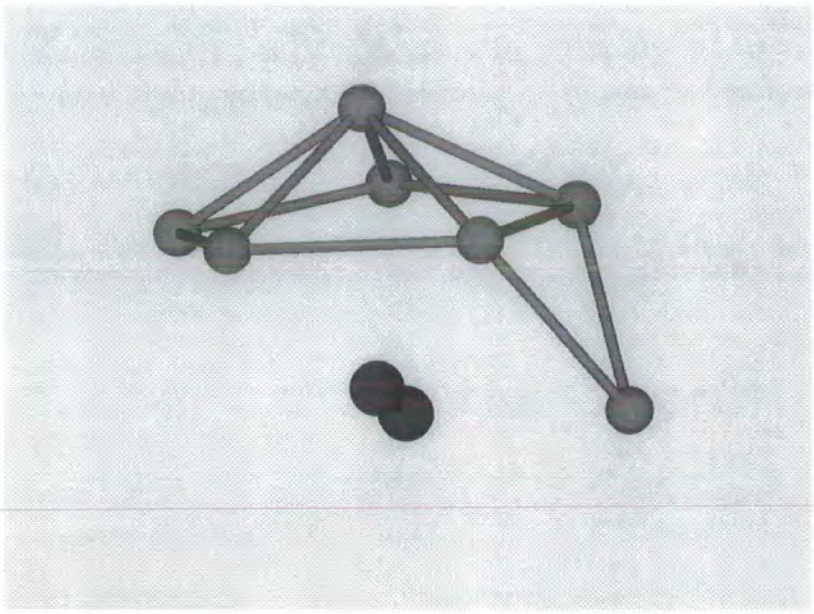

Figure 5.17: Ne_7N_2 $V_{7,1}$ structure

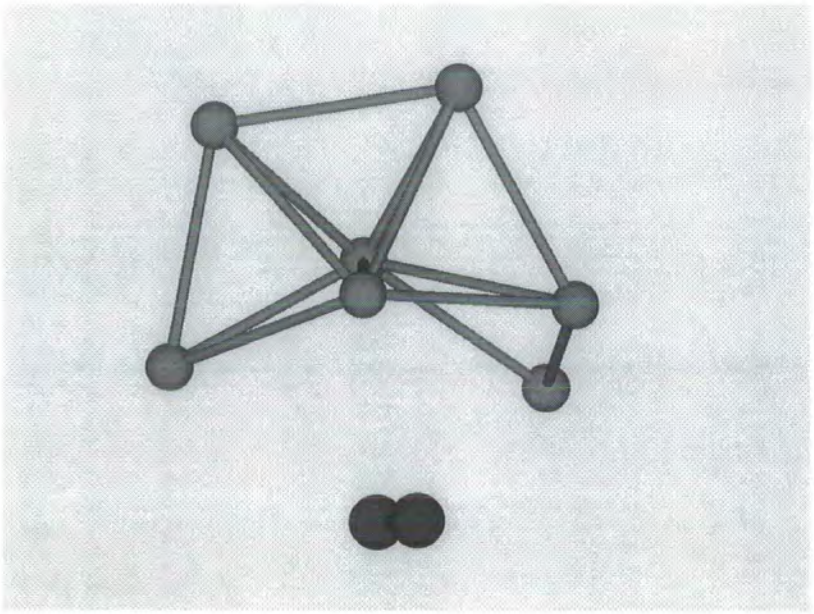

Figure 5.18: Ne_7N_2 $V_{7,2}$ structure

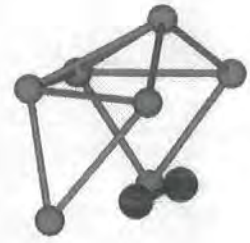

Figure 5.19: Ne_7N_2 $V_{7,3}$ structure

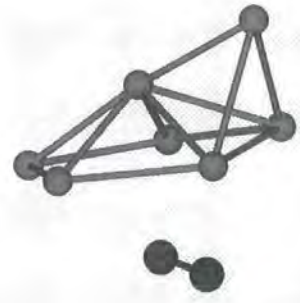

Figure 5.20: Ne_7N_2 $V_{7,4}$ structure

5.2.7 Ne_8N_2

The global minimum for Ne_8N_2 is a part-formed icosahedral cage. This is a fascinating reversal from the Ar_8N_2 system. The Ne_8N_2 system has a part-formed icosahedral cage as its global minimum even earlier that the Ar_nHF system. This structure was the $V_{8,5}$ structure for the Ar_8N_2 system. The first low-lying minimum is a part-formed pure rare gas structure, which was the global minimum for the Ar_8N_2 system. Again with these first two structures we see that the weaker Ne-Ne interaction produces to very different behaviour. The $V_{8,3}$ structure illustrates this point very clearly. It is another part-formed icosahedral structure, but this

time the two lowest atoms of the cage sit on either side of the N_2 instead of being adjacent to each other, as in the global minimum. This structure was not found at all in the Ar_8N_2 system, as the rare gas-N_2 angle is not 90° and therefore the two Ar atoms prefer to sit next to each other. In the Ne_nN_2 system though the relatively high strength of the Ne-N_2 interaction compared to the Ne-Ne interaction means that this structure is not only found, but is relatively stable. The $V_{8,4}$ structure has two atoms capping adjacent sides of the $V_{6,1}$ (capped pentagon) structure. This was the $V_{8,4}$ structure in the Ar_8N_2 system, and was more stable than the part-formed icosahedral cage.

All of the above structures have shown that the weaker Ne-Ne interaction leads to cages being formed around the N_2, as the global minimum or a low-lying structure. It is also becoming clear that as n increases the structure of the global minimum and the low-lying minima are becoming more and more dominated by the Ne-N_2 interaction. In the Ar_nN_2 systems as n increases the structures were dominated by the Ar-Ar interaction. As a result of this the two systems become more and more dissimilar. A very good example of the divergence of the two rare gas systems is given by the $V_{8,2}$ and $V_{8,3}$ structures of Ar_8N_2, which are both within 2 cm^{-1} of the global minimum. Yet in the Ne_8N_2 system these two structures are found to be very unstable. They were only stable in the Ar_8N_2 system because of the dominance of the Ar-Ar interaction.

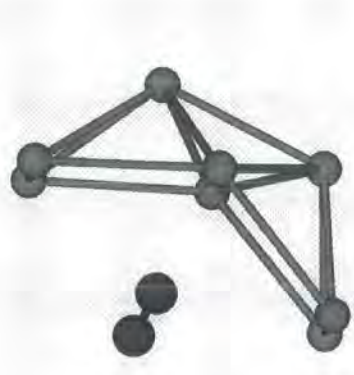

Figure 5.21: Ne_8N_2 $V_{8,1}$ structure

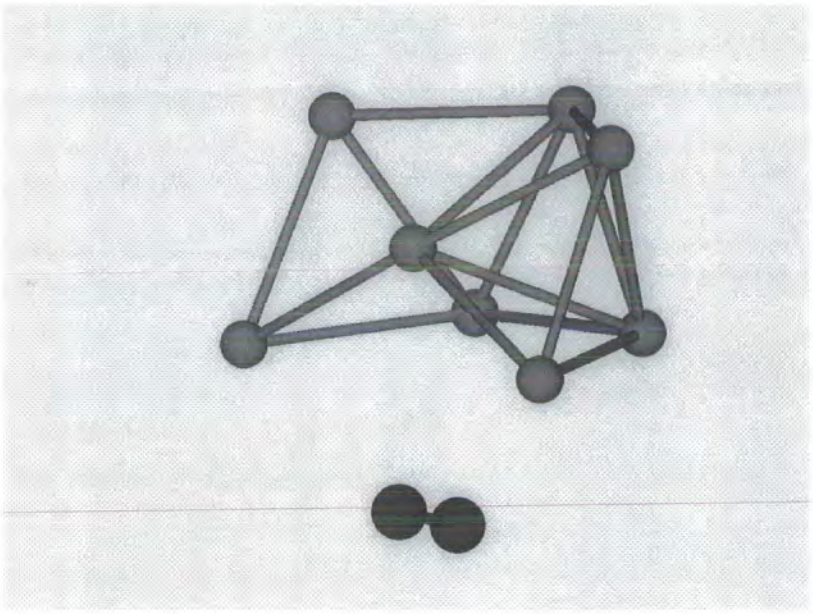

Figure 5.22: Ne_8N_2 $V_{8,2}$ structure

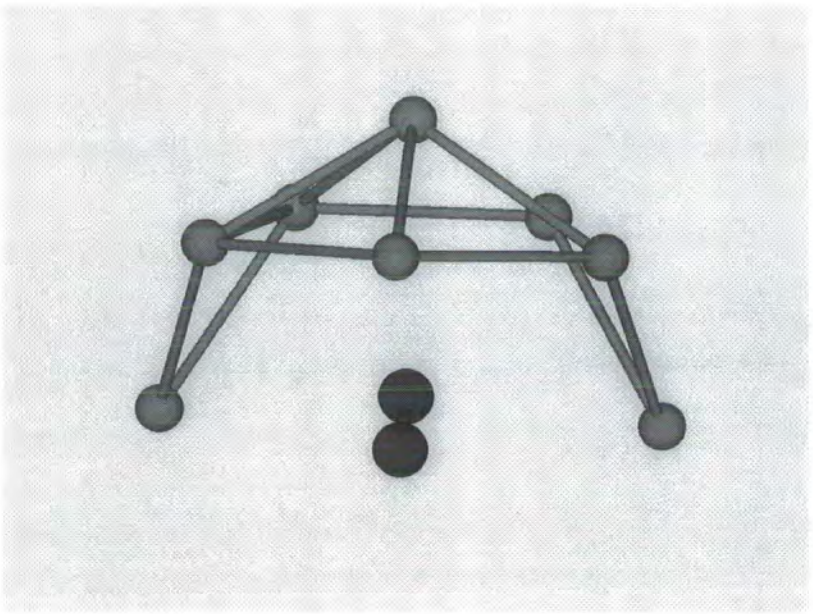

Figure 5.23: Ne_8N_2 $V_{8,3}$ structure

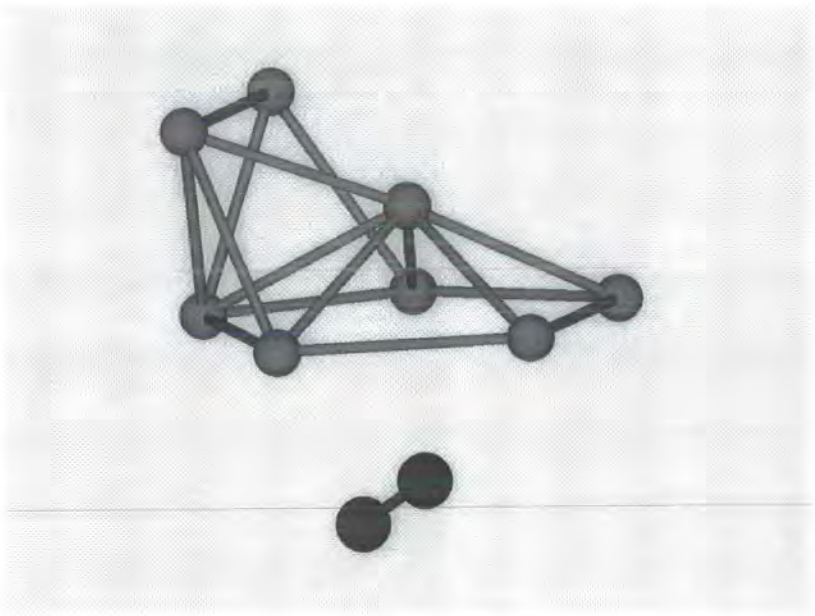

Figure 5.24: Ne_8N_2 $V_{8,4}$ structure

5.2.8 Ne_9N_2

The global minimum is the part-formed icosahedral cage, and follows from the $V_{8,1}$ and $V_{7,3}$ structures. The first low-lying minimum has one of the three Ne atoms in the bottom part of icosahedral $V_{9,1}$ structure on the opposite side of the N_2. We did not find the $V_{9,2}$ structure in our search of the Ar_9N_2 system, as it maximises the rare gas-N_2 interactions at the expense of the rare gas-rare gas interaction. The $V_{9,3}$ structure has the $V_{6,1}$, capped pentagon structure, capped by the remaining three Ne atoms. This is a structure we considered as a global minimum for the Ar_9N_2 system, but saw that the large Ar-Ar interaction did not favour it.

The remaining structures for Ne_9N_2 are complicated. They are basically capped versions of the three structures so far described, where one of the Ne atoms is removed and used as the capping atom. There are thus many structures that are similar in energy and it becomes difficult to be certain that no minima have been missed. We have found the basic structures of the system and all the complications reveal little more about the forces shaping the system. Such

complications occur in all systems, with six or more rare gas atoms, that I have studied, but in other systems the complications did not show up so early. There are usually four to six basic structures, which I will discuss for each system. These are followed by capped derivatives of the basic structures. In general I do not discuss the capped structures because there are many variants, so that it is easy to miss a structure. The capped structures are also in general less stable that the none capped structures. I do however try to find most of the capped structures, in order to understand the system fully, and to prevent an alternative structure being missed.

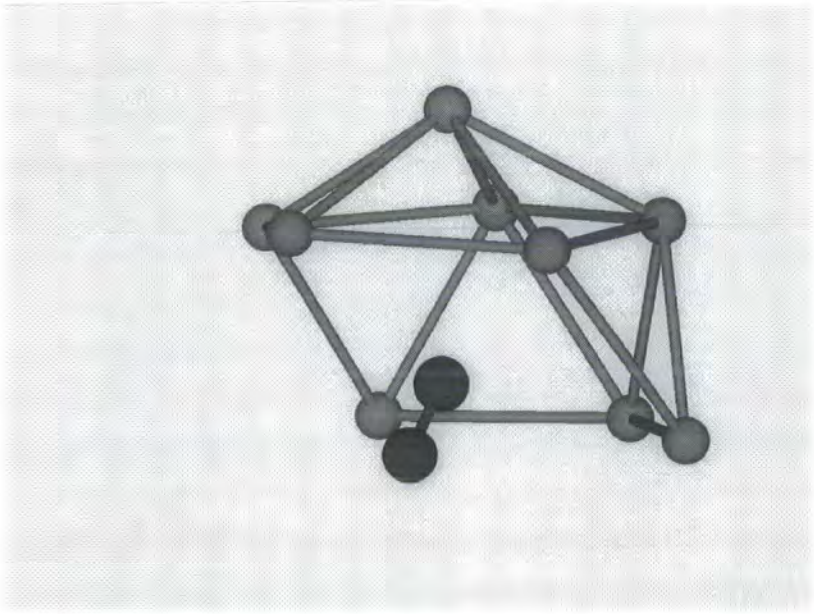

Figure 5.25: Ne_9N_2 $V_{9,1}$ structure

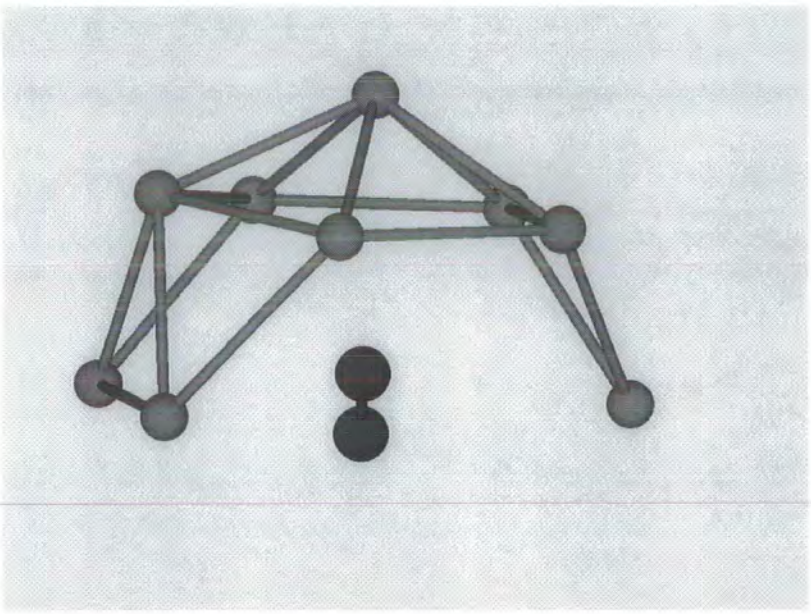

Figure 5.26: Ne_9N_2 $V_{9,2}$ structure

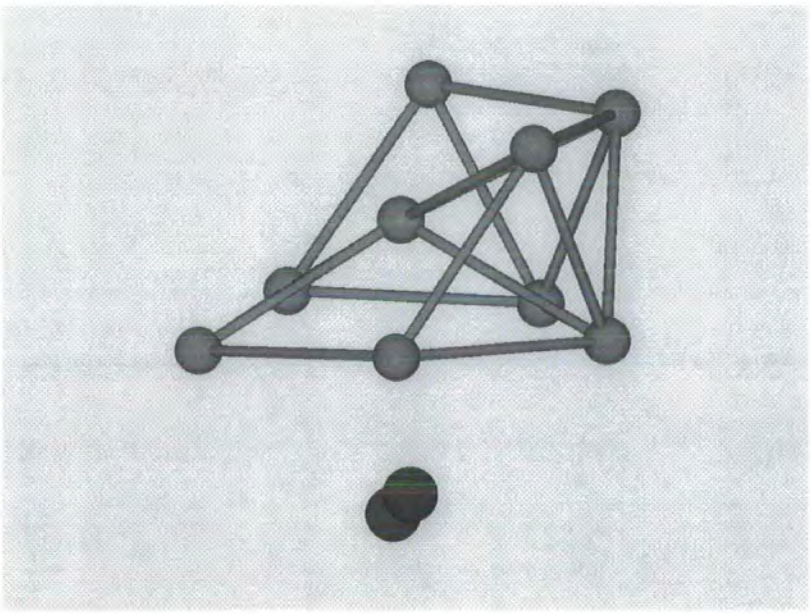

Figure 5.27: Ne_9N_2 $V_{9,3}$ structure

5.2.9 $Ne_{10}N_2$

The global minimum for $Ne_{10}N_2$ is a part-formed icosahedral cage following on from the $V_{8,1}$ and $V_{9,1}$ structures. The $V_{10,2}$ structure is a part-formed pure rare gas cage, with the N_2 sitting under the cage. This structure was a surprise, as we have not seen much evidence for this type of structure and its derivatives in the Ne_8N_2 or Ne_9N_2 systems. Its presence shows that even though the Ne-N_2 interaction is the dominant one, there is still an determined interplay and balancing of the rare gas-N_2 and rare gas-rare gas interactions. The $V_{10,3}$ structure has the $V_{6,1}$ capped pentagon structure with three Ne atoms capping adjacent faces of the Ne_6 substructures; the 10th Ne atom capping sitting above the three atoms in the upper ring of the structure, and directly above the top atom in the pentagon substructure. The $V_{10,4}$ structure is like the $V_{10,3}$ structure, except that all four capping atoms cap the Ne_6 substructure. The $Ne_{10}N_2$ system is much more like the $Ar_{10}N_2$ system than we would have expected from the smaller Ne_nN_2 systems. In stark contrast to the Ne_8N_2 and Ne_9N_2 systems, which had both different structures and relative ordering of the structures to Ar_nN_2, the $Ne_{10}N_2$ system (except for $V_{10,1}$) has not only the same structures but also the same ordering of structures.

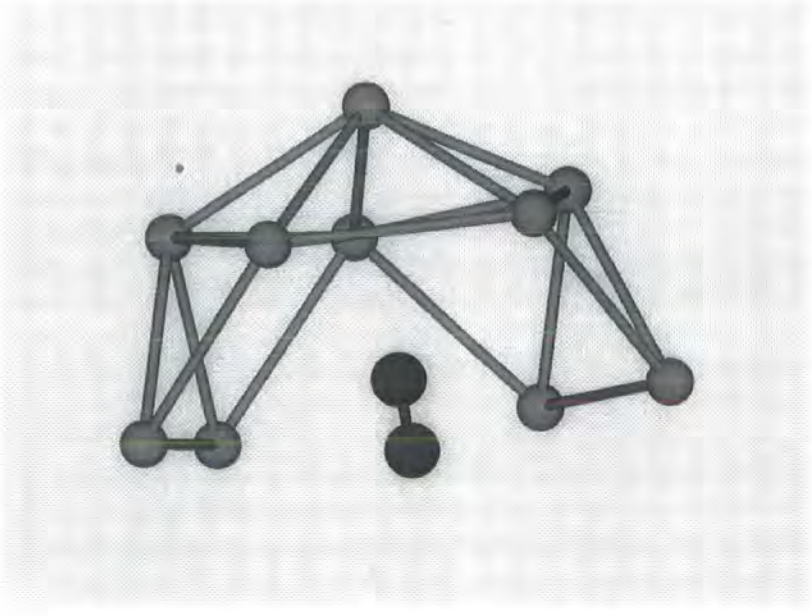

Figure 5.28: $Ne_{10}N_2$ $V_{10,1}$ structure

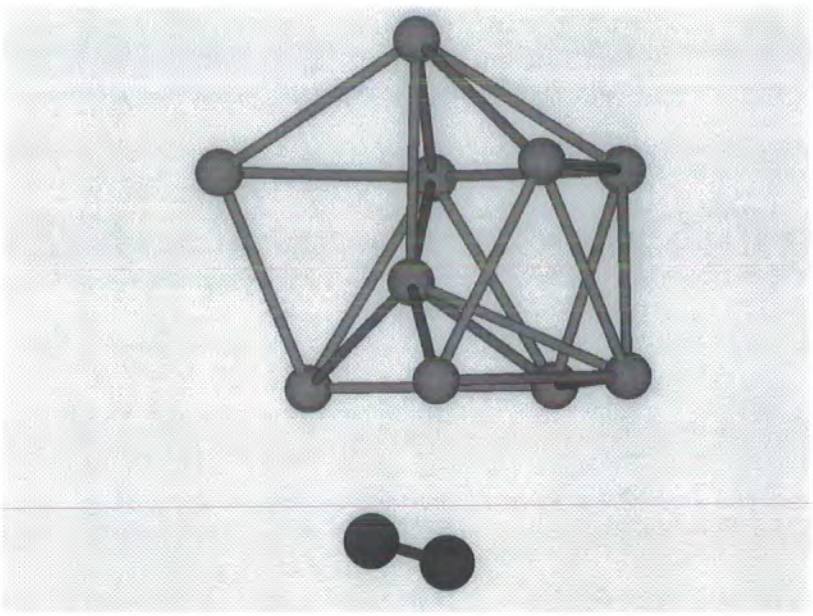

Figure 5.29: $Ne_{10}N_2$ $V_{10,2}$ structure

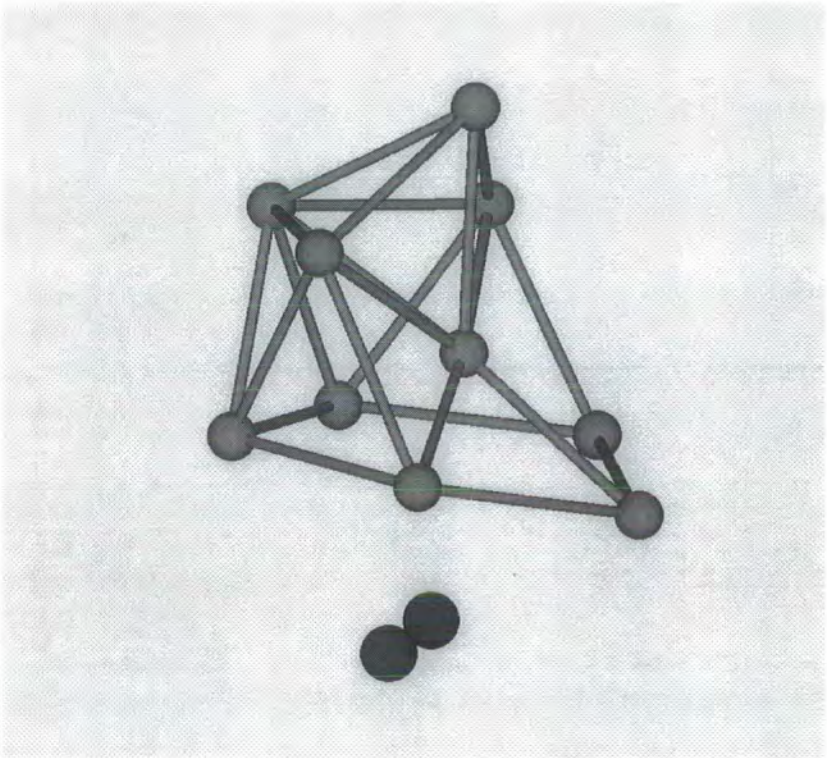

Figure 5.30: $Ne_{10}N_2$ $V_{10,3}$ structure

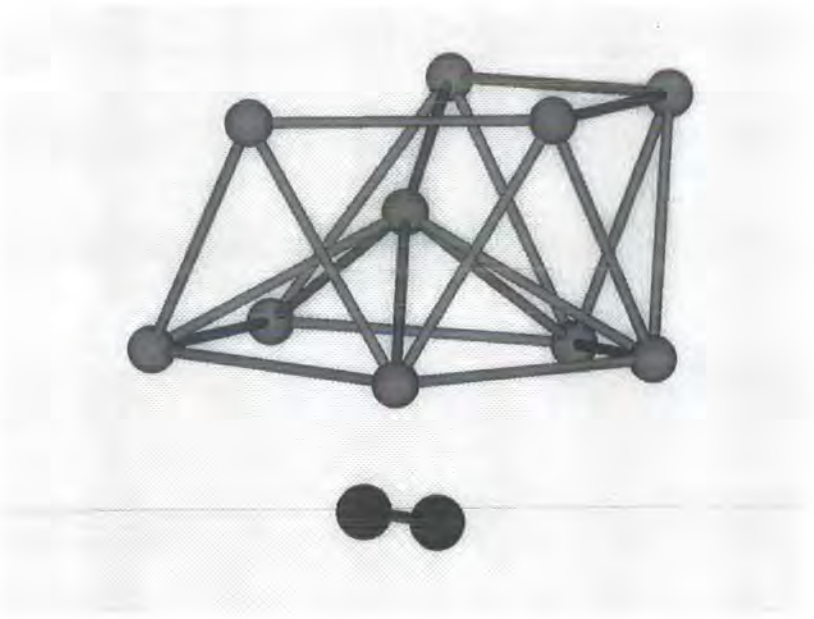

Figure 5.31: $Ne_{10}N_2$ $V_{10,4}$ structure

5.2.10 $Ne_{11}N_2$

The global minimum for the $Ne_{11}N_2$ system is the pure rare gas Ne_{12} structure, with the N_2 sitting underneath it. Unlike the $Ar_{11}N_2$ system there are not two versions of the pure rare gas structure, one with it pointing along the structure and the other with the N_2 pointing across the structure. This means that when the N_2 is lying across the bottom of the neon structure in the $Ne_{11}N_2$ system it can rotate to lie along the structure without having to climb out of a well. This is probably due to the lower anisotropy of the Ne-N_2 potential energy surface.

This difference between the two rare gas-molecule systems may be an unphysical artefact of the Ne-N_2 potential energy surface. The Ne-N_2 [168] potential energy surface is considerable older than that the Ar-N_2 [164]. The Ne-N_2 potential energy surface did give a reasonable fit to all the available experimental data, and is still used widely in calculations of various properties (such as second virial coefficients and total differential scattering cross sections). The Ar-N_2 surface by contrast has recently been re-investigated. The main feature of the new work on the Ar-N_2 interaction has been to make the potential energy surface more

anisotropic. This may explain why the $Ar_{11}N_2$ system has a second stable position for the N_2 underneath the rare gas cluster, while one is not found in the $Ne_{11}N_2$ system.

The $V_{11,2}$ structure is the $V_{10,4}$ structure with an extra atom above the upper ring of atoms, and directly above the top atom of the pentagonal pyramid. The $V_{11,3}$ structure is also based on the $V_{10,4}$ structure, but this time the last Ne atom occupies the last free capping position on the side of the pentagon substructure. The $V_{11,4}$ structure is the part-formed icosahedral structure.

The question now is why has Ne_nN_2 suddenly (for $n \geq 10$) started behaving like $Ar_{11}N_2$ system, and will this trend continue? I have called the $V_{8,1}$, $V_{9,1}$, $V_{10,1}$ and $V_{11,4}$ structures icosahedral cages, which they indeed are, but they are subtly different from the icosahedral cages of the Ar_nN_2 system. The icosahedral cages of the Ar_nN_2 systems have the atoms in the bottom ring below the N_2, whereas in the Ne_nN_2 system the atoms in the bottom ring lie around the N_2. This gives us our first clue as to why the Ne_nN_2 system has had its apparent change of mind. The equilibrium distance for the Ar-Ar pair potential is 3.759 Å; whereas the Ne-Ne equilibrium is 3.091 Å. The distance between the top and bottom rings in the two cages are 3.8518 Å for the Ar cage, and 3.040-3.169 Å for the Ne cage. Thus in both cases the atoms in the two rings are separated by approximately their equilibrium distance. However in the Ne cage the bottom ring has to expand to sit around the N_2 at the Ne-N_2 equilibrium distance. This expansion means that the interparticle distance, ranging from 3.25-4.38 Å in the lower ring, is large compared with the Ne-Ne equilibrium distances. In the Ar cages the interparticle distance in the lower ring is approximately 4.02 Å, which is relatively close to the equilibrium distance of Ar-Ar interaction. The extremely large interparticle distance in the lower ring compared to the equilibrium distance for the Ne-Ne cages would normally lead to a highly unfavoured ring structure, but the fact that all five atoms can interact in a 'T shaped' configuration with N_2 stabilises the structure. The fact that the Ne-Ne interaction is too short range means that even though the Ne-N_2 interaction is dominant, the structures that would maximise

that interaction, the icosahedral cage and its derivatives, can not be easily formed. While it is possible to form a distorted icosahedral cage or a capped version of the $V_{10,1}$ structure neither of these structures are energetically favourable compared to those that which allow the rare gas-rare gas interaction to be maximised while still allowing the N_2 to interact with five of the Ne atoms. We therefore see the rare gas-rare gas interaction determining the structures $n \geq 10$ instead of the stronger rare gas-N_2 interactions.

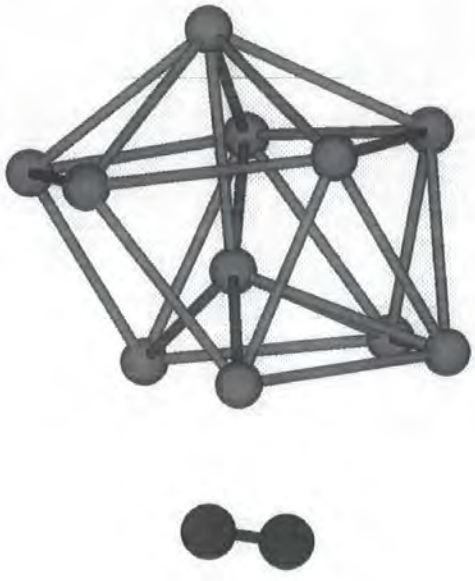

Figure 5.32: $Ne_{11}N_2$ $V_{11,1}$ structure

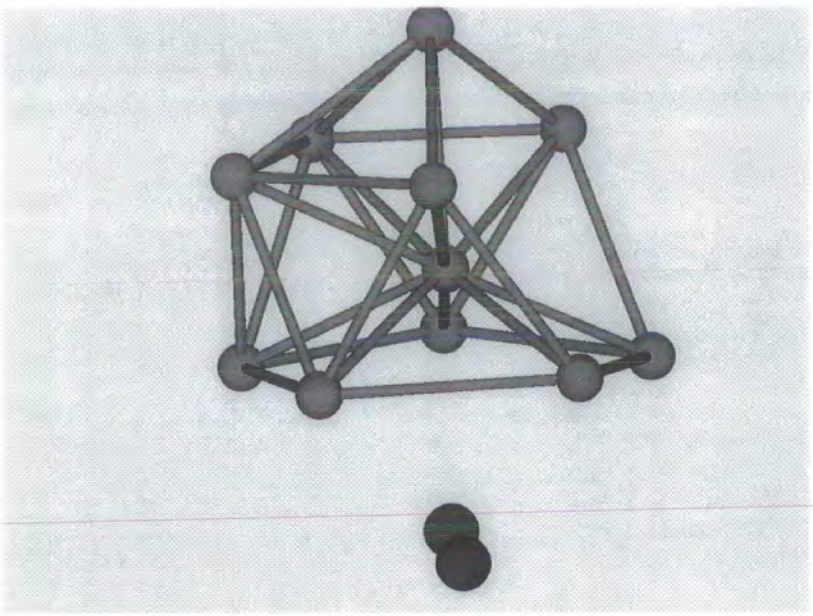

Figure 5.33: $Ne_{11}N_2$ $V_{11,2}$ structure

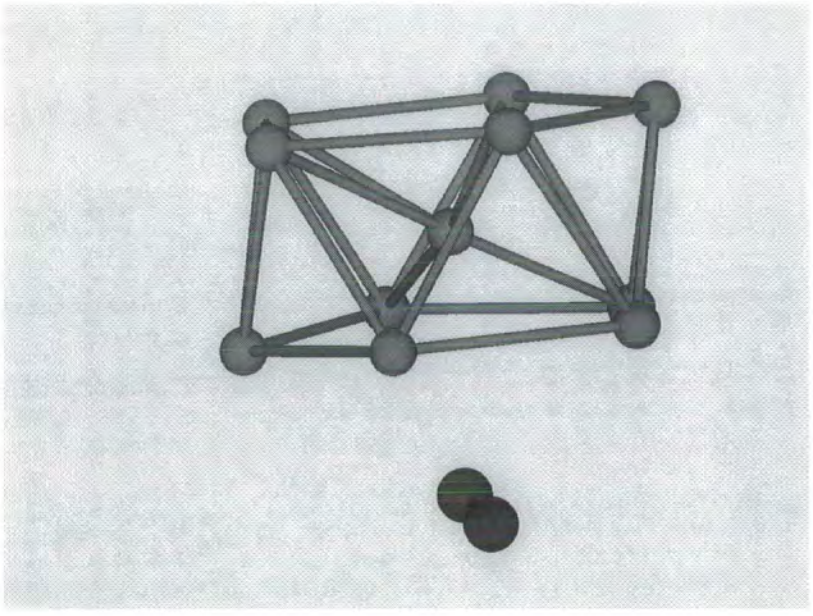

Figure 5.34: $Ne_{11}N_2$ $V_{11,3}$ structure

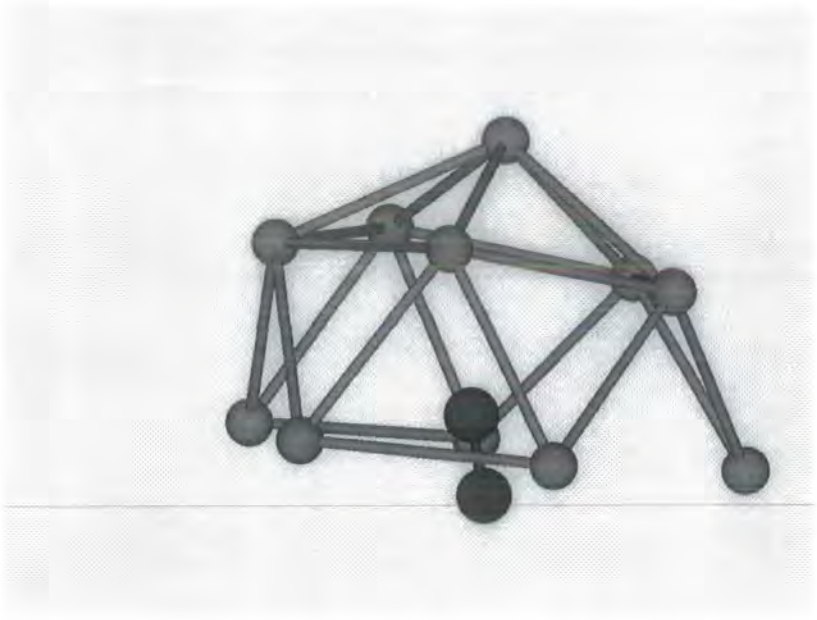

Figure 5.35: $Ne_{11}N_2$ $V_{11,4}$ structure

5.2.11 $Ne_{12}N_2$

The global minimum for the $Ne_{12}N_2$ system is a pure rare gas cage, with the N_2 sitting underneath it. This is the same as the $Ar_{12}N_2$ global minimum, and is a continuation from the $Ne_{11}N_2$ global minimum. The $V_{12,2}$ structure is a continuation of the $V_{11,5}$ structure. It is an irregular cage, with six atoms in the lower ring around the middle of the N_2. We do not find a distorted icosahedral cage because the bottom capping atom would be too far from the Ne atoms in the lower ring of the icosahedral cage if it was to be at its equilibrium distance from the N_2. The six atoms in the lower ring are packed closer to each other than those in the $V_{11,4}$ structure, with interparticle distance ranging from 3.08-4.31 Å. This however is not unfavoured in the Ne_nN_2 system with its short-range rare gas-rare gas interactions. The $V_{12,3}$ structure is a $V_{11,1}$ structure with the last Ne atom lying below the cage, where it interacts in an almost 'T shaped' which allows the Ne atom to interact favourably with the cage structure above.

The $V_{12,4}$ structure is very interesting, and unexpected structure to find. Its relatively high stability is again due to the strong Ne-N_2 interaction that it helps

to maximise. It is actually the $V_{10,1}$ structure, the last cage structure to be a global minimum, with two capping atoms. The first capping neon atom caps one of the top faces on the incomplete side of the cage part-formed icosahedral cage structure, while the second one lies directly below the first capping atom and interacts strongly with the N_2. This causes the top five membered ring of the part-formed icosahedral cage to distort so as to maximise the Ne-N_2 interaction. Many capped $V_{10,1}$ structures were found but their energies were outside our range of interest, and therefore I will not mention them here. There is only one version of the $V_{12,4}$ structure however, because it relies on the lower of the two capping atoms being able to interact with the N_2. This means that the lower capping atom must be placed on the open side of the part-formed cage structure, and the Ne atom capping the top of the structure must be directly above the first capping atom. There are only two possible sites on the $V_{10,1}$ structure where this is true, and the two are equivalent. There is therefore only one structure of interest. This structure very clearly illustrates how the Ne-N_2 interaction still dominates the system, even though the global minimum is not a cage structure. If the two Ne atoms are placed on the side of the cage adjacent to each other the energy of the structure is 1285.129 cm^{-1} which is outside of the energy range we are interested in. Again this show the stabilising effect of the Ne-N_2 on the $V_{12,4}$.

The $V_{12,5}$ structure is like the $V_{12,3}$ structure except that the 12th atom now interacts with the N_2 in a linear configuration, rather than in a 'T shaped' manner. It is therefore energetically less stable. We then find all the capped $V_{11,1}$ structures, where the capping atom interacts with the Ne_{11} cage rather than the N_2. This makes these structures less energetically favoured than the $V_{12,3}$ and $V_{12,5}$ structures, again showing the dominance of the Ne-N_2 interaction over the Ne-Ne interaction. As was discussed in the $Ar_{12}N_2$ system there are seven capping sits for the $V_{11,1}$ structure. They are very close in energy and therefore probable interchangeable in reality.

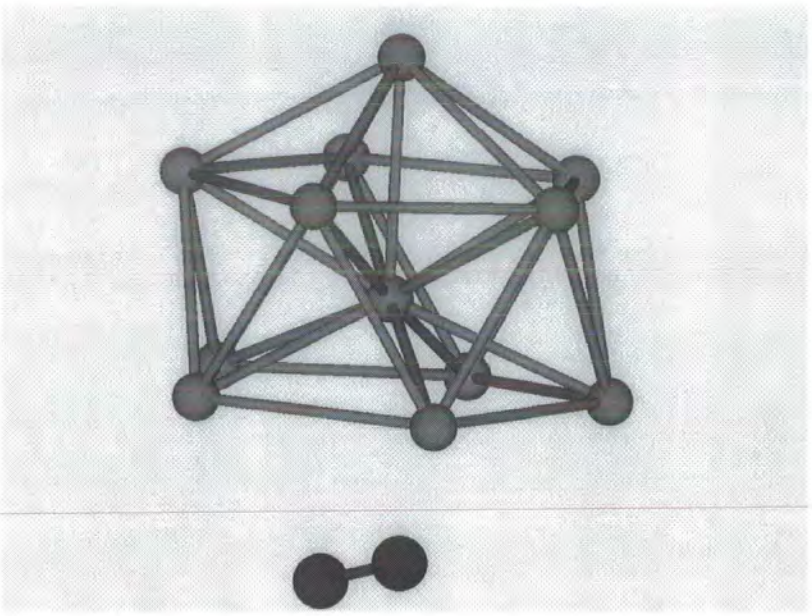

Figure 5.36: $Ne_{12}N_2$ $V_{12,1}$ structure

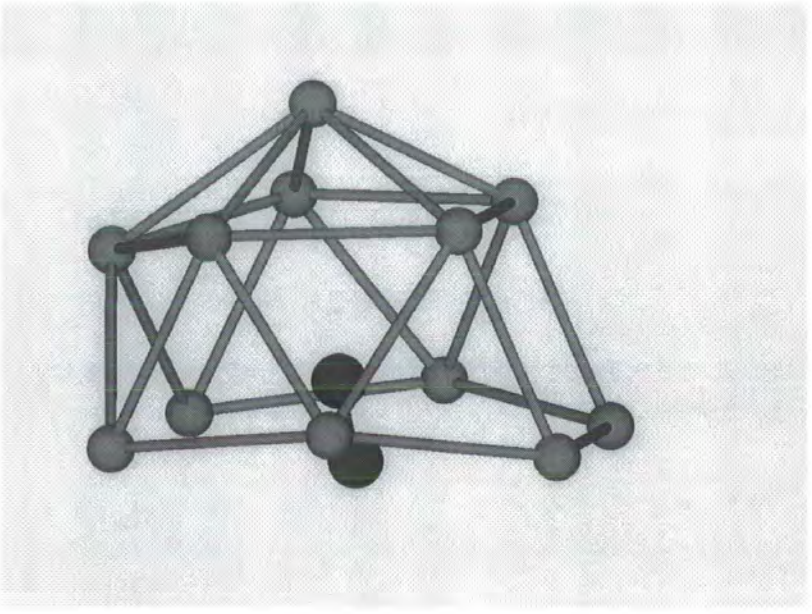

Figure 5.37: $Ne_{12}N_2$ $V_{12,2}$ structure

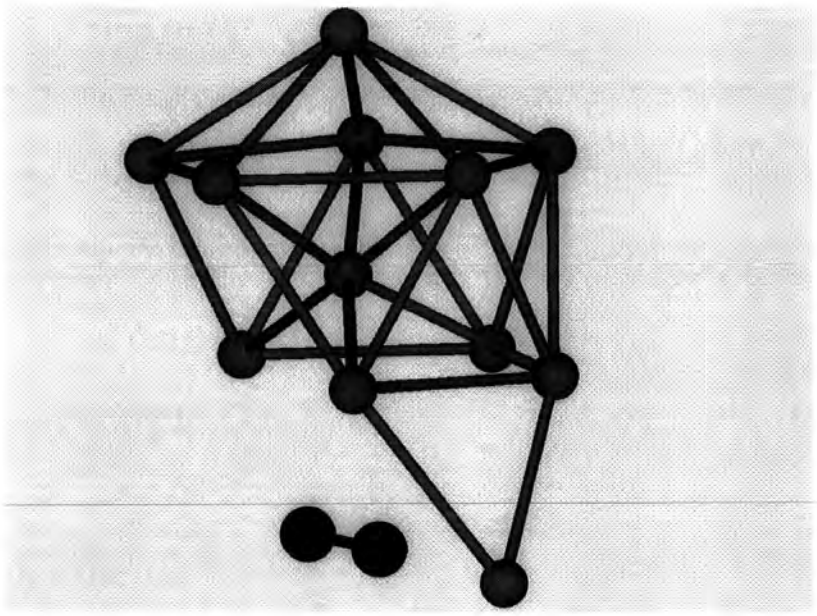

Figure 5.38: $Ne_{12}N_2$ $V_{12,3}$ structure

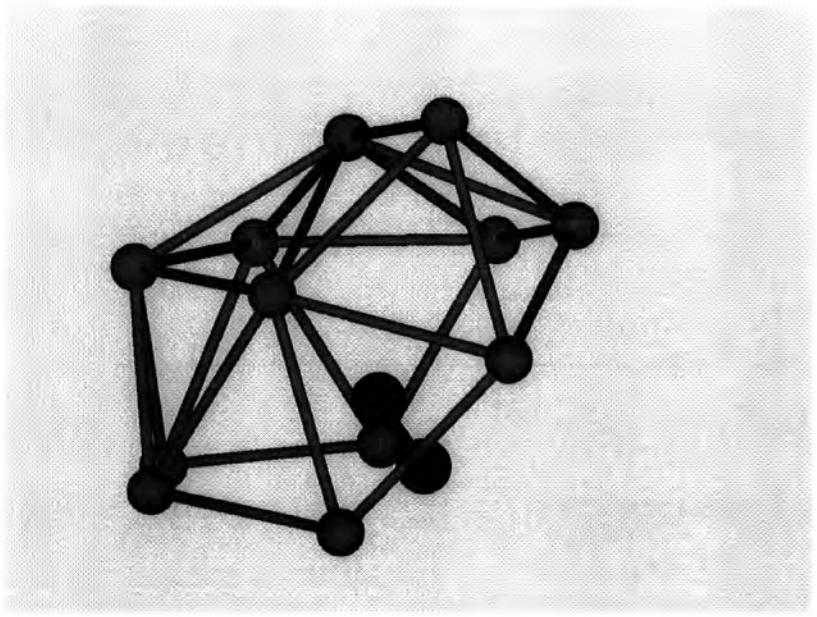

Figure 5.39: $Ne_{12}N_2$ $V_{12,4}$ structure

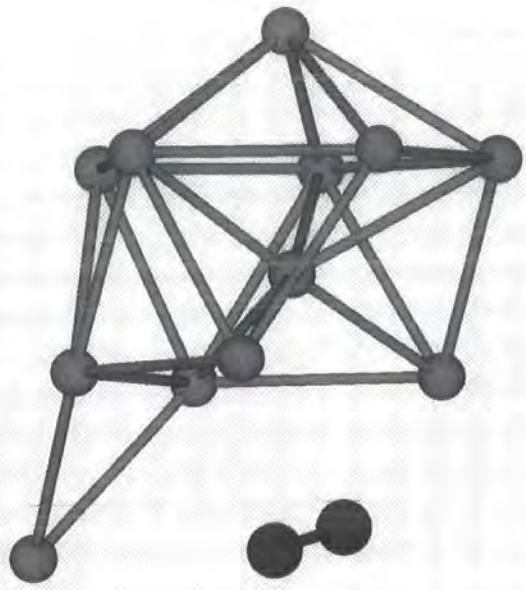

Figure 5.40: $Ne_{12}N_2$ $V_{12,5}$ structure

5.2.12 Ne_nN_2 where $n > 12$

The question that we now need to ask is when does the Ne_nN_2 system have a complete cage structure as the global minimum? At the moment we can use simulated annealing to search the potential energy surface for systems up to $n = 12 - 14$ before it becomes practically impossible, because of the amount of computer time required. For example, a typical $Ne_{12}N_2$ run took approximately 600 minutes of CPU time on one Silicon Graphics R10000. That is for just one simulated annealing run. To be confident that the complete active space of the potential energy surface has been covered usually requires between twenty and thirty simulated annealing runs for different starting positions. The number of simulated annealing runs increases as the number of atoms increases. Figure 5.41 shows a plot of the CPU time taken for each simulated annealing run against n. The graph clearly shows that using simulated annealing to search a surface limits the size of system that can be studied. The increase in the time taken each search as n increases makes searches of larger ($n > 14$) unlikely for the foreseeable future.

It is possible to reduce the scaling of the problem, using physical understanding of what constitutes a good structure. Starting all searches from physically reasonable places on the potential energy surface reduces the chance of being trapped in a local minimum. This allows the simulated annealing algorithm to spend most of its time searching the parameter space of interest, and can make a very significant reduction to the time need for a simulated annealing run. As the value of n increases it becomes increasingly important to select the starting point for each simulated annealing run carefully. It is possible save as much as 100 to 150 minutes by choosing the starting points for the simulated annealing runs well. This of course biases the search, as some structures are effectively eliminated because the simulated annealing search simply cannot reach them. Using more 'selective' simulated annealing searches it may be possible in the near future to study some of the larger systems that are at the moment not possible.

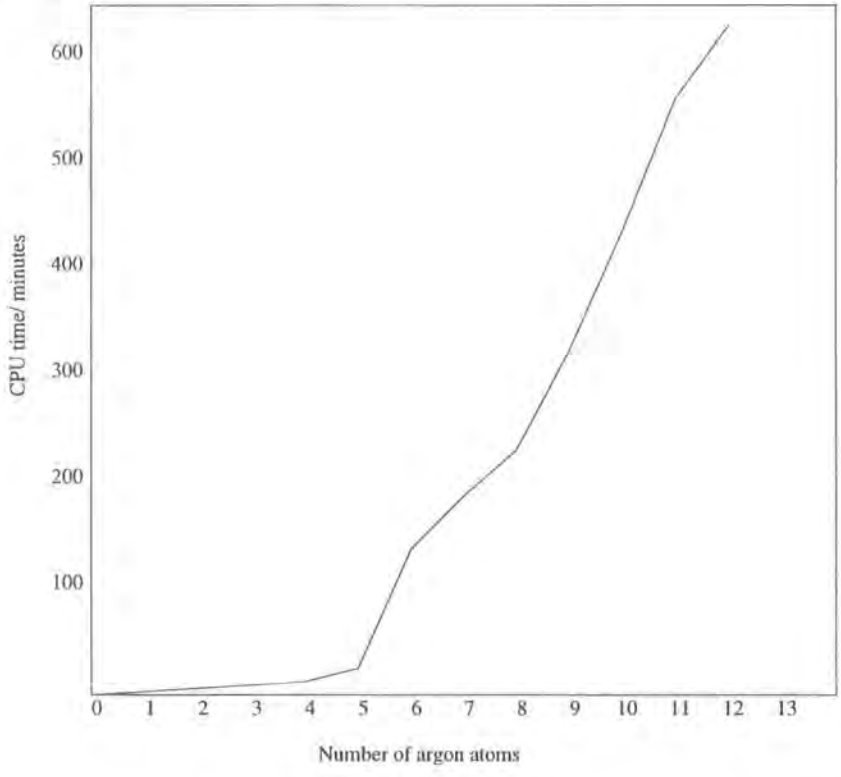

Figure 5.41: Plot CPU time vs. number of Ne atoms in the cluster

The problems above mean that it is difficult to push the simulated annealing

technique to search for the first cage-like global minimum. At this point we need to bring our understanding of the system into play. Instead of searching the potential energy surface for a global minimum and low-lying minima, we can use our physical insight to decide on the most likely first cage structure. Having done this we can use a gradient based minimisation technique to relax the structure to its lowest-energy configuration. This is not a search technique, as we sample only sampling a few points on the potential energy surface. It is however a way of testing ideas for possible structures, which can show if we are on the right track. We can build both a cage structure and some form of multicapped pure Ne_{12} structure. We can then relax both of them to their local minimum, and find out which of the local minima is the lower in energy. If the capped structure is the lower energy structure, we have a valuable answer for that value of n. If the reverse is true and we find that the cage structure is the lower of the two minima, the next question is wether the non-cage structure is the lowest-energy such structure available. We have assumed that we understand the driving forces of the system well enough to be able to make 'good' guess at the structures. This can be a dangerous assumption to make, as we have seen in the rare gas-N_2 system. For instance we did not expect to find the pure rare gas cluster for the global minimum of the $Ne_{12}N_2$ system, on the basis of the $Ne_{10}N_2$ results.

We have seen that the Ne-N_2 interaction dominates the Ne-Ne interaction, although the relatively short range of the Ne-Ne interaction means that we do not find the icosahedral cage structure to be the global minimum for the $Ne_{12}N_2$ system. Yet all indications from our studies on the Ne_nN_2 system lead us to expect a cage structure of some description to be formed as soon as is possible. Even in the $Ne_{12}N_2$ the first low-lying minima is an open cage structure, thus showing the system prevalence for forming cage structures.

We do not know what sort of cage system will be formed for Ne_nN_2. If it is to be more stable than a structure which maximises the rare gas-rare gas interactions, such as some form of capped pure Ne_{12} structure, it must have the Ne-Ne pairs close to their pair potential equilibrium distance. The most obvious cage structure that

will encase the N_2 and still allow the Ne atoms to stay at their equilibrium distance is a tube-like cage, which has a second capped pentagon ($V_{6,1}$) structure sitting underneath the part-formed icosahedral structure. There are two candidates for the part-formed cage onto which we will attach the capped pentagon structure. They are the eleven atom part-formed icosahedral cage structure, $V_{11,4}$, and the twelve atom cage structure ($V_{12,2}$) with six Ne atoms in the base. Both of these structures are likely candidates and so both were tested.

We also need a likely candidate to compete with the cage structures. This of course is very tricky, as we have already said that it is difficult to predict how a system will change as n increases. We have seen that in general the more symmetric a structure is, the more stable it will be. Although this is not always true, as was shown by the $V_{12,4}$ structure, it is a good rule of thumb. It seems likely that the most stable non-cage structure for the $Ne_{17-18}N_2$ system is likely to be based on the pure Ne_{12} structure. The remaining atoms can then either sit around the top or middle of the Ne_{12} structure, or sit underneath the structure and interact with the N_2 in a 'T shaped' manner. This is where we have to look at the systems we have studied and make an educated guess at the most likely structure. Through out our study of the Ne_nN_2 system, we consistently found that the Ne-N_2 interaction is dominant. It thus seems reasonable to assume that the most stable place for the Ne atoms to sit is underneath the pure Ne_{12} structure, and around the middle of the N_2 bond. Again we can put the five or six atoms in the ring, and again both possibilities seem feasible from our experience so far. In the $Ne_{17}N_2$ system we can only have five Ne atoms in the lower ring, but in the $Ne_{18}N_2$ system we could have five atoms in the ring around the N_2 and the last Ne atom capping one of the faces of the neon structure; alternatively we could have six atoms in the ring around the middle of the N_2 molecule. Both of the these structures seem possible and so we tested both.

The results are very interesting. In both $Ne_{17}N_2$ and $Ne_{18}N_2$ the lowest energy structure is that of the cage. In both cases the energy difference is approximately 60 cm^{-1}. This compares with an energy difference of approximately 68 cm^{-1}

in the $Ne_{12}N_2$, in favour of the pure rare gas structure. The fact that the cage structure is so much more energetically stable than the structures based on pure rare gas clusters is very significant. If the energy difference had been small, i.e. less than 10 cm^{-1}, then there would have been some doubt as to whether or not the cage structure was the global minimum. It would be difficult to argue that there was little chance of finding an alternative non-cage structure which could make up the energy difference. However with such a large energy difference we think that it is unlikely that there is a structure for either $Ne_{17}N_2$ or $Ne_{18}N_2$ that will be more stable than the cage structure. It therefore seems likely that in the Ne_nN_2 system the global minima for $n \geq 17$ are going to be cage structures.

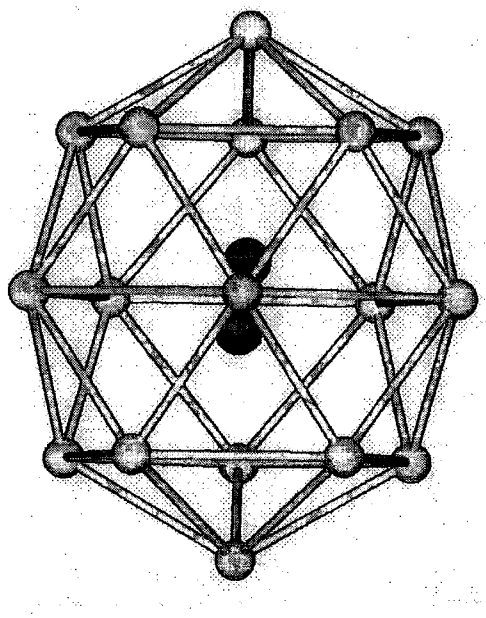

Figure 5.42: $Ne_{17}N_2$ $V_{17,1}$ structure

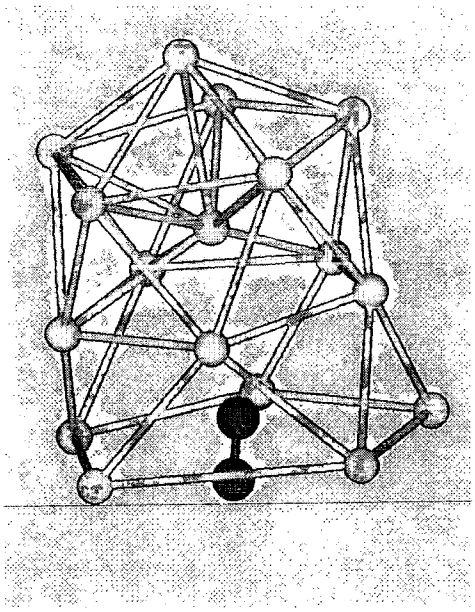

Figure 5.43: $Ne_{17}N_2$ $V_{17,2}$ structure

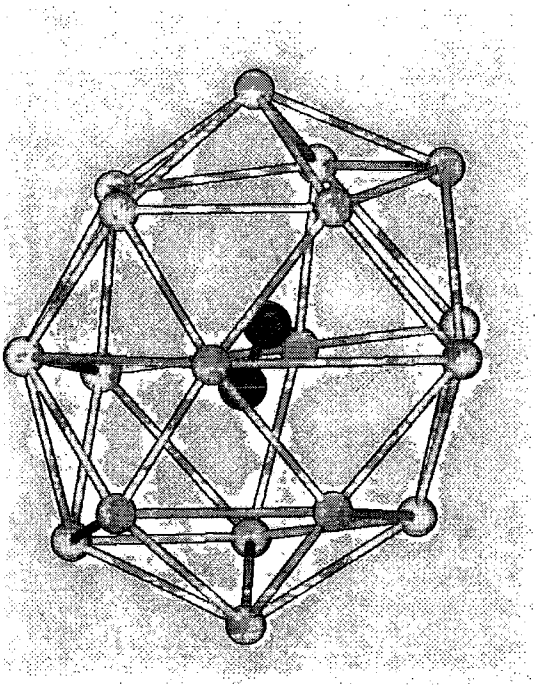

Figure 5.44: $Ne_{18}N_2$ $V_{18,1}$ structure

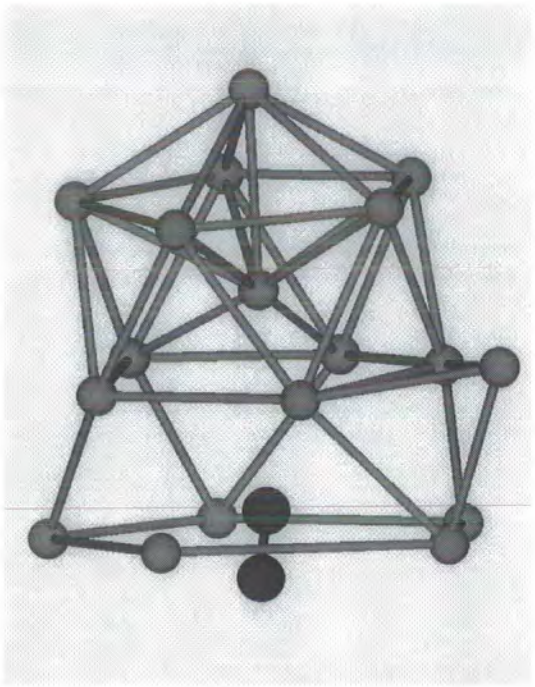

Figure 5.45: $Ne_{18}N_2$ $V_{18,2}$ structure

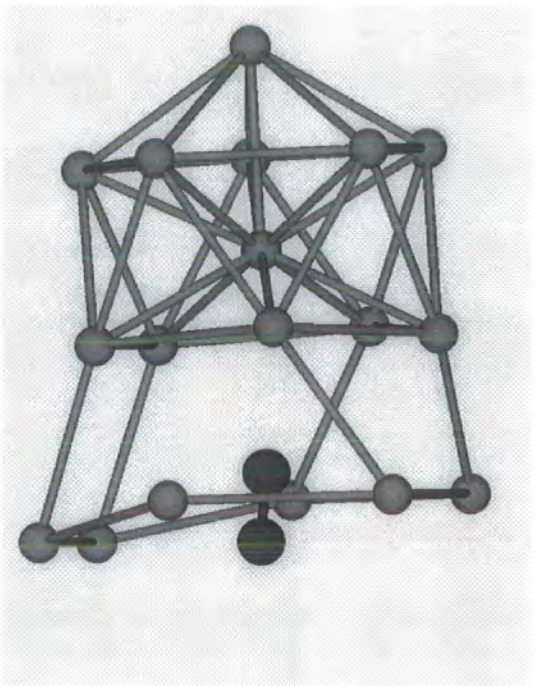

Figure 5.46: $Ne_{18}N_2$ $V_{18,3}$ structure

5.3 Conclusions

We started the work on Ne_nN_2 in order to gain further insight into the interplay between solvent-solvent and solvent-solute interactions, and their effect on the structures found. In Ne_nN_2 we chose a system where the strength of the solvent-solvent interactions is less than that of the solvent-solute interactions, to allow comparisons with Ar_nN_2.

The Ne_nN_2 systems for $n < 6$ have a few new structures in them. These new structures all have the neon atoms clustering around the middle of the N_2 bond. These structures are similar to those of the early Ar_nCO_2 systems [95]. These structures are possible because of the strong Ne-N_2 interactions. However there is not a five membered ring around the middle of the N_2 because the short Ne-Ne interaction distance makes such a configuration energetically highly unfavourable.

In general there were fewer new structures found than in our study of the Ne_nN_2 system. This was to be expected as Ne_nN_2 is much closer in nature to Ar_nN_2 than Ar_nN_2 is to Ar_nHF. We were more interested in the subtle effect that changing the balance between the two types of interaction would have on the system. To make a direct comparison of the two sets of results more difficult, there was the added complication that the two rare gases have different range of interaction. The fact that the neon-neon interaction is shorter than the argon-argon interaction leads to a strange change in the type of structures found for the system as the value of n increases. This leads to a first solvation shell that we would not have been predicted for this system, based on our results for $n \leq 10$. This is a valuable lesson, as it shows us how the range of an interaction can drastically alter the solvation properties.

The effect of the range of an interaction has recently seen by Nesbitt et al. in the Ar_nHCl system [91]. The Ar_nHCl however showed completely different behaviour to Ar_nHF. Instead of having a first solvation shell at $n = 12$ the $Ar_{12}HCl$ global minimum has the argon atoms forming a pure rare gas cluster, and the HCl 'pointing' at the five-atom-base of the argon cluster. This behaviour looks very strange at first because the Ar-HF and Ar-HCl potential both have deep anisotropic

minima about the linear Ar-H-X configuration, and as such it would have been predicted that the two systems would behave in a very similar manner. What causes the two systems to behave so differently is that the equilibrium distance of the Ar-HCl interaction is larger than that of Ar-HF. This means that if the HCl is inside the Ar cluster the Ar atoms have to be further apart, which is energetically unfavourable.

If Ar_nN_2 can be crudely classified as a system dominated by the solvent-solvent interactions, then Ne_nN_2 is one in which the opposite is true. In the Ne_nN_2 system the solvent-solute interaction is dominant. Even though the rare gas-molecule interaction is not as anisotropic as the Ar-HF interaction the Ne_nN_2 system forms a part-formed icosahedral cage structure very easily. Indeed the system has a part-formed icosahedral cage as the global minimum earlier that the Ar_nHF system.

The Ar_nN_2 and Ne_nN_2 systems start to behave very differently for $n \geq 7$, as the dominance of one of the interactions starts to show through clearly in the structures found. It is not just the fact that Ne_7N_2 has a part-formed icosahedral cage that is so surprising, but that the higher n systems become so dominated by cage structures. The relative weakness of the Ne-Ne interaction means that even unsymmetric cages are favoured over more symmetric pure rare gas structures. A good example of the Ne_nN_2 system's propensity to form cages is shown by the $V_{12,4}$ structure. This is a part-formed icosahedral cage, actually the $V_{10,1}$, structure with one of the capping atoms interacting with the N_2 in an almost 'T shaped' manner. This structure is only found in the Ne_nN_2 system, as it requires a relatively strong rare gas-molecule interaction to make the structure stable.

The trend towards cage structures which encase the N_2 molecule makes an abrupt halt at $n = 11$. This was a most unexpected result at the time, although it can be rationalised. The fact that the system appears to change its mind over the forces determining the structure of the system means that a larger cluster is needed to form a complete cage around the N_2. As has been discussed above we have been able to show that the likely global minima for the $Ne_{17}N_2$ and $Ne_{18}N_2$

systems are cage structures, and that this follows the trends of behaviour that we saw in the Ne_nN_2 systems before the problem of the short interaction distance began to effect the structures found.

The unexpected behaviour of the Ne_nN_2 system for $n = 11$ and 12 is an excellent example of the difficulties in simply following a trend in structures when trying to find the minima of a potential energy function. For each value of n we have a completely new potential energy hypersurface, and although there are similarities between the different Ne_nN_2 systems, that is all. To be sure that the global minimum and the other low-lying minima have been found, it is essential to search the surface thoroughly. However, this is not possible for large systems, and we are reduced to other method such as those described in the previous section.

n	$V_{n,1}$ /cm^{-1}	$V_{n,2}$ /cm^{-1}	$V_{n,3}$ /cm^{-1}	$V_{n,4}$ /cm^{-1}	$V_{n,5}$ /cm^{-1}
2	−129.473				
3	−230.174	−210.203			
4	−340.806	−322.431	−291.320		
5	−446.246	−439.543	−435.015	−418.683	
6	−565.572	−558.084	−557.654	−548.175	
7	−678.896	−667.466	−6650625	−662.247	
8	−803.367	−793.986	−789.689	−785.070	−781.301
9	−931.327	−917.775	−914.093		
10	−1056.445	−1048.088	−1042.021	−1040.873	
11	−1201.365	−1196.557	−1195.698	−1177.819	
12	−1383.888	−1319.200	−1316.749	−1312.684	−1308.113
17	−2067.711	−2006.066			
18	−2202.828	−2146.535	−2138.977		

Table 5.1: results for Ne_nN_2

Chapter 6

Three-Body Effects in Rare Gas-Molecule Cluster

6.1 Three-Body Effects

In this chapter we will investigate the effects of three-body interactions on the two rare gas-molecule systems that we have studied. In most pervious work on van der Waals clusters it was assumpted that the potential energy counld be calculated as a sum of the pairwise interactions [101, 159, 91, 95, 14, 131, 22, 47]. There has been much work on the effect of three-body forces on many different systems, [13, 170, 171, 131, 172, 173, 174, 175, 176], but relatively little work on their effect in rare gas-molecule clusters despite their importance in many physical and chemical processes. The lack of investigation is due to two main reasons. Firstly the effects of three-body forces are notoriously difficult to detect by conventional spectroscopic techniques, and secondly they present formidable theoretical difficulties.

In all our studies of rare gas-molecule systems so far we have constructed the potential energy surface to be searched by summing the pairwise interactions. The potential energy surface was then searched using simulated annealing, and structures were refined using a gradient-based minimisation technique. In doing this we ignored any three-body interactions. These three-body interactions were not included, because pairwise interactions account for the majority of the interaction

energy in van der Waals systems. The small but significant effect of three-body interactions was shown by Nesbitt [91] in his work on Ar_nCO_2. He found experimentally that in the case of Ar_2CO_2, with a red shift of 0.89827(27) cm^{-1}, the three-body contribution to the red shift was 0.042 cm^{-1}. While the size of the three-body contribution is different for each system the range is typically between 5 and 15% for rare gas clusters.

Not only is it generally valid to assume pairwise additivity when considering molecular clusters, it is also a necessary simplification as the three-body potential is very expensive to evaluate. It would be impossible to use simulated annealing, at the present time, to search a potential energy surface which included three-body effects. This is shown quite clearly by the results of the gradient-based search routine on the three-body potential energy surface. Starting a gradient-based minimisation of the $Ne_{17-18}N_2$ structures on the three-body potential energy surfaces clearly shows the problems of searching such surfaces. The $Ne_{17-18}N_2$ systems both offer good examples of the problems encountered in searching three-body surfaces, because the positions used at the start of the minimisation are not at or very near to a minimum. Because of this, the minimisation for the pairwise surface takes approximately ninety steps to find a minimum. It therefore has to calculate the value of the potential energy surface a very large number of times, just as the simulated annealing search routine would. In the case of the pairwise additive potential energy surface, the minimum was found in 10-15 minutes. For the three-body potential energy surface, the time taken to find the same minimum from the same starting position was between 100 and 150 minutes. A similar scaling could reasonably be expected for a simulated annealing search. Indeed the scaling of the time taken for a three-body simulated annealing search could be even worse, as in simulated annealing the potential energy subroutine is call many more times than in a typical gradient-based minimisation routine. As a single simulated annealing search of a large cluster, for example $Ar_{12}N_2$, takes seven hundred minutes of CPU time, increasing the time by a factor of ten or more would make a full search of the system infeasible.

The above discussion shows that we will have to use a gradient-based search technique to study three-body effects in rare gas-molecule clusters. The problem is gradient-based search techniques are highly sensitive to the starting position of the search. As the potential energy surface becomes more complicated, gradient-based search routines becomes more and more sensitive to the choice of starting position. The addition of three-body terms to each point in configuration space will make the potential energy surface even more complicated, both in terms of evaluation and of topology. The energy at any given point in parameter space for the pairwise surface is

$$E(x) = \sum V_{\text{Rg-Rg}}(x_i, x_j) + \sum V_{\text{Rg-Mol}}(x_i, x_j); \tag{6.1}$$

whereas the energy at any point of the three-body surface is,

$$\begin{aligned} E(x) &= \sum V_{\text{Rg-Rg}}(x_i, x_j) + \sum V_{\text{Rg-Mol}}(x_i, x_j) \\ &+ \sum V^{\text{3B}}_{\text{Rg-Rg}}(x_i, x_j, x_k) + \sum V^{\text{3B}}_{\text{Rg-Mol}}(x_i, x_j, x_k). \end{aligned} \tag{6.2}$$

The pairwise terms remain dominant.

Since the three-body surface is more difficult to search that the two-body surface, the choice of starting position is even more critical. The most logical place to start the searches of the three-body surface are the minima of the pairwise potential energy surface, as the pairwise contributions are larger the the three-body terms. This assumes that the effect of the three-body terms on the potential does not move the minima too far in configuration space, and that the three-body terms do not form barriers in configuration space that would trap the search routine and stop it from finding a new minimum.

The main rare gas-rare gas three-body term and the only one that we consider here is the Axilrod-Teller [177] triple dipole dispersion interaction, which is of the form

$$V^{\text{AT}}_{\text{3-body}} = \nu_{ABC} \left(\frac{3 \cos\theta_A \cos\theta_B \cos\theta_C + 1}{(R_{AB} R_{BC} R_{CA})^3} \right) \tag{6.3}$$

Where θ_A, θ_B and θ_c are the angles of the triangle formed by the three atoms, and R_{AB}, R_{BC} and R_{CA} are the interparticle distance. The values of the coefficients ν_{ABC} for various rare gas systems have been given by Kumar and Meath [178].

The rare gas rare-molecule three-body potential also includes a triple-dipole dispersion term [179], and this is the only term considered here. The triple-dipole dispersion energy (DDD) for the interaction of three linear Σ-state molecules, A, B and C, is [179]

$$
\begin{aligned}
DDD &= \frac{(1+3\cos\theta_A\cos\theta_B\cos\theta_C)C_9(a,b,c)}{R_{ab}^3R_{bc}^3R_{ac}^3} \qquad (6.4)\\
&\times Re\,[\,1-\Gamma(a)W(\theta_a,\phi_a,\theta_A,\theta_B)\\
&- \Gamma(b)W(\theta_b,\phi_b,\theta_A,\theta_B)\\
&- \Gamma(c)W(\theta_c,\phi_c,\theta_A,\theta_B)\\
&+ \Gamma(a,b)W(\theta_a,\phi_a,\theta_b,\phi_b,\theta_A,\theta_B)\\
&+ \Gamma(a,c)W(\theta_a,\phi_a,\theta_c,\phi_c,\theta_A,\theta_B)\\
&+ \Gamma(b,c)W(\theta_b,\phi_b,\theta_c,\phi_c,\theta_A,\theta_B)\\
&+ \Gamma(a,b,c)W(\theta_a,\phi_a,\theta_b,\phi_b,\theta_c,\phi_c,\theta_A,\theta_B)\,]\,. \qquad (6.5)
\end{aligned}
$$

Where angles θ_i $(i = A, B, C)$ are as defined in equation 6.3, as are the three interparticle distances R_{AB}, R_{BC} and R_{CA}, and the angles θ_i and ϕ_i $(i = a, b, c)$ describe the orientation to the linear molecules. In the case of the rare gas-molecule clusters of interest here we do not have three linear Σ-state molecules. Instead we have two rare gas atoms interacting with linear Σ-state molecule. If we arbitrarily chose the linear Σ-state molecule to be the 'C' molecule then all angular terms in the $Re[\cdots]$ bracket of equation 6.5 that involve the 'A' or 'B' molecules will be zero, as the rare gas atoms can have no angular dependency. The above considerations lead to the following equation for rare gas-rare gas-molecule three-body triple-dipole dispersion energy,

$$
\begin{aligned}
DDD &= \frac{(1+3\cos\theta_A\cos\theta_B\cos\theta_C)C_9(a,b,c)}{R_{ab}^3R_{bc}^3R_{ac}^3}\\
&\times Re\,[1-\Gamma(c)W(\theta_c,\phi_c,\theta_A,\theta_B)]\,, \qquad (6.6)
\end{aligned}
$$

where the $C_9(a, b, c)$ and $\Gamma(c)$ coefficients have been calculated by McDowell et al. [180]. Using the shorthand Ω_c for θ_c, ϕ_c, the angular part of equation 6.6 is

$$
W(\Omega_c,\theta_A,\theta_B) = \left(\frac{4\pi}{5}\right)^{1/2}[\,Y_2^2(\Omega_c)(Q_1+\sqrt{6}P_{11}) + Y_2^1(\Omega_c)
$$

$$\left(Q_8 + 3\sqrt{6}P_{10} - \frac{3}{\sqrt{6}}P_{12}\right) + Y_2^0(\Omega_c)(Q_2)\,]\,, \tag{6.7}$$

where $Y_l^m(\Omega_c)$ are spherical harmonics. The $P_{m_1\,m_2}$ terms are

$$P_{m_1\,m_2} = \frac{P_2^{m_1}(\cos\theta_B)P_2^{m_2}(\cos\theta_A)}{(1+3\cos\theta_A\cos\theta_B\cos\theta_C)}, \tag{6.8}$$

where $P_2^{m_1}(\cdots)$ and $P_2^{m_2}(\cdots)$ are associated Legendre functions. The Q_k terms in equation 6.6 are

$$Q_1 = \frac{2}{\sqrt{6}}P_{20} - \frac{4}{\sqrt{6}}P_{11} + \frac{2}{\sqrt{6}}P_{02}, \tag{6.9}$$

$$Q_2 = 1 - P_{11} + 8P_{00}, \tag{6.10}$$

$$Q_8 = \frac{\sqrt{6}}{6}P_{21} + \frac{\sqrt{6}}{3}P_{12} - \frac{8}{\sqrt{6}}P_{10} - \frac{10}{\sqrt{6}}P_{01}. \tag{6.11}$$

To evaluate the three-body potential, we need to define all the three-atom and two atom-molecule interactions over which we want to sum. In a rare gas cage must count every triad of rare gas atoms, which will be designated $A\,B\,C$. If we think about the number of possible triads that we could form where $A \neq B \neq C$, in the Ar_4N_2 cluster, the possibilities are shown in table 6.1, where the four argon atoms are designated 1, 2, 3 and 4.

A	B	C	A	B	C
1	2	3	3	1	2
1	2	4	3	1	4
1	3	2	3	2	1
1	3	4	3	2	4
1	4	2	3	4	1
1	4	3	3	4	2
2	1	3	4	1	2
2	1	4	4	1	3
2	3	1	4	2	1
2	3	4	4	2	3
2	4	1	4	3	1
2	4	3	4	3	2

However as can be seen from table 6.1 most of the possible combinations are actually the same three atoms, but assigned to a different atom label (e.g. A, B or C). Obviously if the three-body interaction for atoms 1, 2 and 3 is accounted for with $A = 1$, $B = 2$ and $C = 3$, then we have to discount all other $A\ B\ C$ triads that contain atoms 1, 2 and 3. If we keep only the first example of each triad found then the unique triads left from table 6.1 are shown in table 6.1.

A	B	C
1	2	3
1	2	4
1	3	4
2	3	4

Table 6.1:

There is an analytical expression for the number of unique combinations of objects that can be form fromed a group of objects. These expressions can be used to check that we find all possible unique combinations. For a given number of atoms n and with r atoms in each combination, the total number of possible unique combinations is

$$C_r^n = \frac{n!}{(n-r)!r!}. \tag{6.12}$$

In the case of three-body interactions, this formula simplifies to

$$C_r^n = \frac{n!}{(n-3)!3!}. \tag{6.13}$$

Which in turn simplifies to

$$C_r^n = \frac{n \cdot (n-1) \cdot (n-2)}{6}. \tag{6.14}$$

This formula gives the correct number of triads, but it does not give the actual triads. To find the triads a subroutine was written, based on the above discussion. To provide the rare gas triads to the rare gas three-body potential routine the following algorithm was implemented. The three triad members ($A\ B\ C$) were

generated by looping over all possibilities of atom combinations, from one to the number of rare gas atom in the cluster. This is done by setting up three consecutive loops; the first loop is for A, the second for B and the third for C. After the second loop the algorithm checks to see if A and B are the same. If they are the same the algorithm moves on to cheque the next A and B combination. If they are not the same the third loop is entered, and the algorithm checks to see if the $A = C$ or $B = C$; if either of these conditions is true then the algorithm moves onto the next value of C in the loop. If $C \neq A$ or B them we have found a possible combination of atoms to use as a three-body triad, in our calculation. We now must test to see if the combination we have found is unique. The first triad to make it to this point is by definition unique, and so is automatically stored. All subsequent triads are then tested, by a subroutine described below, to see whether or not they are unique. If the triad is unique then it is store along with the others so far found, and used to test all subsequent triads.

To test whether a triad is unique or not, a second algorithm is used. In this a new triad (denoted $A_{new}\, B_{new}\, C_{new}$) is sequentially tested against each of the previously stored triads. For each unique triad(denoted $A\, B\, C$) each member is tested against each member of the new triad, to see whether or not they are the same. That is to say to see whether A_{new} or B_{new} or C_{new} is the same as A, B or C. Every time this condition is true a counter, which is zeroed for each unique triad that is tested, is increased by one, and the three members of the unique triad are tested against the next member of the new triad. If after all three members of the new triad have been tested the counter is equal to three the subroutine returns to the main program, where the new triad is not stored and the next possible combination is tried. If however the counter is not equal to three then the next previously accepted triad is tested in the same fashion. If at the end of this algorithm a count value of three has not been achieved, meaning that the new triad is not just a permutation of one of the previously stored unique triads, then the subroutine returns to the program and the new triad is stored as an accepted triad. When all possible combinations of $A\, B\, C$ have been tried, and the unique

triads have been determined, the number of accepted triads is checked against the analytical expression in equation 6.14. If these two numbers agree with each other then the unique triads are passed to the main gradient minimisation routine, where they are used to calculate the three-body interaction energy of the rare gas cage. Algorithms for the two programs described above is given in the appendix of this chapter.

To calculate the three-body interaction for the rare gas-rare gas-molecule interaction we have to find the rare gas-molecule triads. To do this we use the same method as in the calculation of the rare gas three-body interaction energy. There are however some slight differences. The formula (6.6) for the rare gas-molecule three-body interaction energy is defined with the molecule as the third member of the three-body triad. The subroutine to form the rare gas-molecule triads therefore only has to loop over the A and B members of the triads. That is to say that it only has to find the unique combinations of the rare gas atoms that will interact with the nitrogen molecule. [1]

The analytical expression of the total number of triads in each rare $\mathrm{gas}_n\mathrm{N}_2$ system, where one member of the triad is fixed, is given by equation 6.12 with $r = 2$, and is given by the following expression

$$C_r^n = \frac{n!}{(n-2)!2!}. \tag{6.15}$$

This leads to the expression

$$C_r^n = \frac{n \cdot (n-1)}{2}. \tag{6.16}$$

[1] The method just described for the calculation of the rare gas triads can be replaced by a simpler method, in which the triads are created by looping over $C > B > A$. A similar method can also be used for the rare gas-molecule triads by looping over $C > B$, and fixing A. In the texted I have described the method we accually used, although in any future work the simpler method would, and should, be used.

6.2 Results

6.2.1 Ar_nN_2

The result of the reoptimisation of the two-body structures using the three-body potential energy surface was that no qualitatively new structures were found, though the ordering sometimes changes. As the structures have not changed, I shall describe the three-body structures in terms of the two-body structures. To distinguish between the two potential energy surfaces, any designation of a structure from the three-body surface will be shown as $V^{3B}_{n,m}$. So for example if it is stated that the $V^{3B}_{12,2}$ structure is the $V_{12,7}$ structure this means that the first low-lying minimum of the three-body surface is the sixth low-lying minimum of the two-body surface. The fact that no new structures were found was not a surprise, as the three-body contribution to the total energy of the system is small. We thought that we might see some distortion of the two-body structures, which we do find. The distortion are however small. In the Ar_nN_2 system the argon-argon distances increase by between 0.01 and 0.02 Å, while argon-nitrogen distances increase by between 0.015 and 0.03 Å. In the Ne_nN_2 system the increases in the two distances is smaller: the neon-neon distances increase by between 0.003 and 0.01 Å, while the neon-nitrogen distances increase by between 0.005 and 0.02 Å. We do however see quite a lot of re-arrangement in the relative ordering of the two-body structures. In the main this involves a pair of low-lying minima switching their relative positions, for example the two-body $V_{6,4}$ and $V_{6,5}$ structure switch positions in the three-body systems for both Ar and Ne. The relative ordering of the three-body structures compared to the two-body structures is shown in table 6.2. The effect of the change in ordering is most noticeable in the $Ar_{12}N_2$ structures, where the ordering is completely different. The global minimum is unchanged, but the gap to the next low-lying minimum is significantly smaller than in the two-body case. The first low-lying minimum is now the icosahedral cage structure, which was previously the $V_{12,7}$ structure. The full set of changes is shown in table 6.2. The reason for the icosahedral cage being so energetically

favoured is that it minimises the energetically unfavourable triangular three-body Ar-Ar interactions, which are more numerous than the Ar-N_2 interactions. The $Ar_{12}N_2$ system rearrages so much because all the structures are so close in energy. They are mostly in fact capped $V_{11,1}$ structures, where the capping atom interacts with one face of the structure or with the N_2 molecule. This means the subtle effects of the three-body forces show up more clearly in the $Ar_{12}N_2$ system that in other Ar_nN_2 systems.

Another effect of including three-body terms is that the energy gap between consecutive structures is in general smaller. The reason for this is that the two-body interactions and the three-body interaction tend to drive the structure in different ways. That is to say that the two-body interaction energies are −ve and three-body interaction energies are +ve for most molecular configurations. It is only the fact that the two-body forces are stronger than the three-body forces that stops more structures altering their relative positions.

n	$V^{3B}_{n,1}$	$V^{3B}_{n,2}$	$V^{3B}_{n,3}$	$V^{3B}_{n,4}$	$V^{3B}_{n,5}$	$V^{3B}_{n,6}$	$V^{3B}_{n,7}$	$V^{3B}_{n,8}$	$V^{3B}_{n,9}$	$V^{3B}_{n,10}$
3	$V_{3,1}$									
4	$V_{4,1}$	$V_{4,2}$								
5	$V_{5,1}$	$V_{5,2}$	$V_{5,3}$	$V_{5,4}$						
6	$V_{6,1}$	$V_{6,2}$	$V_{6,3}$	$V_{6,5}$	$V_{6,4}$	$V_{6,6}$				
7	$V_{7,1}$	$V_{7,2}$	$V_{7,3}$	$V_{7,4}$						
8	$V_{8,1}$	$V_{8,2}$	$V_{8,3}$	$V_{8,4}$	$V_{8,5}$					
9	$V_{9,1}$	$V_{9,2}$	$V_{9,3}$	$V_{9,5}$	$V_{9,4}$					
10	$V_{10,1}$	$V_{10,2}$	$V_{10,3}$	$V_{10,4}$						
11	$V_{11,1}$	$V_{11,2}$	$V_{11,3}$	$V_{11,4}$	$V_{11,5}$					
12	$V_{12,1}$	$V_{12,7}$	$V_{12,2}$	$V_{12,4}$	$V_{12,8}$	$V_{12,5}$	$V_{12,6}$	$V_{12,10}$	$V_{12,9}$	$V_{12,3}$

Table 6.2: Ar_nN_2 three-body minimisation results from two-body starting positions

n	$V_{n,1}$ (cm^{-1})	$V_{n,2}$ (cm^{-1})	$V_{n,3}$ (cm^{-1})	$V_{n,4}$ (cm^{-1})	$V_{n,5}$ (cm^{-1})	$V_{n,6}$ (cm^{-1})
3	−590.961					
4	−889.866	−885.807				
5	−1218.189	−1192.854	−1190.279	−1187.710		
6	−1581.919	−1550.193	−1521.217	−1499.403	−1499.325	−1494.231
7	−1893.669	−1891.213	−1865.228	−1852.890		
8	−2290.375	−2288.654	−2287.911	−2258.752	−2256.917	
9	−2686.016	−2684.691	−2663.344	−2659.426	−2656.762	
10	−3083.189	−3059.755	−3050.679	−3048.917		
11	−3552.890	−3543.522	−3527.426	−3521.122	−3475.751	
12	−4104.445	−3884.746	−3874.246	−3873.468	3872.793	−3871.621

Table 6.3: results for three-body Ar_nN_2

6.2.2 Ne_nN_2

The results for the three-body Ne_nN_2 system are shown in table 6.4. Yet again we see that the energy differences between consecutive structures is less than in the two-body systems. We also find that not only are the structures from the two-body searches found, but their ordering relative to each other is the virtually the same (see table 6.4. There is in fact only one occasion on which the ordering changes. It should also be noted that the $Ne_{12}N_2$ system has the same ordering of structures as in the two-body case. The reason for the relatively small effect of the three-body forces on the Ne_nN_2 system is that the three-body interactions involving neon are so small. So for example the rare gas-rare gas three-body interaction energy of the $V^{3B}_{12,1}$ structures for the argon and neon systems are 153.010 cm^{-1} and 20.950 cm^{-1} respectively. This is a factor of 7.5 difference between argon and neon, whereas the ratio of the two-body interactions is a little over 3. The ratio of the three-body rare gas-molecule interactions is about five, where the two-body ratio is only two. These two facts together mean that the three-body forces disturb the Ne_nN_2 system less than the Ar_nN_2 system.

n	$V^{3B}_{n,1}$	$V^{3B}_{n,2}$	$V^{3B}_{n,3}$	$V^{3B}_{n,4}$	$V^{3B}_{n,5}$	
3	$V_{3,1}$	$V_{3,2}$				
4	$V_{4,1}$	$V_{4,2}$	$V_{4,3}$			
5	$V_{5,1}$	$V_{5,2}$	$V_{5,3}$	$V_{5,4}$		
6	$V_{6,1}$	$V_{6,3}$	$V_{6,2}$	$V_{6,4}$	$V_{6,5}$	$V_{6,6}$
7	$V_{7,1}$	$V_{7,2}$	$V_{7,3}$	$V_{7,4}$		
8	$V_{8,1}$	$V_{8,2}$	$V_{8,3}$	$V_{8,4}$	$V_{8,5}$	
9	$V_{9,1}$	$V_{9,2}$	$V_{9,3}$			
10	$V_{10,1}$	$V_{10,2}$	$V_{10,3}$	$V_{10,4}$		
11	$V_{11,1}$	$V_{11,2}$	$V_{11,3}$	$V_{11,4}$		
12	$V_{12,1}$	$V_{12,2}$	$V_{12,3}$	$V_{12,4}$	$V_{12,5}$	

Table 6.4: Ne_nN_2 three-body minimisation results from two-body starting positions

n	$V_{n,1}$ (cm^{-1})	$V_{n,2}$ (cm^{-1})	$V_{n,3}$ (cm^{-1})	$V_{n,4}$ (cm^{-1})	$V_{n,5}$ (cm^{-1})	$V_{n,6}$ (cm^{-1})
3	−227.602	−208.573				
4	−336.172	−318.352	−289.034			
5	−439.715	−433.099	−428.760	−412.852		
6	−556.942	−549.146	−549.139	−540.168	−536.606	−533.265
7	−688.156	−656.511	−655.251	−651.917		
8	−790.432	−780.260	−777.317	−772.067	−768.275	
9	−915.786	−902.965	−898.224			
10	−1038.399	−1028.675	−1023.090	−1021.818		
11	−1177.621	−1173.423	−1172.429	−1157.250		
12	−1354.969	−1292.562	−1290.965	1289.592	−1282.705	
17	−2026.960	−1965.359				
18	−2159.514	−2103.169	−2095.317			

Table 6.5: results for three-body Ne_nN_2

6.3 Random Move Minimisation(RMM)

In our studies of three-body forces so far we have always started the gradient-based search from the starting positions found by the simulated annealing searches because, as stated previously, the three-body potential is very expensive to calculate. The main problem with this method is that it relies on the same structures existing for the global minimum and local minima in the two-body and three-body potential energy surfaces. This has however not been demonstrated. In this section we will attempt to provide some evidence that our assumptions about the three-body potential energy surface are valid.

The question is how can we attempt to explore a surface that is too expensive to search with simulated annealing? The surface is far too complicated to be search completely with a gradient-based search routine, which is not too expensive to use. The number of starting positions that would be required for a complete search of the potential energy surface, with a gradient-based search technique, would be very large indeed, especially as the number of rare gas atoms in the cage increased. This brings us back to the structures found by the simulated annealing searches of the two-body potential energy surface, which we believe are good starting positions. The problem is that the gradient-based search will not be able to leave a potential well, if we start it in one. This is not a problem if we are indeed starting our searches in the global minimum or a low-lying minimum of the three-body potential energy surface, but we cannot know that this is true. There may well be a minimum near the starting position, found by the simulated annealing search, that is lower in energy that the starting point, or one of the other low-lying minima found by the simulated annealing search of the two-body surface. Yet because there is no downhill path connecting the two minima, the gradient-based search of the three-body potential energy surface will not find the new minimum. So how do we overcome this problem? We have to use a gradient-based method; and we need to keep the good starting positions found be the simulated annealing searches. However we must find some way of not becoming trapped in the well around the starting position.

One obvious way of searching the three-body potential energy surface is to try to alter our simulated annealing search. If we could make the number of steps small enough it might be possible to do a limited simulated annealing search of the surface. This has some very attractive advantages. Within the limits of the number of steps we could take, it would allow us to explore the whole surface. The problem however is that, as the size of the clusters increases, the number of steps needed increases, and eventually simply becomes too large. As an alternative to doing a full simulated annealing search we could just search the local parameter space around the previously found minima. This would be a 'quick' simulated annealing search. It could be done by using the two-body minima as starting positions, setting the number of random steps to be very small (100-1000), and reducing the temperature quickly. Again this idea looks promising, as it would certainly allow us to escape to local parameter space. The problem with this strategy is that it fundamentally will not work with simulated annealing. This is because, unlike a gradient-based search where starting close to a minimum increases the likelihood of finding the minimum, a simulated annealing search may not find the starting minimum, even if it is the global minimum. The reason for this is that a simulated annealing search can take large energetically unfavoured steps while the simulated temperature is high. This allows it to test a large volume of parameter space, but if the system is annealed too quickly, the search can become stuck in an energetically unfavoured local minimum. This problem can be solved by making the number of random steps between each temperature step large. However this is not a practical solution for three-body potential energy surfaces. In general even for large searches, such as in the larger two-body clusters, it is not advisable to start at a structure which is likely to be a minimum. Instead it is better to start the search at a point in configuration space near to the structure of the minimum. We can therefore not use the previously found structures as starting points for quick simulated annealing searches, nor can we use a full simulated annealing search starting from near the previously found structures.

The way in which we overcame these problems is very simple. As has already

been stated we have to use a gradient-based technique, because of the expense of evaluating the potential energy surface. We have therefore written a program that alters each co-ordinate of the rare gas cluster by a random amount. After the co-ordinates of the cluster have been altered a gradient-based search routine is used to find the nearest minimum from the new starting position. This search routine will be designated RMM. It is similar in philosophy to the quick simulated annealing runs that have been suggested, because both searches assume that any new minimum will be close to one of the two-body minima and both algorithms aim to use a random search of the local parameter space to find the new minimum.

The co-ordinates from the two-body simulated annealing search are read in by the main program. They are then sent to a subroutine 'rand', where each of the $3n$ co-ordinates is altered. In the rand subroutine for each of the $3n$ co-ordinates two random numbers (in the range 0-1) are generated. The first random number is multiplied by a pre-set factor (called max step) to give the magnitude of the step; the second random number is then used to determine the sign (i.e. +ve or -ve) of the step. This is done by setting a flag positive if the random number is less than a 0.5, or negative if it's a 0.5 or more. The sign of the move is then multiplied by the magnitude of the move, and added to the co-ordinate being altered.

Depending on the size of the random steps, the cluster from the simulated annealing searches could be slightly distorted or completely altered. We are not interested in just slightly distorting the cluster, as this would almost certainly result in the starting structure being found again. We need to alter the starting cluster structure sufficiently to give the gradient-based refinement routine a chance of finding any low-lying minima that are close by in parameter space. The larger the step size the more likely it is that the refinement will not return to the original minimum. It is of course possible that it will simply find one of the other previously found minima. If however there are other low-lying minima in the three-body potential energy surface we might have to question our assumption about the three-body potential energy surface.

The distortions to the two-body simulated annealing structures are by their

nature random, so that we have to do more than one search to have any confidence in our conclusions. The problem with repeated numbers of RMM runs is that because the cage is distorted to such a large extent, each refinement takes 5 to 10 times longer than the previous three-body minimisations. This means that some of the searches on larger clusters take 100 to 150 minutes of CPU time[2]. We test approximately 40 minima for both rare gas-nitrogen systems. We are therefore limited by the number of times we can run all the clusters through the RMM procedure.

There is no guarantee that we will find a new minimum from the RMM procedure. It is not a cheap version of simulated annealing. More importantly we are still prone to all the problems associated with minimising a very complicated N-dimensional function, with a gradient-based technique. The RMM technique is simply the most efficient, and perhaps the only, way of sampling the local configuration space. If we are correct in our assumption that the three-body forces only alter the two-body structures slighty, and that therefore the same structures exist for the minima on both the two-body and three-body potential energy surfaces, then the starting positions will be the only minima in the local configuration space. In effect all we will have done is to start the search on the side of the potential well. Alternatively we may have started the search from a plateau, with a downhill path to the original minimum. In either case the gradient minimisation routine will return to the original minimum. If however the three-body forces fundamentally alter the topology of the local parameter space, we should expect to find that a significant number of the randomise and minimise searches will fail to return to their original minimum.

In the searches of the three-body potential energy surface we only use the first few minima from each Ar_nN_2 systems as starting points for the gradient-based searches of the three-body surface. However, the effects of the three-body forces, are subtle and two orders of magnitude smaller than those of the two-body forces. They do affect the relative ordering of the low-lying minima and also bring the

[2]again on one R10000

energy differences between the consecutive clusters down considerably. The effect of the three-body forces is not uniform, as the geometry of a structure controls the magnitude of the three-body forces. It is therefore possible that a low-lying minimum that was not discussed and studied could represent a structure lower in energy on the three-body surface than one of the two-body low-lying minima. This is especially true for the Ar_nN_2 and Ne_nN_2 systems, which have very closely space minima compared to the Ar_nHF system.

It is therefore important that we find a way of eliminating this possibility. We could simply test all the low-lying minima that we ignore in the search of the two-body potential energy surface. This is not a very attractive option, because there are a very large number of possible minima that would have to be tested. For example in the $Ar_{12}N_2$ system the energy difference between the global minimum and the first low-lying minimum is approximately 200 cm^{-1}. There are then ten low-lying minima within the next 50 cm^{-1} of the $V_{12,2}$ structure. Since we cannot test all the two-body structures, our only left option is to look for evidence of high energy minima becoming more energetically favoured.

6.3.1 Energy-Limited RMM Search

When we randomly move the cluster atoms we find that most of the changes of co-ordinates increase the energy. As the clusters get larger the cumulative effect of small increases in the energy due to each co-ordinate change can give the new starting position an energy of 10^3 to 10^4 cm^{-1}. When this happens the search routine fails, either because the number of iterative steps exceeds a pre-set value or the search routine cannot find its way back to the region of interest. The reason for these large energies is that, in the random move process, two or more rare gas atoms are moved too close each other, or one or more rare gas atom is moved to close too the N_2. When this happens the two-body energy is large and positive. This sort of search behaviour does not tell us anything useful about the three-body potential energy surface. We need to restrict the structures to the volume of local configuration space where low-lying minima are likely to be found, and away from

repulsive regions of configuration space which may be difficult to leave. To do this we simply added an extra condition in to the random move subroutine. The condition prevents any random move for making the total energy of the system larger than a preset value, in our case 1000 cm^{-1}.

This method of limiting the maximum energy of the cluster could also lead to problems. In particular there is the possibility that the alteration of one co-ordinate could lead to an increase in the energy to almost 1000 cm^{-1}, and that all subsequent moves will be small. This particular problem seems not to be a practical problem however. This is because in general the moves that are accepted do not push the total energy of the system to 1000 cm^{-1} in one go, and moves can also decrease the total energy of the system. We could have eliminated this problem by setting a maximum change to the energy for any given change in the co-ordinates. This method of limiting the total energy was not used because it would not be possible to allow a large enough change in any one co-ordinate to successfully sample the local configuration space, while at the same time preventing the total energy becoming to large.

6.4 Results obtained from RMM for Ar_nN_2

For both the argon and the neon clusters a RMM search was done with a small step size of 0.2 Å. These tests were not to search for other nearby minima, unlike the RMM searches with larger maximum step sizes. The point of these searches was to give the two-body structures 'a bit of a jiggle' before the two-body structures were minimised. This would prevent the search routine from not finding the minimum value of each minimum due to the minimisation routine being started to close to the minimum. This can be thought of as a pseudo-annealing process. As can been seen from figures 6.6 and 6.12 these two searches confirm that we have indeed found the bottom of the well in all our minimisations of the two-body structures.

For the Ar_nN_2 system the RMM search results with a maximum step size of

$\frac{2}{3}$ Å were slightly surprising because so many searches fail, whereas in the Ne_nN_2 system the same step size was found to be much more successful. We found that if the step size was reduced to $\frac{1}{2}$ Å then the searches were much more successful at re-finding the original minimum. This is due to two factors. The first is that in Ar_nN_2 the Ar-Ar interaction is dominant, whereas in Ne_nN_2 it is the Ne-N_2 interaction that dominates. The second factor is that the N_2 molecule does not move during the minimisation process, so that the maximum change in the rare gas-rare gas interaction distance is greater than that of the rare gas-molecule interaction distance. These two facts combined mean that the argon clusters are more likely to move to a region of high energy in comfiguration space, and the searches are therefore more likely to fail.

Another interesting point to notice about the energy-limited searches is that with the largest maximum step size (max step = 1.5 Å) we start to see the searches finding other minima. These other minima are not new structures, but structure previously found in our searches of the two-body surface. What is happening is the random moving of atoms places the starting configuration for the search outside the valley that leads to the original minimum. The fact that the searches still only find previously found minima is a good indication that there are no low-lying minima nearby that we have missed. Indeed that we have to take such a large maximum step size to leave the local region of each minimum is a clear indication that we have the most stable structure for the three-body surface.

One type of result that has not been mentioned so far is that the search sometimes finds the original starting structure, but does not find its exact energy. The reason for this is unclear. It is probably caused by the starting position being too far from the bottom of the well. This causes the search routine to minimise along an unusual path, so that its convergence criteria are met before it has found the absolute minimum. This problem is more likely to happen in searches of the surface where the addition of extra terms to the potential function make the surface more complicated. If the structure's co-ordinates were to be moved by a small amount and the resulting structure minimised the exact minimum energy

would be found. These results have been marked as having failed, but to separate them from the straightforward failures they are marked by a star '*' in the results tables.

We sometimes find that the cluster has been so distorted that the search routine passes its maximum number of iterations, and the search is terminated. Sometimes when this happens the search is near the original starting minimum, on other occasions the search is nowhere near the original minimum. To reduce the likelihood of this type of result we doubled (500 $\rightarrow$ 1000) the number of iterations allowed for each search. For searches that were near the original minima at five hundred iterations this was successful. For some searches however even 1000 iterations is not enough. It is not practical to increase the maximum number of interaction much beyond 1000 because of the time taken to complete each search, especially considering that there are 40 searches to be carried out for each maximum step size.

n	$V_{n,1}$	$V_{n,2}$	$V_{n,3}$	$V_{n,4}$	$V_{n,5}$	$V_{n,6}$
3	√					
4	√	√				
5	√	√	√	√		
6	√	√	√	√	×*	√
7	√	√	√	√		
8	√	√	√	√	√	
9	√	√	√	√	√	
10	√	√	√	√		
11	√	√	√	√	√	
12	√	√	√	√	√	√

Table 6.6: Ar_nN_2 random move results($\Delta = 0.2$ Å)

n	$V_{n,1}$	$V_{n,2}$	$V_{n,3}$	$V_{n,4}$	$V_{n,5}$	$V_{n,6}$
3	√					
4	√	√				
5	√	√	√	√		
6	√	√	×	×	√	√
7	√	√	×*	√		
8	×	×*	×*	√	√	
9	√	√	√	√	√	
10	√	×	√	√		
11	√	√	√	√	√	
12	√	√	√	√	√	√

Table 6.7: Ar_nN_2 random move results($\Delta = 0.5$ Å)

n	$V_{n,1}$	$V_{n,2}$	$V_{n,3}$	$V_{n,4}$	$V_{n,5}$	$V_{n,6}$
3	√					
4	×	√				
5	√	√	√	√		
6	√	√	×	×	×	×
7	√	√	√	×		
8	×	×	×	×	×	×
9	√	×	√	×	√	
10	√	×	×	×		
11	×	×	√	√		
12	√	√	√	√	×	×

Table 6.8: Ar_nN_2 random move results($\Delta = \frac{2}{3}$ Å)

n	$V_{n,1}$	$V_{n,2}$	$V_{n,3}$	$V_{n,4}$	$V_{n,5}$	$V_{n,6}$
3	√					
4	√	√				
5	√	√	√	√		
6	√	√	$V_{6,3}$	√	√	×*
7	√	√	√	√		
8	√	×*	√	×	√	
9	√	×	×	√		
10	√	×	×	×		
11	√	×	×	×	×	
12	√	×	√	√	×	×

Table 6.9: Ar_nN_2 random move results($\Delta = \frac{2}{3}$ Å),$E_{max} = 1000$ cm^{-1}

n	$V_{n,1}$	$V_{n,2}$	$V_{n,3}$	$V_{n,4}$	$V_{n,5}$	$V_{n,6}$
3	√					
4	√	√				
5	√	√	√	$V_{5,3}$		
6	√	√	×*	√	×*	×*
7	√	√	×*	√		
8	√	×	×	√	×	
9	×	×	√	×	×	
10	×	×	√	√		
11	√	$V_{11,1}$	√	√	√	
12	√	√	√	√	√	√

Table 6.10: Ar_nN_2 random move results($\Delta = 1$ Å),$E_{max} = 1000$ cm^{-1}

n	$V_{n,1}$	$V_{n,2}$	$V_{n,3}$	$V_{n,4}$	$V_{n,5}$	$V_{n,6}$
3	√					
4	×*	√				
5	$V_{5,2}$	√	√	√		
6	$V_{6,3}$	√	$V_{6,1}$	√	×	$V_{6,1}$
7	×	√	√	√		
8	√	×	×	√	×	
9	×	×*	√	×	×	
10	×	$V_{10,1}$	×	√		
11	√	√	×	×	√	
12	√	√	$V_{12,1}$	$V_{12,1}$	$V_{12,1}$	√

Table 6.11: Ar_nN_2 random move results($\Delta = 1.5$ Å),$E_{max} = 1000$ cm^{-1}

6.5 Results Obtained from RMM for Ne_nN_2

In the neon system, just as in the argon system, we find that some searches find other three-body minima in the same system. Some searches also find the original starting structure but do not find the exact minimum energy.

For the Ne_nN_2 system the first step size tried was 0.5 Å. This represents one-sixth of the equilibrium bond distance. Therefore the total distance between any two atoms could alter by up to a third of the equilibrium bond distance. This is a very large possible change. For example if we were to take two atoms interacting at their equilibrium distance then they could be moved apart by 1 Å in the x, y and z co-ordinates. This would lead to a total change in the interaction distance of 1.73 Å. This would mean that two atoms that were previously interacting at a distance of 3.04 Å, were now interacting at a distance of 4.77 Å. Alternatively the two atoms could move closer together by the same amount, and then be interaction at a distance of 1.27 Å. The difference in energy between these three distances is considerable. At their equilibrium distance the Ne-Ne interaction energy is 29

cm^{-1}, at 1.27 Å its approximately 1000 cm^{-1}, whereas at 4.77Å it is approximately 3 cm^{-1}. In the gradient-based searches the N_2 is not moved, and because of this the maximum change in the Ne-N_2 is 0.87 Å. The fact that the Ne-N_2 potential energy function depends on both R and θ means that it is more difficult to judge the effects of the altering the Cartesian co-ordinates of the Ne Atoms. It is however clear that it will have a significant effect.

While the non-energy-limited runs with a maximum step size of 0.5 Å (table 6.13) are very successful at re-finding the original two-body minima, they are less successful when the maximum step size is increased to $\frac{2}{3}$ or 1 Å (see tables 6.14 and 6.15). In the main these searches fail because they either exceed the maximum number of iterations, or because they find a structure outside the energy range of interest. Both of these problems are caused by the fact that the starting energy of the search is too high, and from this high energy point the search cannot find its way back down to the original starting minimum. This problem will clearly get worse the larger the maximum step size becomes, as the random alteration to the co-ordinates of the rare gas atoms makes it more likely that two atoms will move very close to each other.

These two unlimited energy large step size searches do however produce one very interesting result. They both show a new structure for the search started from the $V_{6,2}$ two-body starting structure. The new structure is a square pyramid ($V_{5,1}$) structure with the sixth neon atom lying level with the N_2 and interacting in a 'T shaped' manner. This is a structure that was found in the two-body simulated annealing searches, but was not low enough in energy to be of interest. Now however, because the structure has relatively few rare gas-rare gas interactions, it is more energetically favoured.

The fact that this is the only example of a structure which moves into the energy range of interest is encouraging because this was one type of behaviour of the three-body system about which we were concerned. If this type of behaviour were more common we would have expected to see more examples in the medium sized($n = 5-8$) clusters. In the larger clusters the process of rearrangement would

probably be too complicated, and lead to a starting structure with too high an energy for the behaviour to have be seen. We are therefore reliant on the smaller clusters to show this behaviour. We can say that while it is possible for a structure to move into our energy range of interest, it appears not to happen very often.

When the same step sizes are used in the energy-limited searches the results are much better. This is especially true for the maximum step size equals $\frac{2}{3}$ Å. The results for both step sizes are shown in the tables 6.16 and 6.17.

Another result of interest produced by the energy-limited RMM searches is shown in table 6.18. Searches started from the two-body $V_{9,1}$ and $V_{9,3}$ structures both found the same new structure. The new structure was however outside the energy range of interest. It is encouraging that the energy-limited searches found the new structure, as it shows that the energy limit does not prevent the RMM search leaving the local starting minimum.

n	$V_{n,1}$	$V_{n,2}$	$V_{n,3}$	$V_{n,4}$	$V_{n,5}$	$V_{n,6}$
3	√	√				
4	√	√	√			
5	√	√	√	√		
6	√	√	√	√	√	√
7	√	√	√	√	√	√
8	√	√	√	√	√	
9	√	√	√			
10	√	√	√	√		
11	√	√	√	√		
12	√	√	√	√	√	

Table 6.12: Ne_nN_2 random move results($\Delta = 0.2$ Å)

n	$V_{n,1}$	$V_{n,2}$	$V_{n,3}$	$V_{n,4}$	$V_{n,5}$	$V_{n,6}$
3	√	√				
4	√	√	√			
5	√	√	√	√		
6	√	√	√	√	×*	√
7	√	√	√	√		
8	√	√	√	√	√	
9	×	√	√	√		
10	√	√	×	√		
11	√	√	√	√		
12	√	√	√	√	√	

Table 6.13: Ne_nN_2 random move results($\Delta = 0.5$ Å)

n	$V_{n,1}$	$V_{n,2}$	$V_{n,3}$	$V_{n,4}$	$V_{n,5}$	$V_{n,6}$
3	√	√				
4	×	√	√			
5	√	×	×*	√		
6	×	×	×	√	×*	√
7	×	×	√	×		
8	×	×	×	×	×*	
9	×	×	×			
10	×	×	×	×		
11	√	×	×	×		
12	×	×	×	×	×	

Table 6.14: Ne_nN_2 random move results($\Delta = \frac{2}{3}$ Å)

n	$V_{n,1}$	$V_{n,2}$	$V_{n,3}$	$V_{n,4}$	$V_{n,5}$	$V_{n,6}$
3	√	√				
4	×	√	√			
5	√	×	√	√		
6	×	×	×	√	×	√
7	×	×	√	×		
8	×	×	×	√	×*	
9	×	×	×			
10	×	×	×	×		
11	√	×	×	×		
12	×	×	×	×	×	

Table 6.15: Ne_nN_2 random move results($\Delta = 1$ Å)

n	$V_{n,1}$	$V_{n,2}$	$V_{n,3}$	$V_{n,4}$	$V_{n,5}$	$V_{n,6}$
3	√	√				
4	√	√	√			
5	√	√	×*	$V_{5,2}$		
6	√	√	√	√	×*	√
7	√	√	×	√		
8	√	√	√	√	√	
9	√	×	×			
10	×*	√	√	$V_{10,2}$		
11	√	×	×	√		
12	×	√	√	√	√	

Table 6.16: Ne_nN_2 RMM results($\Delta = \frac{2}{3}$ Å):$E_{max} = 1000$ cm^{-1}

n	$V_{n,1}$	$V_{n,2}$	$V_{n,3}$	$V_{n,4}$	$V_{n,5}$	$V_{n,6}$
3	√	√				
4	√	√	√			
5	√	√	√	×*		
6	×	√	×	√	×	√
7	√	√	√	√		
8	√	√	√	×	×*	
9	√	√	√	√		
10	√	√	√	√		
11	√	$V_{11,3}$	√	√		
12	√	√	√	√	$V_{12,1}$	

Table 6.17: Ne_nN_2 RMM results($\Delta = 1$ Å):$E_{max} = 1000$ cm^{-1}

n	$V_{n,1}$	$V_{n,2}$	$V_{n,3}$	$V_{n,4}$	$V_{n,5}$	$V_{n,6}$
3	×	√				
4	√	√	√			
5	√	$V_{5,1}$	×*	$V_{5,3}$		
6	√	$V_{6,1}$	×	√	×	$V_{6,1}$
7	√	√	√	$V_{7,2}$		
8	√	√	×	×	×*	
9	×	√	×			
10	×	√	√	√		
11	×	×	×	√		
12	√	√	×	×*	√	

Table 6.18: Ne_nN_2 RMM results($\Delta = 1.5$ Å):$E_{max} = 1000$ cm^{-1}

6.6 Conclusions

When looking at the results from the various types of RMM searches, it is more useful to consider the general pattern of the results than any one set of them due to the random nature of the distortion of the original geometry.

The first and most important conclusion to be drawn from the results for the three-body potential energy surface is that the two-body structures are in the low-lying minima of the three-body surface. There are a couple of structures which show that it is possible for new structures to be found in the three-body systems. These results are however the exception rather than the rule. The results of adding three-body forces are usually more subtle. They result in a convergence in the energy of structures. In some cases, such as the $V_{6,4}^{3B}$ and $V_{6,4}^{3B}$ structures of the Ar_nN_2 system, this leads to very small energy differences between consecutive structures. The three-body forces can also cause massive re-arrangement of a system if there are many two-body structures close in energy. This effect is best shown in the $Ar_{12}N_2$ system.

One result that is immediately noticeable from looking at the results of the various RMM searches on both potentials is that certain structures are more robust to the process of the random alteration of their co-ordinates than others. In general the smaller the cluster the more likely it is that a RMM search will return to the original starting minimum. But even for large clusters there are structures which are more robust than others. For example in the Ne_nN_2 system the $V_{11,1}$ structure is re-found for all RMM searches except the energy limited search where the maximum step size is 1.5Å. The $V_{9,1}$ structure shows the opposite behaviour, and is only re-found for the energy limited search with a maximum step size of $\frac{2}{3}$Å.

Some of the minima are more likely to be found than others. In particular the Ar_nN_2 systems $V_{12,1}$ structure is found from four RMM of other minima in the energy limited search with a maximum step of 1.5Å, as shown in table 6.11. This is probably due to the large energy difference between the global minimum and the other low-lying minima. It is however noteworthy that the $Ne_{12}N_2$ system

does not show a similar behaviour to the $Ar_{12}N_2$ system, even though it also has a large energy gap between the global minimum and the low-lying minima. This is because, for a given maximum step size, the rare gas-rare gas distances change more than the rare gas-molecule distance, and in the Ar_nN_2 systems it is the Ar-Ar interaction which dominates. Therefore the Ar_nN_2 system is more likely to convert from one structure to another, as the cage can be perturbed more and still be in an energetically favourable configuration. We did not use the RMM search algorithms on the $V_{17,m}$ and $V_{18,m}$ structures because to search about either of these structures would be prohibitively expensive. This is clearly shown by the fact that the time taken to minimise these two structures on the three-body surface was of the order of 100-150 minutes. Therefore even after a small random change in each co-ordinate it would take a very large amount of CPU time to complete the minimisation.

6.7 Appendix

6.7.1 Argon Three-Body Triad Code

For n argon atoms

6.7.2 main program

loop1 A 1 $\rightarrow n$

loop2 B 1 $\rightarrow n$

If $A = B$ goto end of B loop2

loop3 C 1 $\rightarrow n$

IF $A = C$ or $B = C$ goto end of C loop3

IF ABC is not first triad stored call cheq subroutine

if check digit less than 3 (i.e. that the triad is a new triad) store triad

Endloop3

Endloop2

Endloop1

6.7.3 cheq subroutine

This routine checks to see if new triad is a permutation of a previously stored triad.

Stores $A\,B\,C$ triad as $A_{new}\,B_{new}\,C_{new}$

check digit set to zero

loop1 1 $\rightarrow$ number of triad already accepted

previously accepted triad temporarily as $A_{old}\,B_{old}\,C_{old}$

If $A_{new} = A_{old}$ or

$A_{new} = B_{old}$ or

$A_{new} = C_{old}$

then add one to check digit

If $B_{new} = A_{old}$ or

$B_{new} = B_{old}$ or

$B_{new} = C_{old}$

then add one to check digit

If $C_{new}\ A_{old}$ or

$C_{new} = B_{old}$ or

$C_{nnew} = C_{old}$

then add one to check digit

Chapter 7

Conclusions and Future Directions

In this thesis two main types of rare gas clusters have been investigated. The first is rare gas trimers. We have calculate vibrational energy levels for several different species of rare gas trimer. We have also investigate the affect of the Eckart conditions on the embedding of rotating axes into rare gas trimers.

Future work on the rare gas trimers could involve the further investigation of mixed trimers, as well as calculation of their rotational constants and possibly their wavefunctions.

We have also studied the two important rare gas-molecule cluster prototypes Ar_nN_2 and Ne_nN_2, which were previously unstudied, using simulated annealing. From our studies we have gained a greater understanding of the interplay of solvent-solvent and solvent-solute interactions in determining the low energy structures of a system. We have used this understanding to predict possible solvation structures for both systems. We have also investigated, as fully as possible, the effects of three-body interactions on the low energy structures.

The field of weakly bound clusters of atoms and molecules is still an expanding one. There are still many systems, such as rare gas CO or CO_2, which have not been investigated thoroughly either by theory of experiment. One problem for the theoretical investigation of all rare gas-molecule clusters is the availability of suitable rare gas-molecule potentials. This is especially true for calculations of the red shifts of such clusters. In addition there is also a need for further development

of minimisation techniques, to allow the investigation of larger clusters. Recent advances such as genetic algorithms hold considerable potential improvements in the size of clusters that can be studied.

The field of weakly bound clusters has had a history of close experimental and theoretical collaboration and development, which will hopefully continue in the future. In particular experimental information on the red shift of a cluster, and even red shift proportionality constants will lead to a much deeper understanding of these systems.

Bibliography

[1] K. Liu, J. D. Cruzan, and R. J. Saykally, Science 271, 929 (1996).

[2] F. A. Gianturco, M. Venanzi, and A. S. Dickinson, Mol. Phys. 65, 585 (1988).

[3] F. A. Gianturco, M. Venanzi, and A. S. Dickinson, Mol. Phys. 65, 563 (1988).

[4] F. A. Gianturco and M. Venanzi, J. Chem. Phys. 91, 5352 (1989).

[5] F. R. W. McCourt, C. C. K. Wong, and P. Casavecchia, J. Chem. Phys. 93, 4699 (1990).

[6] L. Beneventi, P. Casaveccia, G. G. Volpi, and U. Buck, J. Chem. Phys. 89, 4671 (1988).

[7] L. Beneventi, P. Piergiorgio, and G. G. Volpi, J. Chem. Phys. 85, 7011 (1986).

[8] C. F. Roche, A. Ernesti, J. M. Hutson, and A. S. Dickinson, J. Chem. Phys. 104, 2156 (1996).

[9] H. S. Gutowsky et al., J. Chem. Phys. 86, 569 (1987).

[10] Y. Xu, W. Jãger, and M. C. L. Gerry, J. Chem. Phys. 99, 919 (1993).

[11] Y. Xu, W. Jãger, and M. C. L. Gerry, J. Chem. Phys. 100, 4171 (1994).

[12] J.-U. Grabow, J. Chem. Phys. 102, 1181 (1995).

[13] J. M. Hutson, J. A. Beswick, and N. Halberstadt, J. Chem. Phys. 90, 1337 (1989).

[14] J. M. Hutson and S. Jain, J. Chem. Phys. 91, 1 (1989).

[15] A. R. Cooper, S. Jain, and J. M. Hutson, J. Chem. Phys. 98, 1 (1993).

[16] J. G. Frey and B. J. Howard, Chem. Phys. 99, 415 (1985).

[17] J. G. Frey and B. J. Howard, Chem. Phys. 99, 427 (1985).

[18] R. M. Whitnell and J. C. Light, J. Chem. Phys. 89, 3674 (1988).

[19] R. M. Whitnell and J. C. Light, J. Chem. Phys. 90, 1774 (1989).

[20] A. Ernesti and J. M. Hutson, Chem. Phys. Lett. 222, 257 (1993).

[21] L. Wolniewicz and J. Hinze, J. Chem. Phys. 101, 9817 (1994).

[22] A. Alijah, L. Wolniewicz, and J. Hinze, Mol. Phys. 85, 1106 (1995).

[23] A. Alijah, L. Wolniewicz, and J. Hinze, Mol. Phys. 85, 1125 (1995).

[24] C. Eckart, Phys. Rev. 47, 552 (1935).

[25] J. K. G. Watson, Mol. Phys. 15, 479 (1968).

[26] J. Watson, Mol. Phys. 19, 465 (1970).

[27] C. D. Carney, L. L. Sprandel, and C. W. Kern, Adv. Chem. Phys. 37, 305 (1978).

[28] J. M. Hutson and B. J. Howard, Mol. Phys. 41, 1123 (1980).

[29] J. Tennyson and B. T. Sutcliffe, J. Chem. Phys. 77, 4061 (1982).

[30] J. Tennyson and B. T. Sutcliffe, Mol. Phys. 58, 1053 (1986).

[31] J. M. Hutson, J. Chem. Soc. Faraday Trans. 2 82, 1163 (1986).

[32] J. Hutson, Comput Phys Communications 84, 1 (1994).

[33] D. E. Manolopoulos, Ph. D. Thesis, Cambridge University. (1986).

[34] R. G. Gordon, J. Chem. Phys. 51, 14 (1969).

[35] A. M. Dunker and R. G. Gordon, J. Chem. Phys. 64, 4984 (1976).

[36] B. R. Johnson, J. Chem. Phys. 67, 4086 (1977).

[37] B. R. Johnson, J. Chem. Phys. 69, 4678 (1978).

[38] B. R. Johnson, J. Chem. Phys. 73, 5051 (1980).

[39] B. R. Johnson, J. Chem. Phys. 79, 1906 (1983).

[40] B. R. Johnson, J. Chem. Phys. 79, 1916 (1983).

[41] Z. Bačić and J. Light, Ann. Rev. Phys. Chem 40, 469 (1989).

[42] Z. Bačić and J. C. Light, J. Chem. Phys. 85, 4594 (1986).

[43] J. C. Light, I. P. Hamilton, and J. V. Lill, J. Chem. Phys. 82, 1400 (1985).

[44] J. V. Lill, G. A. Parker, and J. C. Light, Chem. Phys. Lett. 89, 483 (1982).

[45] C. Leforestier, J. Chem. Phys. 106, 8527 (1997).

[46] Q. Wu, D. Zhang, and J. H. Zhang, J. Chem. Phys. 103, 2548 (1993).

[47] T. Carrington, M. J. Bramley, J. W. Tromp, and G. C. corey, J. Chem. Phys. 100, 6175 (1994).

[48] S. K. Gregurick and M. H. Alexander, J. Chem. Phys. 104, 2684 (1996).

[49] L. T. Wille, Chem. Phys. Lett. 133, 405 (1957).

[50] I. M. Navon, F. B. Brown, and D. H. Robertson, Comp. Chem. 89, 95 (1990).

[51] J. A. Niesse and H. R. Mayne, J. Chem. Phys. 105, 4700 (1996).

[52] Q. Wu, D. Zhang, J. H. Zhang, and Z. Bačić, J. Chem. Phys. 102, 2315 (1995).

[53] D. J. Nesbitt, Faraday Discuss. Chem. Soc. 97, 1 (1994).

[54] M. Quack and M. A. Suhm, Theor. Chim. Acta 93, 61 (1996).

[55] E. J. Bohac and R. E. Miller, J. Chem. Phys. 99, 1537 (1993).

[56] R. C. Cohen and R. J. Saykally, J. Chem. Phys. 96, 1024 (1992).

[57] M. J. Elrod and R. J. Saykally, J. Chem. Phys. 103, 933 (1995).

[58] D. J. Nesbitt, M. D. Schuder, C. M. Lovejoy, and R. Lascola, J. Chem. Phys. 99, 4346 (1993).

[59] M. A. Suhm and D. J. Nesbitt, Chem. Soc. Rev. 24, 45 (1995).

[60] J. Han, Z. Wang, and A. L. McIntosh, J. Chem. Phys. 100, 7101 (1994).

[61] J. M. Lisy and D. W. Michael, J. Chem. Phys. 85, 2528 (1986).

[62] M. A. Suhm, J. T. Farrell, and D. J. Nesbitt, J. Chem. Phys. 98, 5985 (1993).

[63] D. Luckhaus, M. Quack, and U. Schmitt, Phys. Chem. 99, 457 (1995).

[64] G. T. Fraser, Int. Rev. Phys. Chem. 10, 189 (1991).

[65] Z. S. Haung and R. E. Miller, J. Chem. Phys. 91, 6613 (1989).

[66] S. S. Xantheas and T. H. Dunning, J. Chem. Phys. 99, 8774 (1993).

[67] S. S. Xantheas, J. Chem. Phys. 100, 7523 (1994).

[68] J. K. Gregory and D. C. Clary, J. Chem. Phys. 102, 7817 (1995).

[69] Z. Bačić, D. Sabo, and T. Leutwyler, Chem. Phys. Lett. 244, 283 (1995).

[70] Z. Bačić and R. E. Miller, J. Phys. Chem. 100, 12945 (1996).

[71] S. Suzuki, P. G. Green, and R. E. Dasgupta, Science 257, 942 (1992).

[72] J. D. Augspurger, C. E. Dykstra, and T. S. Zwier, J. Chem. Phys. 96, 7252 (1992).

[73] P. L. A. Popelier and A. J. Stone, Faraday Discuss. Chem. Soc. 97, 243 (1994).

[74] A. J. Gotch and T. S. Zwier, J. Chem. Phys. 96, 3388 (1992).

[75] A. J. Gotch and T. S. Zwier, J. Chem. Phys. 96, 3402 (1992).

[76] B. M. Cheng, J. R. Grover, and E. A. Walters, Chem. Phys. Lett. 232, 364 (1995).

[77] R. N. Pribble, A. W. Garrett, K. Haber, and T. S. Zwier, J. Chem. Phys. 103, 531 (1995).

[78] P. M. Maxton, M. W. Schaeffer, and P. M. Felker, Chem. Phys. Lett. 241, 603 (1995).

[79] Y. T. Lee, M. Okumura, L. I. Yeh, and J. D. Myers, J. Chem. Phys. 94, 3416 (1990).

[80] A. W. Castleman and R. G. Keeses, Chem. Rev. 86, 589 (1986).

[81] J. M. Lisy, Vibrational Spectroscopof cluster ions (John Wiley & son, New York, 1993).

[82] S. Leutwyler and J. Bösiger, Chem. Rev. 90, 489 (1990).

[83] S. Leutwyler and J. Jortner, J. Phys. Chem. 91, 5558 (1987).

[84] S. Leutwyler and J. Bösiger, Z. Phys. Chem. N.F. 154, 31 (1987).

[85] M. A. Kmetic and R. J. LeRoy, J. Chem. Phys. 95, 6271 (1991).

[86] M. A. Kmetic and R. J. LeRoy, JCP 95, 6271 (1991).

[87] S. Goyal and D. L. S. G. Scoles, jcp 102, 2302 (1995).

[88] J. M. Adams and R. M. Stratt, J. Chem. Phys. 93, 1358 (1990).

[89] D. J. Nesbitt, Chem. Rev. 88, 843 (1988).

[90] A. McIlroy, R. Lascola, C. M. Lovejoy, and D. J. Nesbitt, J. Phys. Chem. 96, 2636 (1991).

[91] D. T. Anderson, S. Davis, and D. J. Nesbitt, J. Chem. Phys. 107, 1115 (1997).

[92] H. S. Gutowsky et al., J. Chem. Phys. 86, 569 (1987).

[93] H. S. Gutowsky et al., J. Am. Chem. Soc. 109, 5653 (1987).

[94] H. S. Gutowsky et al., J. Chem. Phys. 83, 4817 (1985).

[95] J. M. Sperhac, M. J. Weida, and D. J. Nesbitt, J. Chem. Phys. 104, 2202 (1996).

[96] T. D. Klots, J. Chem. Phys. 87, 5315 (1987).

[97] T. D. Klots, J. Chem. Phys. 87, 4383 (1987).

[98] M. J. Elrod, J. G. Loeser, and R. J. Saykally, J. Chem. Phys. 98, 5352 (1992).

[99] M. J. Elrod, D. W. Steyert, and R. J. Saykally, J. Chem. Phys. 95, 3182 (1991).

[100] J. M. Hutson, BOUND computer code, distribution by Collaborative Computer Project No. 6 of the UK Science and Engineering Research Council Version 1 (1983) to verson 5 (1993). The BOUND program is avalible by anonymous ftp from Internet address krypton.dur.ac.uk. .

[101] Z. Bačić, S. Liu, J. W. Moskowitz, and K. E. Schmidt, J. Chem. Phys. 100, 7166 (1994).

[102] S. Leutwyler and J. Bösiger, Chem. Rev. 90, 489 (1990).

[103] S. Goyal, G. N. Robinson, D. Schutt, and G. Scoles, J. Chem. Phys. 95, 4186 (1991).

[104] W. H. Press, S. A. Teukolsky, W. T. Vetterling, and B. P. Flannery, Numerical Recipes in FORTRAN. The Art of Scientific Computing (Cambridge University, Cambridge, 1992).

[105] J. Nichols, H. Taylor, P. Schmidt, and J. Simons, J. Chem. Phys. 92, 340 (1990).

[106] C. J. Cerjan and W. H. Miller, J. Chem. Phys. 75, 2800 (1981).

[107] R. L. Asher, D. A. Micha, and P. J. Brucat, J. Chem. Phys. 96, 7683 (1992).

[108] S. Kirkpatrick, S. D. G. Jr., and M. P. Vecchi, Science 220, 4598 (1983).

[109] L. Davis, Genetic Algorithms and Simulated Annealing (Pitman, London, 1987).

[110] J. T. Ngo and J. Marks, Protein Eng. 5, 313 (1992).

[111] J. T. Ngo, J. Marks, and M. Karplus, The Protein Folding Problem and Tertiary Structure Prediction (Birkhäuser, Boston, 1994).

[112] L. T. Wille and J. Vennik, J. Phys. A 18, L419 (1985).

[113] M. R. Garey and D. S. Johnson, Computers and Intractability: A Guide to the Theory of NP-Completeness (Freeman, San Francisco, 1979).

[114] D. M. Deaven, N. Tit, J. R. Morris, and K. M. Ho, Chem. Phys. Lett. 256, 195 (1996).

[115] D. E. Goldberg, Genetic Algorithms in Search, Optimization, and Machine Learning (Addison-Wesley, Reading,MA, 1989).

[116] D. E. Manolopoulos, J. Chem. Phys. 85, 645 (1986).

[117] B. Johnson, J. Comput. Phys. 13, 445 (1973).

[118] J. Tennyson, Comp. Phys. Reports 4, 1 (1986).

[119] J. Tennyson, S. Miller, and J. Henderson, in Methods in Computational Chemistry. Vol. 5,ed. (S.Wilson, Plenum, New York, 1991).

[120] D. G. Truhlar, D. W. Olson, A. C. Jeanotte, and J. Overend, J. Am. Chem. Soc. 98, 2373 (1976).

[121] M. Shapiro and G. G. Balint-Kurti, J. Chem. Phys. 71, 1461 (1979).

[122] J. M. Hutson, Adv. Mol. Vibrat. Coll. Dyn. A1, 1 (1991).

[123] M. Tamir and M. Shapiro, Chem. Phys. Lett. 31, 166 (1975).

[124] R. T. Pack, J. Chem. Phys. 60, 634 (1974).

[125] P. McGuire and D. J. Kouri, J. Chem. Phys. 60, 2488 (1974).

[126] R. D. Levine, J. Chem. Phys. 49, 51 (1968).

[127] H. Mayer, J. Phys. A 8, 1562 (1975).

[128] R. C. Whitten and F. T. Smith, J. Math. Phys. 9, 1103 (1968).

[129] W. Zickendraht, Ann. Phys. 18, 35 (1965).

[130] D. M. Brink and G. R. Satchler, Angular Momentum (Oxford University, Oxford, 1968).

[131] A. Ernesti and J. M. Hutson, J. Chem. Phys. 103, 3386 (1995).

[132] R. A. Aziz, J. Chem. Phys. 99, 4518 (1993).

[133] R. A. Aziz and M. J. Slaman, J. Chem. Phys. 130, 187 (1989).

[134] F. Luo et al., J. Chem. Phys. 98, 3564 (1993).

[135] F. Luo et al., J. Chem. Phys. 100, 4023 (1994).

[136] E. S. Meyer, J. C. Mestar, and I. F. Silvera, J. Chem. Phys. 100, 4021 (1994).

[137] R. A. Aziz, J. Chem. Phys. 94(12), 8047 (1991).

[138] R. A. Aziz et al., J. Chem. Phys. 70, 4330 (1979).

[139] A. R. Janzen and R. A. Aziz, J. Chem. Phys. 103, 9626 (1995).

[140] R. J. Vos, J. H. van Lenthe, and F. B. van Duijneveldt, J. Chem. Phys. 93, 643 (1990).

[141] B. Liu and A. D. McLean, J. Chem. Phys. 91, 2348 (1989).

[142] F. Luo et al., J. Chem. Phys. 98, 9687 (1993).

[143] M. J. Jamieson, A. Dalgarno, and M. Kimura, Phys. Rev. A 51, 2626 (1995).

[144] T. Cornelius and W. Glöckle, J. Chem. Phys. 85(7), 3906 (1986).

[145] S. Nakaichi-Maeda and T. K. Lim, Phys. Rev. A 28(2), 692 (1983).

[146] H. S. Huber and T. K. Lim, J. Chem. Phys. 68, 1006 (1978).

[147] W. Schllopf and J. P. Toennies, Science 260, 25 (1994).

[148] W. Schllopf and J. P. Toennies, J. Chem. Phys. 104, 1155 (1995).

[149] V. N. Efimov, Yad. Fiz 12, 1080 (1970).

[150] E. Fermi, PR 71, 666 (1947).

[151] J. M. Blatt and J. D. Jackson, PR 76, 18 (1949).

[152] J. Al-Khalili, Physics World June, 33 (1996).

[153] D. A. Barow and R. A. Aziz, Chem. Phys. 89, 1689 (1988).

[154] S. C. Carter, I. M. Mills, and N. C. Handy, J. Chem. Phys. 99, 4379 (1993).

[155] J. M. Hutson, Ann. Rev. Phys. Chem. 41, 123 (1990).

[156] J. E. B. Wilson, J. C. Decius, and P. C. Cross, Molecular Vibrations: The Theory of Infrared and Raman Vibrational Spectra (MaGraw-hill Publishing Company Ltd, London, 1955).

[157] A. Sayvetz, J. Chem. Phys. 7, 383 (1939).

[158] D. Papousek and M. R. Aliev, Molecular Vibrational-Rotational spectra (Elsevier, Amsterdam, 1982).

[159] Z. Bačić, S. Liu, J. W. Moskowitz, and K. E. Schmidt, J. Chem. Phys. 101, 6358 (1994).

[160] Z. Bačić, S. Liu, J. W. Moskowitz, and K. E. Schmidt, J. Chem. Phys. 101, 10181 (1994).

[161] Z. Bačić, S. Liu, J. W. Moskowitz, and K. E. Schmidt, J. Chem. Phys. 103, 1829 (1995).

[162] B. Numerov, Publs. Observatoire Central Astrophys. Russ. 2 18, 188 (1933).

[163] R. A. Aziz and H. H. Chen, J. Chem. Phys. 67, 5719 (1977).

[164] A. K. Dham, F. R. W. McCourt, and W. J. Meath, J. Chem. Phys. 103, 8477 (1993).

[165] J. M. Hutson, J. Chem. Phys. 96, 5098 (1992).

[166] J. M. Hutson et al., J. Chem. Phys. 105, 9130 (1996).

[167] F. Y. Naumkin, Mol. Phys. 90, 875 (1997).

[168] M. S. Bowers, K. T. Tang, and J. P. Toennies, J. Chem. Phys. 88, 5465 (1988).

[169] K. T. Tang and J. P. Toennies, J. Chem. Phys. 80, 3726 (1984).

[170] A. R. Cooper and J. M. Hutson, J. Chem. Phys. 98, 5337 (1993).

[171] A. Ernesti and J. M. Hutson, Phys. Rev. A 51, 239 (1995).

[172] J. Rak, M. M. Szczesniak, G. Chalasinski, and S. M. Cybulski, JCP 107, 10215 (1997).

[173] A. Ernesti and J. M. Hutson, JCP 106, 6288 (1997).

[174] G. Chalasinski, J. Rak, M. Szczesniak, and S. M. Cybulski, JCP 106, 3301 (1997).

[175] J. T. Farrell and D. J. Nesbitt, JCP 105, 9421 (1996).

[176] M. Lewerenz, JCP 104, 1028 (1996).

[177] B. M. Axilrod and E. Teller, J. Chem. Phys. 11, 299 (1943).

[178] A. Kumar and W. J. Meath, Mol. Phys. 54, 823 (1985).

[179] S. A. C. McDowell, A. Kumar, and W. J. Meath, Mol. Phys. 87, 845 (1996).

[180] S. A. C. McDowell and W. J. Meath, Mol. Phys. 90, 713 (1997).

Appendix A

Conferences, Courses and Seminars Attended

CCP6 Workshop, 'Intramolecular Dynamics in the Frequency and Time Domains'. Oxford University, 15th-16th December 1994.

Molecular Collisions in the Atomsphere. University of Durham 8th-11thJune 1995

Institute of Physics one day meeting on Atoms and Limits of Quantum Theory. 14th July 1995

Royal Society of Chemistry High Resolution Spectroscopy Group. Conference on High Resolution Spectroscopy (Annual meeting of the HRSG). Reading University, 17th-19th December 1995.

6th Annual Informal Northern Universities Meeting on Chemical Physics. Newcastle Universities 4th July 1996.

Charles Coulson Summer School in Theoretical Chemistry. Oxford University 8th-18th September 1996.

Photoionisation Dynamics, Rydberg States and Large Amplitude Motion. University of York 3rd-5th November 1996.

The following pages contain lists of the seminars in the chemistry department from 1994-1997. These marked with an asterisk were attended.

1994 - 1995 (August 1 - July 31)

1994

October 5 Prof. N. L. Owen, Brigham Young University, Utah, USA
Determining Molecular Structure - the INADEQUATE NMR way

October 19 Prof. N. Bartlett, University of California
Some Aspects of Ag(II) and Ag(III) Chemistry

November 2 * Dr P. G. Edwards, University of Wales, Cardiff
The Manipulation of Electronic and Structural Diversity in Metal Complexes - New Ligands

November 3 Prof. B. F. G. Johnson, Edinburgh University
Arene-metal Clusters

November 9 Dr G. Hogarth, University College, London
New Vistas in Metal-imido Chemistry

November 10 Dr M. Block, Zeneca Pharmaceuticals, Macclesfield
Large-scale Manufacture of ZD 1542, a Thromboxane Antagonist Synthase Inhibitor

November 16 Prof. M. Page, University of Huddersfield

Four-membered Rings and b-Lactamase

November 23 Dr J. M. J. Williams, University of Loughborough
New Approaches to Asymmetric Catalysis

December 7 Prof. D. Briggs, ICI and University of Durham
Surface Mass Spectrometry

1995

January 11 Prof. P. Parsons, University of Reading
Applications of Tandem Reactions in Organic Synthesis

January 18 * Dr G. Rumbles, Imperial College, London
Real or Imaginary Third Order Non-linear Optical Materials

January 25 Dr D. A. Roberts, Zeneca Pharmaceuticals
The Design and Synthesis of Inhibitors of the Renin-angiotensin System

February 1 * Dr T. Cosgrove, Bristol University
Polymers do it at Interfaces

February 8 Dr D. O'Hare, Oxford University
Synthesis and Solid-state Properties of Poly-, Oligo- and Multidecker Metallocenes

February 22 Prof. E. Schaumann, University of Clausthal
Silicon- and Sulphur-mediated Ring-opening Reactions of Epoxide

March 1 Dr M. Rosseinsky, Oxford University
Fullerene Intercalation Chemistry

March 22 Dr M. Taylor, University of Auckland, New Zealand
Structural Methods in Main-group Chemistry

April 26 Dr M. Schroder, University of Edinburgh
Redox-active Macrocyclic Complexes : Rings, Stacks and Liquid Crystals

May 4 Prof. A. J. Kresge, University of Toronto
The Ingold Lecture Reactive Intermediates : Carboxylic-acid Enols and Other Unstable Species

POST GRADUATE COLLOQUIA, LECTURES AND SEMINARS FROM INVITED SPEAKERS
1995 - 1996 (August 1 - July 31)

1995
October 11 * Prof. P. Lugar, Frei Univ Berlin, FRG
Low Temperature Crystallography

October 13 Prof. R. Schmutzler, Univ Braunschweig, FRG.
Calixarene-Phosphorus Chemistry: A New Dimension in Phosphorus Chemistry

October 18 Prof. A. Alexakis, Univ. Pierre et Marie Curie, Paris,
Synthetic and Analytical Uses of Chiral Diamines

October 25 Dr.D.Martin Davies, University of Northumbria
Chemical reactions in organised systems.

November 1 Prof. W. Motherwell, UCL London
New Reactions for Organic Synthesis

November 3 Dr B. Langlois, University Claude Bernard-Lyon
Radical Anionic and Psuedo Cationic Trifluoromethylation

November 8 Dr. D. Craig, Imperial College, London
New Stategies for the Assembly of Heterocyclic Systems

November 15 Dr Andrea Sella, UCL, London
Chemistry of Lanthanides with Polypyrazoylborate Ligands

November 17 Prof. David Bergbreiter, Texas A&M, USA
Design of Smart Catalysts, Substrates and Surfaces from Simple Polymers

November 22 Prof. I Soutar, Lancaster University
A Water of Glass? Luminescence Studies of Water-Soluble Polymers.

November 29 Prof. Dennis Tuck, University of Windsor, Ontario, Canada
New Indium Coordination Chemistry

December 8 Professor M.T. Reetz, Max Planck Institut, Mulheim
Perkin Regional Meeting

1996
January 10 * Dr Bill Henderson, Waikato University, NZ
Electrospray Mass Spectrometry - a new sporting technique

January 17 * Prof. J. W. Emsley , Southampton University
Liquid Crystals: More than Meets the Eye

January 24 Dr Alan Armstrong, Nottingham Univesity

Alkene Oxidation and Natural Product Synthesis

January 31 Dr J. Penfold, Rutherford Appleton Laboratory,
Soft Soap and Surfaces

February 7 Dr R.B. Moody, Exeter University
Nitrosations, Nitrations and Oxidations with Nitrous Acid

February 12 Dr Paul Pringle, University of Bristol
Catalytic Self-Replication of Phosphines on Platinum(O)

February 14 Dr J. Rohr, Univ Gottingen, FRG
Goals and Aspects of Biosynthetic Studies on Low Molecular Weight Natural Products

February 21 Dr C R Pulham , Univ. Edinburgh
Heavy Metal Hydrides - an exploration of the chemistry of stannanes and plumbanes

February 28 Prof. E. W. Randall, Queen Mary & Westfield College
New Perspectives in NMR Imaging

March 6 Dr Richard Whitby, Univ of Southampton
New approaches to chiral catalysts: Induction of planar and metal centred asymmetry

March 7 Dr D.S. Wright, University of Cambridge
Synthetic Applications of Me2N-p-Block Metal Reagents

March 12 RSC Endowed Lecture - Prof. V. Balzani, Univ of Bologna
Supramolecular Photochemistry

March 13 * Prof. Dave Garner, Manchester University
Mushrooming in Chemistry

April 30 Dr L.D.Pettit, Chairman, IUPAC Commission of Equilibrium Data
pH-metric studies using very small quantities of uncertain purity

1996 - 1997 (August 1 - July 31)
1996
October 9 Professor G. Bowmaker, University Aukland, NZ
Coordination and Materials Chemistry of the Group 11 and Group 12 Metals : Some Recent
Vibrational and Solid State NMR Studies

October 14 Professor A. R. Katritzky, University of Gainesville,University of Florida, USA
Recent Advances in Benzotriazole Mediated Synthetic Methodology

October 16 Professor Ojima, Guggenheim Fellow, State University of New York at Stony Brook
Silylformylation and Silylcarbocyclisations in Organic Synthesis

October 22 Professor Lutz Gade, Univ. Wurzburg, Germany
Organic transformations with Early-Late Heterobimetallics: Synergism and Selectivity

October 22 * Professor B. J. Tighe, Department of Molecular Sciences and Chemistry, University of Aston
Making Polymers for Biomedical Application - can we meet Nature's Challenge?
Joint lecture with the Institute of Materials

October 23 Professor H. Ringsdorf (Perkin Centenary Lecture), Johannes Gutenberg-Universitat, Mainz, Germany
Function Based on Organisation

October 29 * Professor D. M. Knight, Department of Philosophy, University of Durham.
The Purpose of Experiment - A Look at Davy and Faraday

October 30 Dr Phillip Mountford, Nottingham University
Recent Developments in Group IV Imido Chemistry

November 6 Dr Melinda Duer, Chemistry Department, Cambridge
Solid-state NMR Studies of Organic Solid to Liquid-crystalline Phase Transitions

November 12 * Professor R. J. Young, Manchester Materials Centre, UMIST
New Materials - Fact or Fantasy?
Joint Lecture with Zeneca & RSC

November 13 Dr G. Resnati, Milan
Perfluorinated Oxaziridines: Mild Yet Powerful Oxidising Agents

November 18 Professor G. A. Olah, University of Southern California, USA
Crossing Conventional Lines in my Chemistry of the Elements

November 19 Professor R. E. Grigg, University of Leeds
Assembly of Complex Molecules by Palladium-Catalysed Queueing Processes

November 20 Professor J. Earnshaw, Deptartment of Physics, Belfast
Surface Light Scattering: Ripples and Relaxation

November 27 Dr Richard Templer, Imperial College, London
Molecular Tubes and Sponges

December 3 Professor D. Phillips, Imperial College, London
"A Little Light Relief" -

December 4 * Professor K. Muller-Dethlefs, York University
Chemical Applications of Very High Resolution ZEKE Photoelectron Spectroscopy

December 11 Dr Chris Richards, Cardiff University
Sterochemical Games with Metallocenes

1997
January 15 Dr V. K. Aggarwal, University of Sheffield
Sulfur Mediated Asymmetric Synthesis

January 16 Dr Sally Brooker, University of Otago, NZ
Macrocycles: Exciting yet Controlled Thiolate Coordination Chemistry

January 21 Mr D. Rudge, Zeneca Pharmaceuticals
High Speed Automation of Chemical Reactions

January 22 Dr Neil Cooley, BP Chemicals, Sunbury
Synthesis and Properties of Alternating Polyketones

January 29 Dr Julian Clarke, UMIST
What can we learn about polymers and biopolymers from computer-generated nanosecond movie-clips?

February 4 Dr A. J. Banister, University of Durham
From Runways to Non-metallic Metals - A New Chemistry Based on Sulphur

February 5 Dr A. Haynes, University of Sheffield
Mechanism in Homogeneous Catalytic Carbonylation

February 12 Dr Geert-Jan Boons, University of Birmingham
New Developments in Carbohydrate Chemistry

February 18 Professor Sir James Black, Foundation/King's College London
My Dialogues with Medicinal Chemists

February 19 Professor Brian Hayden, University of Southampton
The Dynamics of Dissociation at Surfaces and Fuel Cell Catalysts

February 25 Professor A. G. Sykes, University of Newcastle
The Synthesis, Structures and Properties of Blue Copper Proteins

February 26 Dr Tony Ryan, UMIST
Making Hairpins from Rings and Chains

March 4 Professor C. W. Rees, Imperial College
Some Very Heterocyclic Chemistry

March 5 Dr J. Staunton FRS, Cambridge University
Tinkering with biosynthesis: towards a new generation of antibiotics

March 11 Dr A. D. Taylor, ISIS Facility, Rutherford Appleton Laboratory
Expanding the Frontiers of Neutron Scattering

March 19 * Dr Katharine Reid, University of Nottingham

Probing Dynamical Processes with Photoelectrons